Space Science Reviews (2026) 222:56
https://doi.org/10.1007/s11214-026-01308-4

Evolution and Observable Properties of Rocky Planet Atmospheres

Marie-Luise Steinmeyer[1] · Lena Noack[2] · Philipp Baumeister[2] · Keiko Hamano[3,4] · M.J. Way[5,6] · Doris Breuer[7] · Kanako Seki[8] · Caroline Brachmann[2,7] · Fabrice Gaillard[9] · Manuel Scherf[10] · Svetlana V. Berdyugina[11] · Brice-Olivier Demory[12]

Received: 1 December 2025 / Accepted: 25 June 2026

Abstract
The atmospheric composition of rocky exoplanets offers an important tool for constraining the properties of the interior of this type of planet, beyond what is possible from measurements of their mass and radius alone. However, the interpretation of these observations requires an understanding of the complex interplay of a larger number of coupled planetary and atmospheric processes. This review provides an overview of the current state of knowledge regarding rocky exoplanet atmospheres, beginning with their formation and escape mechanisms. We specifically highlight the importance of long-term interaction between the atmosphere, the surface, and the interior on rocky planets. Furthermore, this review addresses the influence of biological activity and photochemical reactions on the atmospheric compositions. Consequently, establishing how these different processes contribute to shaping the atmospheres of rocky exoplanets during their evolution is fundamental for the characterization of these planets with future space missions and ground-based surveys.

Keywords Exoplanets · Exoplanet atmospheres · Exoplanet atmospheric evolution · Exoplanet observation · Extrasolar rocky planets

1 Introduction

Three decades after the discovery of the first exoplanet around a Sun-like star by Mayor and Queloz (1995), the focus of the field has shifted from the mere detection of exoplanets to their detailed characterization. The atmospheres of rocky exoplanets are of particular interest.

This review provides a summary of the major findings on the formation, evolution, and properties of rocky exoplanet atmospheres.

1.1 Atmospheres in the Solar System

Our understanding of planetary atmospheres is mainly derived from laboratory experiments as well as from the observed diversity of atmospheres in the present-day solar system (Fig. 1). The composition of the atmospheres of the gas and ice giants (Jupiter, Saturn,

Extended author information available on the last page of the article

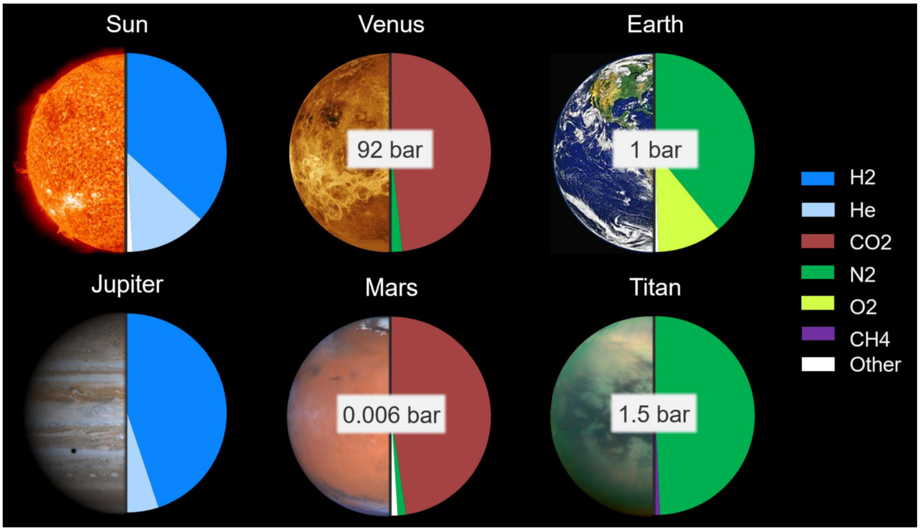

Fig. 1 There are three main types of atmospheric compositions observed in the solar system: primordial atmospheres (Sun and gas giants), carbon-dioxide-dominated atmospheres (Venus and Mars), as well as nitrogen-dominated atmospheres (Earth and Titan)

Uranus, and Neptune) is, at least with respect to their main components, remarkably similar to the solar atmosphere. This indicates their primordial origin from the planetary nebula during the accretion phase of planets, where the main gases available in the system (hydrogen and helium, as well as trace amounts of other gases) were gravitationally captured by the accreting planets (e.g. Hayashi et al. 1979). For the rocky planets in the Solar System, it is generally believed that they either never accreted a primordial atmosphere or that they lost their primordial atmosphere during the early stages of their evolution via different mechanisms (e.g., Lammer et al. 2018).

Venus and Mars, the two neighboring planets of our Earth, both harbor a CO_2-dominated atmosphere, despite their different locations at the inner and outer edge of the habitable zone (e.g. Kasting et al. 1993), and their different planetary masses (Venus being almost as massive as Earth, but Mars only one tenth of the mass of Earth). The striking difference between these two atmospheres is the surface pressure – with Venus' atmospheric pressure being about 100 times the pressure of Earth, and Mars' about 1/100. Several studies (e.g. Jakosky et al. 2018; Sakai et al. 2018; Scherf and Lammer 2021; Lichtenegger et al. 2022; Hu and Thomas 2022; Thomas et al. 2023) have tried to link the thin atmosphere on Mars with atmospheric loss processes and its magnetic field (see Sect. 2), but it is still a topic of active debate.

The third type of atmosphere observed in the present-day solar system is nitrogen-dominated and appears on four very different bodies – on Earth and Titan, and, as collisionless exospheres, on Pluto and Triton. Titan has a reduced chemistry nitrogen-dominated atmosphere with trace amounts of methane, (e.g. MacKenzie et al. 2021), while on Earth, the nitrogen-dominated atmosphere together with a strong oxygen contribution is linked to the existence of life (Schirrmeister et al. 2015; Sproß et al. 2021) and the invention of photosynthesis. Pluto and Triton, in contrast, both have tenuous N_2-dominated exospheres with minor amounts of CO and CH_4 that originate from vapor-pressure equilibria with their icy surfaces (e.g., Scherf et al. 2025). The question of how Earth's atmosphere would look like

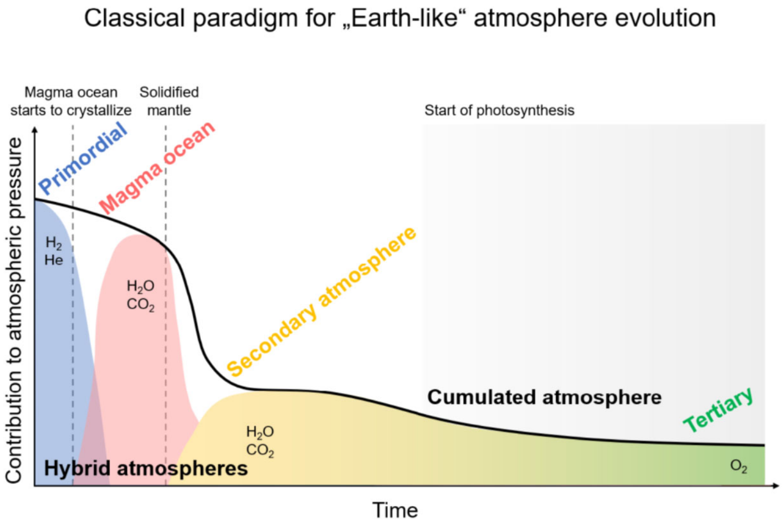

Fig. 2 Sketch for the atmospheric evolution of an Earth-like planet from accretion (primordial atmosphere) via magma ocean crystallization and outgassing to a secondary atmosphere shaped by volcanic outgassing, or (in the case of Earth) by life (tertiary atmosphere)

today if life had never evolved on Earth is a topic of active debate, especially in light of the discovery of rocky exoplanets in the habitable zone (HZ) around other stars. Although a lifeless Earth is likely similar to the late Hadean/early Archean eon, there are indications of similar or lower atmospheric pressure levels of nitrogen than today. For example, Marty et al. (2013) used isotopic data for 3.0–3.5 Ga to find that N_2 was 0.5–1.1 bar. Avice et al. (2018) found at 3.3 Ga that pN_2 was similar or lower than today. Using a variety of different methods (e.g., fossil raindrops, lava vesicle sizes, oxidation of micrometeorites) at ∼2.6–2.7 Ga, the total pressure could have been as low as 0.23 bar (Som et al. 2012, 2016; Rimmer et al. 2019). Higher CO_2 partial pressures in the Archean (Catling and Zahnle 2020) are supported by the work of Kanzaki and Murakami (2015), Charnay et al. (2017), Lehmer et al. (2020a), Feulner et al. (2023). The evolution of the post-accretion period of Earth's atmosphere – or of any of the rocky bodies' atmospheres – remains poorly understood. Studies have produced a wide range of possible atmospheres (from highly reduced to oxidized) in the magma ocean phase (e.g. Bower et al. 2019; Maurice et al. 2024) for which there are few constraints. For the other rocky bodies in the solar system, there is little information on the nature of the atmosphere during the accretion and magma ocean stage, although Titan's nitrogen isotope indicates that its atmosphere mainly comes from the accretion of NH_3 ice and complex N-bearing organics (Miller et al. 2019; Erkaev et al. 2021).

Secondary outgassing by volcanic activity shapes the atmosphere of rocky planets during their long-term evolution. Note that for geological studies, the term secondary outgassing often does not encompass the magma ocean phase, whereas from an astronomer point of view as well as within this review chapter (see Fig. 2) a secondary atmosphere includes any outgassing from the interior including dissolution of volatiles from the magma ocean (e.g. Bower et al. 2019; Maurice et al. 2024). It should be noted that the atmospheric composition can differ from the composition of volcanic gases expected to be degassed at the surface of a planet based on the local melt composition and redox state, as gases may remain dissolved in the melt based on their solubility depending on the already existing atmospheric partial pressures (e.g. Gaillard and Scaillet 2014; Gaillard et al. 2022b; Sossi et al. 2023).

The atmosphere can change over geological timescales through different processes. These may include material in-fall (e.g., meteorites, comets), various atmospheric escape processes (Gronoff et al. 2020), condensation of different species, weathering processes at the surface (Walker et al. 1981), or even large volcanic outgassing (e.g. Wignall 2011; Bond and Grasby 2017). In the case of Earth, biology led to an oxygen-rich atmosphere after the Great Oxygenation Event more than 2.5 Gyr ago (e.g. Alcott et al. 2019). We term this the tertiary atmosphere in Fig. 2.

1.2 Atmospheres of Exoplanets

Beyond the solar system, different direct and indirect methods exist to detect and characterize planetary atmospheres. The first detection of an exoplanetary atmosphere was achieved for the hot Jupiter HD209458b using transit spectroscopy by Charbonneau et al. (2002), who measured an additional dimming of the star in the sodium resonance doublet by about 200 parts per million (ppm) as compared to the nearby continuum. This technique has become a leading approach for detecting exoplanetary atmospheres and characterizing their gaseous composition.

Whether an exoplanet is a gas giant or rocky planet can be determined indirectly based on their size, via transit spectroscopy, and the bulk density, via mass estimation using radial velocity measurements. Based on current observations, alongside theoretical work, rocky planets may be roughly limited to $< 1.5\,R_\oplus$ (Rogers 2015; Fulton et al. 2017b; Petigura et al. 2022), although this value has been challenged by other statistical analyses of mass-radius data yielding values of $1.23^{+0.44}_{-0.22}$ (e.g. Chen and Kipping 2016). In general, the radius gap is mostly a population-level property, and classifying individual planets by their location relative to the gap is to be treated with caution (see e.g, the discussion in Baumeister, Miozzi, et al. 2025, this collection). The location of the radius gap further depends strongly on the stellar type and the orbital period (Petigura et al. 2022; Ho and Van Eylen 2023; Parc et al. 2024; Venturini et al. 2024). Outliers have been repeatedly detected, and for each assumed transition mass/radius from rocky to sub-Neptune planets (with large fractions of volatiles in the form of gases, liquids and/or ices), there will be individual planets of smaller mass/radius with an extended radius (likely not rocky), such as L 98-58b (Demangeon et al. 2021) or Kepler-138 d (Piaulet et al. 2023), as well as larger planets with high densities indicating rocky planets. There is the suggested super-Mercury Kepler-107c with (based on current observations) $10\,M_\oplus$ and $1.6\,R_\oplus$ (Bonomo et al. 2023) leading to a density even higher than expected for a scaled-up Mercury planet. This suggests very small fractions of silicate materials mixed with heavy metals, while leaving almost no room for a substantial atmosphere. Rocky super-Earths and gaseous sub-Neptunes may actually share a common origin, with different atmospheric loss processes dividing the sample into two subgroups (see Sect. 2.3).

Another indirect indication of an atmosphere comes from the evaluation of flux variations during the orbit (phase-curves). In particular, measurements of the rise and ebb of an exoplanet's flux can provide constraints on a potential atmosphere. Depending on the wavelength, exoplanet phase-curves may probe predominantly thermal or reflective components of the planet's outgoing radiation, or their combination (e.g., Wong 2021),

The first detection of thermal radiation from an exoplanet (Deming et al. 2005) and subsequent infrared phase-curve measurements (Knutson et al. 2007) allowed for the detection of clear atmosphere signatures on hot Jupiters. The thermal phase-curve amplitude was found to be significantly smaller than the planet's thermal emission measured during the occultation by the star (eclipse). This flux difference pointed to a significant part of the heat being recirculated from the day-side to the night-side of the planet. This recirculation was further corroborated by the East-ward shift of the phase-curve peak induced by the characteristic strong super-rotation occurring in the atmospheres of tidally-locked planets (Showman and Guillot 2002). Direct imaging studies of young gas giants also indicate cloudy and dusty atmospheres (e.g., Marois et al. 2010).

Optical phase-curves inform about the atmosphere's reflective properties, such as the wavelength-dependent geometrical albedo and the presence of hazes and clouds. For example, Rayleigh scattering on gas-phase atoms and molecules and small particles (haze, aerosols, etc.) produces a characteristic blueward slope in transit spectra. This was first found on the hot Jupiter HD189733b using transit spectroscopy at wavelengths longer than 550 nm (Pont et al. 2008). A high albedo of this exoplanet in the blue (at 450 nm and shorter) was first determined using polarized-light optical phase-curves (Berdyugina et al. 2008, 2011) and subsequently confirmed by near-UV secondary eclipse spectroscopy (Evans et al. 2013). Thus, the Rayleigh slopes and high geometrical albedoes of exoplanets may indicate the presence of the atmospheres, hazes and clouds (e.g., Demory et al. 2013; Sing et al. 2016).

The same general principles apply to the smaller rocky exoplanets. While there are hints of an atmosphere surrounding 55 Cnc e (Mahapatra et al. 2017; Hu et al. 2024), the definitive evidence for an atmosphere around a rocky planet orbiting a cool star is still lacking. The absence of such atmospheres have been confirmed in several cases, either from thermal phase-curve measurements (e.g. Kreidberg et al. 2019) or occultations for those rocky exoplanets subject to high instellation (e.g. August et al. 2025; Meier Valdes et al. 2025). For more temperate planets (Venus-like or slightly hotter), such as TRAPPIST-1b and TRAPPIST-1c, current observations are still compatible with both an airless or atmosphere scenario (e.g. Greene et al. 2023; Zieba et al. 2023; Ducrot et al. 2025).

The true characterization of the atmospheric chemical composition needs spectroscopic measurements to identify individual species in the atmosphere – via transmission, reflection or emission spectroscopy. For gas giants and sub-Neptunes, these methods have been successfully applied to detect a variety of gases such as Na I, H_2O, CH_4, CO_2, CO, and SO_2 (e.g., Charbonneau et al. 2002; Belu et al. 2011; Wakeford et al. 2018; Benneke et al. 2024; Powell et al. 2024; Beatty et al. 2024; Kempton and Knutson 2024).

Scattering on particles (aerosols) in exoplanetary atmospheres, such as cloud condensations and photochemical hazes, reduces the contrast of spectral signatures of gas-phase molecules, that makes them challenging to detect (e.g. Fauchez et al. 2019). In some extreme cases, even flat spectra have been observed, strongly suggesting the presence of aerosol-rich atmospheres (e.g., Kreidberg et al. 2014; Gao et al. 2021). Overall, observations by *Hubble*, *Spitzer* and JWST reveal that aerosols are common in exoplanetary atmospheres, but disentangling particle sizes, composition and their height distribution in models remains a challenge due to multiple degeneracies.

Featureless or heavily muted transmission spectra of lower-mass exoplanets (sub-Neptunes/super-Earths) is a pattern that emerged in early observations (e.g., Kreidberg et al. 2014) and consistently strengthened by the current JWST data and atmospheric retrievals (e.g., Fauchez et al. 2019; Madhusudhan et al. 2025). Along with the detection of multiple carbon-bearing molecules (CH_4, CO_2) and molecules previously hidden by aerosols, JWST data expose new inconsistencies that aerosol models must explain, in particular the complexity and heterogeneity of these atmospheres. For example, high metallicity, non-equilibrium chemistry (e.g., Jaziri et al. 2025) as well as organic and graphite hazes in carbon-rich atmospheres (e.g., Li et al. 2025) can explain some of the observed features.

In the future, spectra from rocky planets at large angular separations from their host stars can be directly observed in the optical and infrared using imaging coronography (e.g., Wolff et al. 2024), nulling interferometry (Quanz et al. 2022), etc. A detailed overview of different current and future observational capabilities from space and ground is given in Lagage et al. (2026, this collection).

2 Formation and Loss Processes of Atmospheres

2.1 Formation

Figure 2 shows that the atmosphere of a rocky planet can be separated into primordial and secondary atmospheres. The primordial atmosphere (Sect. 2.1.1) is formed from gas of the accretion disk during planet formation. The secondary atmosphere (Sect. 2.1.2) is composed of volatiles that are initially brought to the planet with colliding planetesimals, impacting asteroids and comets, and are later released by various outgassing processes: During impact outgassing, which occurs particularly during accretion, volatiles are released directly into the atmosphere and do not accumulate in the forming planet at all. For other outgassing processes such as magma ocean outgassing and volcanic outgassing, the volatiles that are initially stored in the planet's interior during accretion are released later.

2.1.1 Primordial Atmospheres

Modern planet formation predicts that rocky planets form at least partly in the protoplanetary disk of the host star (see e.g., reviews by Raymond and Morbidelli 2022; Drążkowska et al. 2023). These disks are mainly composed of gaseous hydrogen and helium (Armitage 2011). If the thermal energy of a gas particle in the vicinity of a protoplanet is not enough to overcome the gravitational pull from the protoplanet, the gas particle is bound to the planet. The radius at which the thermal energy of a gas particle and the gravitational energy of the protoplanet are roughly equal is called the Bondi radius (Ikoma and Genda 2006). Thus, any planet for which the Bondi radius is larger than the radius of the planet itself binds gas from the surrounding protoplanetary disk (Ikoma and Hori 2012; Lee et al. 2014; Ginzburg et al. 2016). As the gas around the protoplanet cools and contracts, more and more gas will be gravitationally bound to the protoplanet (Ikoma and Genda 2006; Lee and Chiang 2015; Ginzburg et al. 2016). This minimum mass is small enough that rocky planets that form within the life-time of the protoplanetary disks will bind a primordial atmosphere.

It is generally assumed that this primordial atmosphere is in hydrostatic equilibrium and consists of an inner convective and an outer radiative region (Piso and Youdin 2014). At the outer boundary, the Bondi radius, the pressure and temperature correspond to the local disk conditions.

The opacity of the atmosphere plays an important role in shaping the profile of the atmosphere by determining the location of the radiative-convective boundary. There are two potential opacity sources, the gas itself and absorption by dust grains (Semenov et al. 2003). The opacity contribution of dust grains depends on their size, as larger grains contribute less to the opacity. However, both analytical and numerical models of dust growth in primordial atmospheres, show that the contribution of dust grains to the opacity is low (Mordasini 2014; Ormel 2014). Therefore, primordial atmospheres can be assumed to be grain-free, with the gas opacity being the dominant opacity source.

The total accreted mass of a primordial atmosphere depends both on the local disk conditions and the optical properties of the atmosphere itself. Figure 3 compares an analytic estimation of the atmosphere mass fraction as a function of planet mass by Ginzburg et

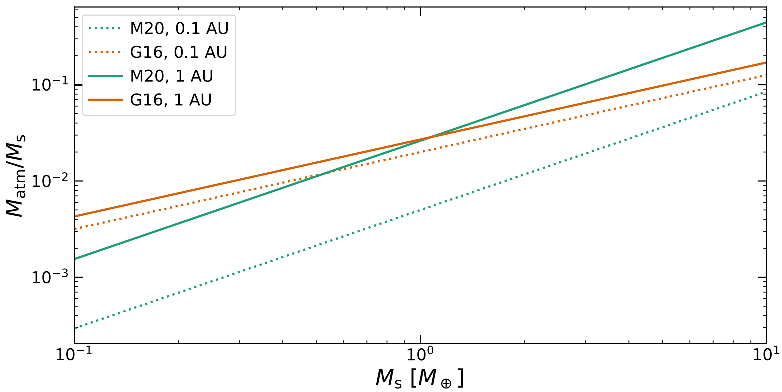

Fig. 3 Comparison of the analytic scaling law for the primordial atmospheric mass fraction ($M_{\rm atm}/M_{\rm s}$) by Ginzburg et al. (2016) (orange line) to the fit to numerical simulations by Mordasini (2020) (green line). Dotted lines refer to planets with an orbital distance of $a = 0.1$ au and solid lines to $a = 1$ au. In all cases, the mass fraction of a primordial atmosphere of an Earth-sized planet is $\sim 1\%$, while a $10\,M_\oplus$ planet has a primordial atmospheric mass fraction of $\sim 10\%$

al. (2016) to the numerical fit by Mordasini (2020). Ginzburg et al. (2016) assume that the atmosphere mass is concentrated in the convective region and find

$$\frac{M_{\rm atm}}{M_s} \approx 0.02 \left(\frac{M_s}{M_\oplus}\right)^{0.8} \left(\frac{T_{\rm eq}}{10^3\,{\rm K}}\right)^{-0.25} \left(\frac{t_{\rm disk}}{1\,{\rm Myr}}\right)^{0.5}. \tag{1}$$

Here $M_{\rm atm}$ is the atmospheric mass, $M_{\rm s}$ the mass of the solid planet, $T_{\rm eq}$ the equilibrium temperature, and $t_{\rm disk}$ the life-time of the disk. Mordasini (2020) on the other hand, use a population synthesis approach to find the mean primordial atmosphere mass fraction as a function of the solid planet mass and the orbital distance a

$$\frac{M_{\rm atm}}{M_s} = 0.005 \left(\frac{M_s}{M_\oplus}\right)^{1.23} \left(\frac{a}{0.1\,{\rm au}}\right)^{0.72}. \tag{2}$$

Both scaling relations estimate that the final primordial atmospheric mass fraction of an Earth-sized rocky planet is $\sim 1\%$ whereas a $10 M_\oplus$ super-Earth can have a primordial atmospheric mass fraction of $\sim 10\%$.

Initially, the composition of the primordial atmosphere corresponds to the composition of the protoplanetary disk. However, if the growth of the planet is dominated by smaller bodies (‘pebbles’), the heating of the atmosphere by the release of gravitational energy leads to an enrichment of the atmosphere in heavier species due to the sublimation of the incoming bodies (Lambrechts et al. 2014; Alibert 2017; Brouwers et al. 2018; Steinmeyer et al. 2023). Fragmentation and ablation of the accreted bodes can further enrich the atmosphere in elements other than H and He (Hori and Ikoma 2011; Venturini et al. 2016; Mol Lous et al. 2024). The long-term evolution of such polluted primordial atmosphere is still uncertain (Vazan et al. 2024).

One important consequence of atmospheric pollution is that it lowers the critical core mass to values as low as a few Earth masses (Hori and Ikoma 2011; Venturini et al. 2015). This is the critical core mass at which a planet enters run-away gas accretion and turns into a gas giant. The existence of super-Earths and sub-Neptunes demonstrates that it needs to be possible to avoid this runaway growth. Possible mechanisms for this are late formation (Lee and Chiang 2016), interrupted accretion due to a gap opening further out in the disk (Fung and Lee 2018; Ginzburg and Chiang 2019), and high opacity atmospheres (Lee et al. 2014). For close-in planets, it has been proposed that the dominant mechanism to avoid run-away gas accretion is the recycling flows between the atmosphere and the surrounding protoplanetary disk (Ormel et al. 2015; Moldenhauer et al. 2022).

While rocky planets will lose their primordial atmospheres during their later evolution, see Sect. 2.2, these initial atmospheres can leave imprints on the planet's interior. The combination of the heat from accretion and the heat produced by radioactive decay leads to the formation of a deep magma ocean. Hydrogen and noble gases such as He and Ne can readily dissolve into the magma ocean and later be sequestered in the mantle and core. The measured $^{3}He/^{4}He$ ratio in Earth's deep mantle is considered evidence for the equilibration between a primordial atmosphere and this early magma ocean (Harper and Jacobsen 1996). The dissolution of hydrogen into the magma ocean also changes its redox state as discussed in Sect. 2.1.2. Furthermore, the sequestration of hydrogen into the interior has been proposed as a mechanism to explain the observed bulk densities of super-Earths (Schlichting and Young 2022; Rogers et al. 2024b). Beyond simple dissolution, chemical reactions between the primordial atmosphere and the magma ocean can further lead to an endogenic production of water with a D/H ratio of nebular gas (Ikoma and Genda 2006; Ikoma et al. 2018).

2.1.2 Secondary Atmosphere

Impact Degassing When a planetary body collides, a shock wave is generated at the point of impact and propagates through the impactor and the rocks near the impact site. The compression caused by the shock wave is irreversible, increasing entropy and converting part of the impactor's kinetic energy into heat. This shock heating induces phase transitions such as degassing, melting, and vaporization, and releases atmophile elements contained in solids (both the impactor and the target's surface) directly into the atmosphere as gases. This process, known as *impact degassing*, is considered to have played an important role in shaping planetary atmospheres throughout planetary formation, from the continuous accretion stage of planetary embryos (Matsui and Abe 1986; Tyburczy et al. 1986; Olson and Sharp 2019; Salvador et al. 2023) to the late accretion phase on fully formed planets (Chyba 1990; Sakuraba et al. 2019; Zahnle et al. 2020). The large number of craters preserved on the ancient surfaces of the Moon, Mercury and icy satellites attests the high frequency of collisions in the early solar system, suggesting that impact degassing played a significant role in the evolution of young terrestrial planets.

The efficiency of impact degassing to devolatilize an accreting planetary body and form an atmosphere increases with the amount of accretion heating, which in turn is related to the size of the growing body and the size of the impactor. As a planet grows, the impact velocities increase due to the increase in radius until partial and then, at larger radii, complete devolatilization of especially water occurs. Water in minerals is released due to the resulting high temperatures. At what planetary radius devolatilization becomes effective also depends on the hydrated minerals, and estimates for complete volatilization range from 1300 km to 2500 km (e.g. Tyburczy et al. 2001). However, experiments have shown that up to 30% of volatiles can be stored in impact melts and projectile survivors (Daly and Schultz 2018). Impact outgassing during accretion is particularly important, as this process determines how much of the volatiles — especially water — is trapped in the forming planet. This can then alter the atmosphere in later stages of magma ocean and volcanic outgassing.

Once the volatile elements are released as gas, the gas composition in the hot vapor cloud in the initial phase is expected to be close to the chemical equilibrium composition due to the high temperature. Chemical equilibrium calculations with bulk elemental abundances similar to those of primitive meteorites indicate that the redox state of iron (iron oxides v.s. metallic iron/iron sulfides) and the amount of atmophile elements are particularly important for the composition and redox state of impact-generated gases (Hashimoto et al. 2007; Schaefer and Fegley 2007, 2010). The gas composition rapidly changes in accordance with the temperature and pressure changes associated with the vapor expansion, and eventually quenches at some point. The quenching conditions are determined by the cooling rate of an impact-induced vapor and the chemical reaction rates, and vary according to gas species. For instance, Zahnle et al. (2020) used a thermochemical kinetics code to estimate that the quenching temperature of NH_3 is about 300 K higher than that of CH_4 for a Vesta-sized impact. In general, the quenching temperature tends to be lower as the size of an impact vapor cloud increases, due to a slower decrease in the internal temperature and pressure.

Ancient Mars is the poster child for an atmosphere by impact degassing. Presently, Mars has a thin atmosphere with global yearly mean surface temperatures of $\sim$–65 C. However, there is ample geologic evidence that Mars in the Noachian eon ($>$ 3.7 Ga) had warm periods (whose length is still debated) where substantial water flowed on the surface (e.g. Wordsworth 2016, and references therein). The seeds of the idea go back at least to Hashimoto et al. (2007), who proposed that impact degassing could have contributed to Earth's atmosphere toward the end of its accretion period, leading to an atmosphere that may have been mainly composed of impact material. Haberle et al. (2019) proposed that a similar mechanism may have occurred on Mars, but in the post-accretion period. The theory is that the impactor creates a short-lived but hot thermal plume and that extant water on the surface of Mars interacts with the impactor's reducing materials to produce H_2 (a powerful greenhouse gas). The authors estimated that if the impactor is $>$100 km in size, it could provide enough H_2 for the planet's mean global surface temperature to rise above 0 °C if it already has a dense CO_2 atmosphere. Earlier work by Wordsworth et al. (2017) had shown using ab-initio calculations that CO_2–H_2 collisionally induced absorption (CIA) had previously been underestimated and could provide significant warming. Subsequent 3-D General Circulation Modeling (GCM) results confirmed that $\sim$10–20% H_2 in a 1–2 bar CO_2atmosphere could provide global and/or local surface temperatures above the freezing point in the Noachian and Hesperian eons (Kamada et al. 2020; Guzewich et al. 2021; Schmidt et al. 2022). However, more recent empirical work by Turbet et al. (2020) has demonstrated that the CO_2–H_2 CIA ab-initio calculations of Wordsworth et al. (2017) may be too optimistic and that the warming provided may be much less. Subsequent 3D GCM simulations by Schmidt et al. (2025) confirm this.

Magma Ocean Outgassing Magma ocean outgassing and solidification is an increasingly active field of research, as it rules the formation of both the initial secondary atmosphere and primordial reservoirs of volatile elements in the planetary mantle. Thus, it defines the starting point from which the secondary atmosphere and mantle reservoirs may evolve via enduring geodynamic processes.

Magma ocean outgassing is the process wherein the atmophile elements dissolved in magma oceans are exsolved to the surface, whereas when surficial gases are dissolved in the magma ocean, one talks about ingassing. In conditions where the exchange of materials between the atmosphere and the magma is most efficient, the mass and composition of the overlying atmosphere can be controlled by gas solubilities into silicate melts. An efficient exchange between the melt and the atmosphere occurs in particular during fractional crystallization. In this process, the heavier crystals sink and the lighter, more volatile melts rise and come into contact with the atmosphere through effective convection in the magma ocean, where the volatiles then exsolve or are ingassed (e.g., Nikolaou et al. 2019; Bower et al. 2022; Salvador and Samuel 2023). In conditions of highly reducing surfaces, the atmosphere consists of H_2 and CO/CH_4, while N is dissolved in magma as nitrides, resulting in an atmosphere that is relatively N-depleted. Conversely, under oxidizing surface conditions, the predominant components are CO/CO_2 and N_2, while the majority of H is dissolved in magma as H_2O, resulting in an atmosphere that is relatively H-depleted.

So far, the effect of magma ocean oxidation (or redox) state on outgassing has mostly been considered as a free parameter, which arbitrarily varies between end-member cases, that is to say, from very reduced to very oxidized (Gaillard et al. 2022a; Bower et al. 2022; Nicholls et al. 2024). Oxygen fugacity f_{O_2} is a proxy that is used to quantify the redox state (amount of oxygen) in the considered system and geochemists have used the iron-wustite (Fe-FeO, labelled IW) as a reference redox buffer. The most reduced systems have ΔIW-6, which indicates oxygen fugacity values that are 6 orders of magnitude lower than the f_{O_2} imposed by the IW buffer. An example of such a reduced system is the mantle of present day Mercury. The most oxidized systems in contrast usually have ΔIW+6, e.g., subduction related magma on Earth.

The provenance of planetary accretion materials, both capture and escape of H_2, and internal redox processes contribute to controlling the magma ocean redox state. The nature of the building blocks of planet accretion, pebble of chondritic origin, planetesimals and planetary embryos, is an obvious parameter controlling magma ocean f_{O_2}. For example, in the solar system, a planet exclusively built from enstatite chondrites should be more reduced, whereas a planet composed of carbonaceous chondrites should be much more oxidized. Similar types of building blocks, with equivalent redox differences, may be expected in other planetary systems (Doyle et al. 2019). Any intermediate magma ocean oxidation states can be attained by a mixture of these end-member materials. The disk processes controlling the provenance of these building blocks (Morbidelli et al. 2015; Johansen et al. 2021) and what controls their redox state is much debated (Righter et al. 2020). Other processes, such as the gravitational capture of nebular gases, a process that has long been discussed in the literature for its consequences in terms of volatile abundances (see review by Ikoma et al. 2018) and its potential effect on the magma ocean oxidation state, remain little investigated (e.g., Young et al. 2023). In all cases, the capture of the solar nebula would raise the H_2/H_2O ratio and thus drive the system toward more reducing conditions. It remains to be studied what type of mineralogy assemblies and exotic speciation could be generated in the planetary interior due to the accretion of H2-dominated primordial atmospheres as is the case for sub-Neptunes. Alternatively, atmospheric escape processes tend to favor H-loss, which should have the opposite effect, i.e., driving an increase in oxygen fugacity (Pierrehumbert 2010a; Katyal et al. 2020). The effect of such escape processes on the magma ocean oxidation state has also been little addressed in a quantitative way.

Internal oxygen redistribution, due to high pressures (> 15 GPa) prevailing deep in the magma ocean, can also affect the oxidation state of the magma ocean. Most identified processes, that is to say, iron disproportionation (Frost et al. 2004) and enhanced stability of ferric iron (Zhang et al. 2024), both favored by high-pressure, and silicon incorporation in the core, favored by high temperature, tend to cause an increase in the magma ocean oxygen fugacity. On the other hand, high temperature enhances the direct dissolution of oxygen in the metallic core, which causes a reduction of the oxygen fugacity of the magma ocean. All these processes are equilibrium processes. As such, they can be short-circuited in the chain of processes forming planets if non-equilibrium processes dominate.

Magma ocean solidification also strongly influences the initial distribution of water and other volatiles in the interior. As a certain amount of water is partitioned into the solidifying minerals, an exponential increase of water in the crystals toward the surface can be expected in particular for fractional crystallization: since volatiles prefer to enter/remain in the melt, the rising melt becomes increasingly enriched with volatile elements as the magma ocean solidifies over time. As a result, the volatile content also increases in materials that crystallize later. The evolving magma ocean liquid is also continuously enriched in oxidized iron as Mg-rich silicates crystallize first. Therefore, Mg-rich cumulates can be found at the core-mantle boundary while Fe-rich cumulates form at the end of magma ocean solidification and remain close to the surface (Elkins-Tanton 2012). This leads to a volatile and non-monotonic density increase toward the surface, resulting in a gravitationally unstable configuration, initiating early mantle convection and mixing the volatiles into the interior.

As described above, fractional crystallization suggests efficient degassing. A depletion of more than 90% of the initial amount of volatiles has been assumed, and even small initial volatile contents (0.05 wt.% H_2O, 0.01 wt.% CO_2) can produce atmospheres in excess of 100 bars (Elkins-Tanton 2008). However, fractional crystallization and degassing are disturbed among others by inefficient crystal-melt segregation, i.e., melt in which incompatible elements are concentrated can be confined in the solid cumulates. The faster the cooling and the slower the compaction, the less efficient is the crystal-melt separation (e.g., Solomatov 2000; Hier-Majumder and Hirschmann 2017). The melt fractions that are trapped in the cumulate pile have been estimated to values of between 1 and 10% (Elkins-Tanton 2008; Hier-Majumder and Hirschmann 2017). Furthermore, if the magma ocean did not comprise the entire mantle, the lower mantle remains primordial and thus more volatile-rich in comparison to the outgassed upper mantle due to magma ocean solidification (Gaillard et al. 2022b). This means that a substantial amount of volatiles may still be present within planets after this early accretion and differentiation process. This water is then outgassed together with CO_2 and other volatiles during subsequent volcanism, as is described in the next section.

The density of such an outgassed atmosphere (neglecting here condensation and atmospheric loss processes) can vary immensely depending on planetary mass, initial volatile content of the outgassing magma ocean, and magma ocean redox state. As an example, Fig. 4 shows the maximum outgassed atmospheric pressure versus planet mass for initial volatile concentrations of 200 ppm CO_2, 200 ppm H_2O and 20 ppm N_2 in the mantle. We consider here three different planetary interior structures (with a small metal core comparable to the Moon, with an Earth-like interior structure, and with a Mercury-like extremely large metal core) assuming either an oxidized magma ocean (solid lines, outgassed species are CO_2, H_2O and N_2, i.e., leading to a COHN-rich atmosphere), a reduced magma ocean (dashed lines, outgassed species considered here are CH_4, H_2 and NH_3) and an extremely reduced magma ocean where all C and N would remain stored in the mantle and only H_2 would be degassed (dotted lines). The planet mass and interior structure (e.g., core-mass fraction X_{CMF}) influence most importantly the mass of the rocky mantle and therefore the total mass of COHN volatiles that can maximally be outgassed, $M_{\text{atm}} \approx M_p(1 - X_{\text{CMF}})$, planet radius,

$$R_{\text{p}} = (7030 - 1840 X_{\text{CMF}} \left(\frac{M_{\text{p}}}{M_{\text{Earth}}}^{0.282} \right),$$

and surface gravitational acceleration $g_0 \approx M/R_{\text{p}}^2 \approx M_{\text{p}}^{0.436}$ (Noack and Lasbleis 2020).

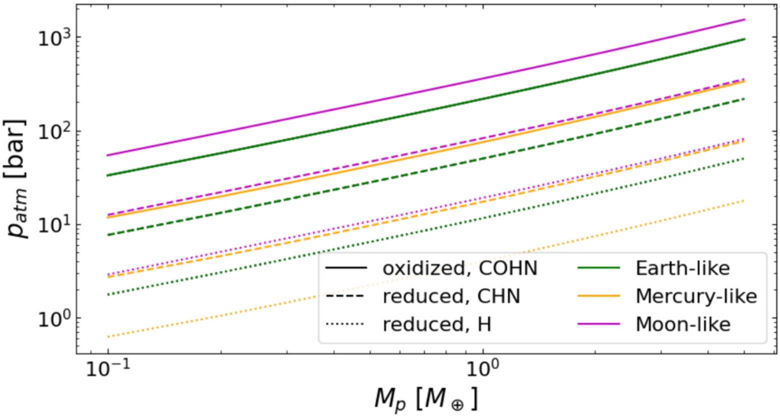

Fig. 4 Rule-of-thumb estimates on maximal outgassed atmospheric pressure over planet mass considering different planetary interior configurations. The initial volatile concentrations in the mantle are 200 ppm CO_2, 200 ppm H_2O and 20 ppm N_2. For more information, we refer the reader to the main text

The resulting atmospheric pressure is then calculated via

$$p_{\mathrm{atm}}[bar] = \frac{M_{\mathrm{atm}} g_0}{4\pi R_{\mathrm{p}}^2} 10^{-5}$$

This simple rule-of-thumb calculation highlights that atmospheric pressures can vary by two orders of magnitude for the same planet mass but different interior configuration: 1) Mercury-like planets would tend to have a factor 3 smaller atmospheric pressure due to the reduced proportion of (volatile-bearing) rocky material; 2) The planet mass impacts the atmospheric pressure by a factor of almost 9 when increasing mass by a factor of 10 (not taking into account solubility effects); and 3) oxidized magma oceans lead to much denser atmospheres, with atmospheric pressures almost five times higher compared to the reduced case and more than ten times higher compared to the extreme case scenario of only H_2 being outgassed.

This simple estimate should of course be taken with caution and only be considered for illustrative purposes to point out that magma ocean atmospheres may vary strongly in density and composition from planet to planet. This example also considered extreme magma ocean redox state scenarios, and for many rocky planets, the atmospheric composition may lie in-between the oxidized and reduced scenarios. Furthermore, the redox state of the magma ocean may change over time due to interior differentiation processes (estimates for Earth suggest an increase of the mantle/magma ocean oxygen fugacity by several orders of magnitude during the accretion, core formation, and magma ocean crystallization, Wood et al. 2006). In addition, outgassing of reduced gases such as H_2 may have further oxidized the magma ocean of early Earth, (Sharp et al. 2013).

Volcanic Outgassing After the solidification of the magma ocean, volatile degassing continues through volcanic activity. Volatiles such as carbon (C), hydrogen (H), oxygen (O), sulfur (S), and nitrogen (N) are stored within the rocks of the mantle and crust. Various geological processes, including heat transfer, decompression, and the introduction of water, can induce the melting of these rocks, leading to the release and partitioning of the stored volatiles into the melt. Being less dense than the surrounding rocks, the melt ascends through the mantle and crust, forming magma diapirs or utilizing fractures and cracks in the brittle crust to rise. As the magma ascends, the decreasing pressure reduces the solubility of dissolved volatiles and eventually leads to the formation of a gas phase when the magma becomes supersaturated. These gas bubbles are subsequently released into the atmosphere either through extrusive volcanism or, in cases where the melt is trapped, through cracks in the overlying rocks, driven by buoyant forces. The composition of these gas bubbles varies depending on factors such as the volatile content of the melt, oxygen fugacity, temperature, and degassing pressure. Melts with high redox states predominantly degas H_2O, CO_2, N_2, and SO_2, whereas at lower redox states, volatiles such as H_2, CO, CH_4 (especially at high pressures), S_2, H_2S and NH_3 are more common (Gaillard and Scaillet 2009, 2014). At low degassing (subaerial) pressures, sulfur is outgassed as SO_2, whereas at higher (submarine or subsurface) degassing pressures, sulfur is outgassed as H_2S, leading to different atmospheric compositions for planetary surfaces covered by oceans compared to atmospheres formed predominantly by continental volcanism (Gaillard et al. 2011).

Additionally, degassing of halogens like HCl and HF is possible and while highly toxic (Giggenbach 1996), they tend to play a less significant role on a global scale. Several studies have aimed to estimate variations in atmospheric composition, pressure, and temperature on exoplanets whose atmospheres are primarily formed through volcanic degassing. To accurately assess outgassing efficiency, key parameters such as the mantle's volatile content, melting fluxes, and oxygen fugacity must be taken into account. Gaillard and Scaillet (2014) highlighted the critical role of pressure in controlling the speciation of volcanic gases: within the pressure range of 50 to 500 bar, carbon species like CO_2 and CO dominate, while at pressures between 50 and 10^{-3} bar, H_2O becomes the most abundant species. At even lower pressures, sulfur-bearing gases prevail. Building on this, Ortenzi et al. (2020) investigated the influence of mantle redox state and planetary size on atmospheric pressure. Their results show that planets with reduced interiors generate thinner atmospheres compared to those with oxidized interiors, due to the higher molecular weight of oxidized volatile species. Moreover, they found that volcanic degassing is most efficient on planets with masses between 2 and 4 Earth masses. This is attributed to greater volatile inventories, increased radiogenic heat production, and elevated mantle temperatures. However, for planets exceeding this threshold, higher lithospheric pressures raise melting temperatures, thereby inhibiting or even preventing volcanic outgassing.

Woitke et al. (2021) developed a simplified equilibrium chemistry model applicable to surface temperatures below 600 K, predicting three distinct compositional atmospheric types for cold terrestrial planets. These types are defined by the relative abundances of four dominant gases: Type A atmospheres consist of NH_3, CH_4, H_2O, and either H_2 or N_2; Type B feature O_2, H_2O, N_2, and CO_2; and Type C are characterized by H_2O, CO_2, CH_4, and N_2. Building on this framework, Brachmann et al. (2025) extended the model by incorporating mantle volatile partitioning and volcanic degassing. Their study revealed a strong dependence of atmospheric chemistry and pressure on mantle oxygen fugacity, surface temperature, and melt production rates. Mantles with oxygen fugacities below ΔIW +1 tend to produce thin, nitrogen-rich Type A atmospheres, while those with higher oxygen fugacities generate H_2O- or CO_2-dominated Type C atmospheres. Surface temperature further modulates gas abundances: H_2O and N_2 are more prevalent at higher temperatures, whereas NH_3 and CH_4 dominate under cooler conditions. Notably, Type B atmospheres cannot be generated by volcanic degassing alone, as O_2 is neither directly released nor formed through equilibrium chemistry. Instead, abiotic O_2 formation requires photodissociation of H_2O molecules.

In a complementary study focused on hotter planets with surface temperatures above 800 K, Liggins et al. (2022) introduced sulfur into the C-H-O-N system and identified three atmospheric classes governed by mantle redox state. Class R atmospheres (oxygen fugacity < ΔIW +0.5) are dominated by H_2, CH_4, and NH_3; Class I atmospheres (oxygen fugacity between ΔIW +0.5 and +2.7) include CH_4, CO_2, CO, and COS; while Class O atmospheres (oxygen fugacity > ΔIW +2.7) are rich in SO_2, S_2O, and polymeric sulfur species (S_x).

It should be noted that the studies referenced here assume a homogeneous and temporally stable oxygen fugacity across a planet's mantle, melt, and atmosphere. However, this is a rough approximation. In reality, oxygen fugacity can vary between these different reservoirs and is influenced by a variety of processes. For example, the degassing of H_2 and CO may oxidize the melt, while sulfur degassing may reduce it (Burgisser and Scaillet 2007; Gaillard and Scaillet 2014). Additionally, atmospheric processes such as the photodissociation of H_2O and the subsequent escape of H_2 can oxidize the atmosphere (Sharp et al. 2013).

The suggested atmosphere classifications therefore also depend on additional factors or processes not yet included, such as planetary composition, evolution of surface temperature under different weathering/condensation scenarios, and atmospheric losses depending among others on the host star.

2.1.3 Current Limitations in Our Understanding of Planetary Atmosphere Formation

Our understanding of planetary atmosphere formation is still constrained by significant approximations and assumptions that require rigorous reassessment. Several major limitations—both experimental and theoretical—persist, demanding focused attention to refine current models.

The degassing and ingassing processes within magma oceans are currently described by solubility laws extrapolated to extreme temperatures and redox conditions, yet these extrapolations lack robust experimental or thermodynamic validation. While widely used by the scientific community, such extrapolations introduce uncertainties that remain difficult to quantify. Moreover, the very nature of species dissolving in magma oceans is not fully understood, particularly for compounds such as H_2, NH_3, and CH_4.

Beyond internal chemistry, the coupling between the primordial and secondary atmospheres presents a modeling challenge. Recent models propose the emergence of hybrid atmospheres, formed by planetary outgassing into a primordial H_2-He envelope (Tian and Heng 2024). The transition from primordial to secondary atmospheres has only recently been approached (Krissansen-Totton et al. 2024). The subsequent ingassing of this primordial atmosphere into the planetary interior — and its geochemical consequences — remains to be constrained. A more versatile modeling approach, capable of integrating exotic conditions beyond standard paradigms, is essential to capture these complex dynamics.

The formation of the metallic core plays a critical role in shaping atmospheric composition through equilibration between the magma ocean and the metallic core. Many key atmophile elements — such as carbon, nitrogen, and hydrogen —also exhibit siderophile tendencies, complicating their partitioning between the core and the atmosphere (Gaillard et al. 2021). This duality necessitates finer modeling of distribution mechanisms during the evolution of the planet.

While the assumption of equilibrium during ingassing and outgassing is convenient, it has been increasingly challenged (Walbecq et al. 2025). Non-equilibrium processes — such as bubble nucleation, volatile diffusion from melt to bubbles, and the balance between advection and convection in extreme magmatic conditions—require systematic study. Validating predictive equations under these high-pressure, high-temperature conditions remains a major experimental and theoretical challenge.

Planetary impacts represent another source of disequilibrium. They play a dual role in the evolution of the atmosphere by acting as volatile reservoirs and triggers for large-scale degassing, while at the same time potentially leading to partial or complete atmospheric loss. Despite their recognized importance, these stochastic events are not yet fully integrated into global models of atmospheric formation.

Finally, the solidification of magma oceans and associated degassing form a complex dynamic system, where internal convection and external radiation interact. Degassing influences the solidification process, which in turn affects convection rates and cooling rates, while solidification itself impacts degassing, creating feedback loops that remain poorly characterized. Additionally, the interplay between stellar irradiation and the nature of the outgassed atmosphere may lead to divergent evolutionary pathways (Hamano et al. 2013). Thus, magma ocean solidification, degassing, atmosphere formation, and stellar irradiation are deeply intermingled processes whose interdependencies require further elucidation.

2.2 Escape

In general, thermal atmospheric escape occurs when the kinetic energy of gas particles in the upper atmosphere exceeds the gravitational binding energy of the planet. The upper atmosphere typically refers to either the region above the homopause or above the mesopause. In the heterosphere, above the homopause, the different atmospheric species are no longer mixed, leading to a stratification by mass. The region above the mesopause is characterized by a positive thermal gradient with altitude. The two boundaries are typically located close to each other. The height of the mesopause on both Earth and Venus is at ≈ 100 km, for exoplanets, the boundary between inner and upper atmosphere is $5-25\%$ bigger than the transit radius (Kite and Barnett 2020; Malsky and Rogers 2020).

Several physical processes can contribute to increasing the energy of the atmospheric particles. This section serves as a brief summary of important mass loss mechanisms. For a detailed discussion on atmospheric escape, we refer the reader to Kubyshkina et al. (2026, this collection).

2.2.1 Thermal Escape Processes

In the case of thermal mass loss, the heating of the planetary atmosphere by external or internal sources drives the escape of the atmosphere. We distinguish two different regimes of thermal escape. In Jeans escape, the upper atmosphere is in hydrostatic equilibrium, and the fraction of the escaping particles corresponds to the high-energy tail of a Maxwell distribution (Jeans 1955; Chamberlain 1963). For strong heating, the upper atmosphere is no longer in hydrostatic equilibrium. The resulting expansion of the atmosphere leads to a bulk outflow of atmospheric gas similar to solar Parker winds (Parker 1965). In contrast to Jeans escape, the outflowing gas remains a collisional fluid. This regime is referred to as hydrodynamic escape. The transition between Jeans and hydrodynamic escape typically takes place when the kinetic energy is the same or greater than the gravitational binding energy of the planet.

The heating source plays an important role in shaping the mass loss rate and the final structure of the planet. In the following, we discuss the two common heating sources for thermal escape.

Boil-Off and Core-Powered Mass Loss Both in the so-called boil-off and core-powered mass loss, the main drivers of the mass loss are the thermal energy reservoir of the planet and the stellar bolometric irradiation[1] (e.g., Ginzburg et al. 2016; Owen and Wu 2016; Tang et al.

[1] Meaning the irradiation across all wavelengths-.

2024). The stellar irradiation heats the atmosphere from above at the same time as the heat flux from the solid planet heats the atmosphere from below.

While the planet is embedded in the disk, the pressure support from the surrounding protoplanetary disk and the solid accretion luminosity allow the primordial atmosphere of the planet to be extended out to its Bondi radius (e.g., Pollack et al. 1996; Ikoma et al. 2000; Piso and Youdin 2014; Stökl et al. 2015). Owen and Wu (2016) find that the atmospheres of low-mass planets remain inflated after the disk disperses, as the cooling time of the atmosphere is longer than the timescale of the disk dispersal. The resulting loss of hydrostatic equilibrium establishes a bulk outflow of atmospheric gas in the form of a hydrodynamic wind (Owen and Wu 2016; Ginzburg et al. 2016).

Boil-off ends when the mass loss timescale becomes shorter than the cooling timescale of the planet (Rogers et al. 2024a; Tang et al. 2024). The typical timescale of boil-off is on the order of a few Myrs, making it a very fast loss process (Owen and Wu 2016; Tang et al. 2024; Rogers et al. 2024a). The remaining mass fraction depends on the solid planet mass and the strength of the irradiation (Owen and Wu 2016; Tang et al. 2024). Models show that boil-off can strip the total primordial atmosphere of planets with $M_\mathrm{p} \lesssim 5\,M_\oplus$ that receive a flux of $F \gtrsim 100\,F_\oplus$ (Fossati et al. 2017; Tang et al. 2024).

The combination of the thermal energy of the solid planet and the bolometric irradiation from the host star continues to drive atmospheric escape over a timescale of Gyrs. This type of atmospheric escape is known as core-powered mass loss. However, most works on the role of core-powered mass loss on the evolution of planets have used a simplified analytical model based on Ginzburg et al. (2018). Recent numerical models by Tang et al. (2024) find that the analytical model overestimates the mass loss due to core-powered mass loss. Further work by Misener et al. (2025) finds that the mass loss rate depends significantly on the ratio of the opacity in the visible and infrared wavelength range. Therefore, boil-off and core-powered mass loss likely only play a role for planets with primordial atmospheres.

Photoevaporation Photoevaporation refers to the hydrodynamic escape of the upper atmosphere driven by the EUV and X-ray (XUV) irradiation received from the host star (e.g., Lopez et al. 2012; Stökl et al. 2014; Owen and Jackson 2012; Owen and Wu 2013). The XUV irradiation heats the upper atmosphere via dissociation and ionization of gas molecules. As the XUV luminosity is especially high for young stars (Ribas et al. 2005; Johnstone et al. 2021a; Kubyshkina et al. 2026, this collection), photoevaporation plays a significant role in the loss of the primordial and magma ocean outgassed atmosphere in the first ~ 100 Myr (e.g., Gillmann et al. 2009; Owen and Wu 2017; Lammer et al. 2018).

Photoevaporation can lead to a complete loss of the primordial atmosphere of rocky planets if the initial mass-loss timescale $t_\mathrm{loss} = M_\mathrm{atm}/\dot{M}_\mathrm{atm}$ is shorter than the phase of high XUV output from the star (Owen and Wu 2017). For close-in planets at roughly 0.1 AU, this is the case for planets up to $6\,M_\oplus$ (Owen and Wu 2013; Mordasini 2020). The duration of the phase with high XUV output, also referred to as the saturation phase of the star, decreases with increasing stellar mass (Jackson et al. 2012; Shkolnik and Barman 2014; McDonald et al. 2019; Johnstone et al. 2021a). In addition, for a given equilibrium temperature planets orbiting young M dwarfs receive a higher XUV flux compared to planets orbiting FGK stars as they are on shorter orbits (Johnstone et al. 2021a). Consequently, photoevaporation is more efficient around low-mass stars. Rocky planets around M dwarfs are therefore less likely to retain atmospheres than planets around more massive stars.

Modeling the variety of physical and chemical processes influencing the escape rates due to photoevaporation is computationally expansive, which is why the escape rates are often estimated using the energy-limited approximation (Watson Astron et al. 1981; Erkaev et al. 2007), i.e.,

$$\dot{M}_{\rm atm} = \eta \frac{\pi R_{\rm XUV}^2 R_{\rm pl}}{4\pi G M_{\rm pl} K}, \tag{3}$$

where G is the gravitational constant, $\dot{M}_{\rm atm}$ is the atmospheric mass loss rate, $F_{\rm XUV}$ is the stellar XUV surface flux at the planet, $R_{\rm XUV}$ is the effective radius where $F_{\rm XUV}$ is absorbed in the atmosphere, $R_{\rm pl}$ and $M_{\rm pl}$ are the planetary radius and mass, respectively, and K accounts for Roche-lobe effects. The heating efficiency, η, is the fraction of the absorbed XUV surface flux that goes into heating. Besides atmospheric type (see below) and local conditions, it depends on the spectral energy distribution (SED) of the XUV flux, whereby a harder SED leads to an increased value for η (Linsky 2025). This implies that active young K and G stars, rapidly rotating stars, and active M dwarfs induce higher η-values.

In addition, η depends on a planet's gravitational potential. Exoplanets with higher gravities have smaller atmospheric scale heights, implying an absorption of the XUV flux at lower atmospheric densities and a smaller value for η (Salz et al. 2016; Linsky 2025). In total, η may vary between roughly 1% and 20% for hydrogen-rich atmospheres (e.g., Shematovich et al. 2014; Salz et al. 2016). For secondary atmospheres, however, heating becomes more complex and depends on various additional factors such as the net energy expanse of the various photochemical reactions and radiative cooling of additional cooling agents such as CO_2 or CO in CO_2-dominated atmospheres (e.g., Johnstone et al. 2018; Yoshida et al. 2022; Van Looveren et al. 2025) and atomic line cooling via oxygen in N_2-O_2-dominated atmospheres (Nakayama et al. 2022).

In the energy-limited approach, the mass loss rate is determined by the ratio of the incoming irradiation and the gravitational binding energy of the planet. However, it has been shown that the energy-limited formula overestimates the escape rate for close-in hydrogen-dominated, highly-irradiated low-mass planets, whereas it underestimates the escape rate for cool planets with more compact atmospheres (Erkaev et al. 2016; Owen and Mohanty 2016). One solution to overcome this is to use pre-calculated grids based on hydrodynamical models (e.g., Kubyshkina et al. 2018).

2.2.2 Non-thermal Mass Loss

In the upper atmosphere of terrestrial exoplanets, collisions become less frequent, and the suprathermal component in the velocity distribution can contribute to atmospheric escape. Two major drivers of non-thermal atmospheric escape are the stellar XUV irradiation and stellar wind. Non-thermal escape mechanisms are categorized into collisional non-thermal escape and stellar wind-induced escape. Photochemical escape and charge exchange (energetic neutral atom production exceeding escape velocity) are major collisional non-thermal escape mechanisms. Stellar wind-induced escape includes ion pickup, atmospheric sputtering, and cold ionospheric outflows (plasma instabilities) for unmagnetized planets, as well as polar wind, auroral outflows, and plasmaspheric drainage plumes for magnetized planets (see Table 2 in Kubyshkina et al. 2026, this collection). The relative importance of these mechanisms depends on planetary conditions, such as atmospheric composition and intrinsic magnetic field.

On Earth-like or heavier planets, where gravitational escape velocity is considerable (11.2 km/s for Earth), thermal escape primarily concerns hydrogen. Heavier species like oxygen, carbon, and nitrogen need to be accelerated to reach escape velocities via non-thermal escape processes. Atmospheric escape of these heavier species, which often constitute a major part of the secondary planetary atmosphere of rocky planets, mainly occurs as ion escape. Neutral atoms or molecules in the upper atmosphere can be ionized by stellar XUV irradiation, charge exchange interactions, or electron impact. Various processes supply planetary ions to the magnetospheres (e.g., Seki et al. 2015, and references therein).

For magnetized planets like Earth, ion escape primarily occurs from the polar ionosphere, corresponding to latitudes higher than the subauroral regions (e.g., Abe et al. 1993; Seki et al. 2001; Yau et al. 2007). Planetary ions outflowing from the polar ionosphere undergo various acceleration and transport in the magnetosphere, with a significant part eventually escaping to the interplanetary space (e.g., Gronoff et al. 2020). Some ions, despite having energies above the escape energy, return to the planetary atmosphere due to magnetospheric convection and plasma processes such as pitch angle scattering by wave-particle interactions. Other escape mechanisms include plasmaspheric drainage plume and ENA production by charge exchange (e.g., Keika et al. 2006; Gronoff et al. 2020, and references therein).

For unmagnetized planets, the stellar wind can interact directly with the planetary upper atmosphere. In addition to Jeans escape (thermal escape), photochemical escape, which we will briefly address in the context of an upper atmosphere's photochemistry in Sect. 5, can be an important mechanism for neutral atmospheric escape (e.g., Amerstorfer et al. 2017; Lillis et al. 2017a). The relative importance of neutral escape compared to ion escape depends on stellar XUV irradiation and planetary mass. As planetary mass increases, the relative importance of ion escape to neutral escape generally becomes higher due to the large escape energy. Major ion escape mechanisms from unmagnetized planets include ion pickup including polar plumes (Curry et al. 2015; Sakakura et al. 2022), atmospheric sputtering (Luhmann and Kozyra 1991), and cold ionospheric outflows (Inui et al. 2019). The cold ionospheric outflow involves various plasma processes causing ion acceleration/heating. Detailed description about the non-thermal escape processes and related observables can be found in Kubyshkina et al. (2026, this collection).

2.2.3 Stripping by Giant Impacts

Giant impacts induce a strong shock wave that propagates through the impactor and the target planet, thereby inducing a global ground motion over them. The atmosphere overlying the surface gains momentum from the ground motion, and, if the propagating shock wave is sufficiently strong, it escapes from the planet on a global scale (e.g. Chen and Ahrens 1997). One-dimensional hydrodynamic simulations indicate that the loss efficiency by this mechanical process is strongly dependent on pre-impact surface conditions, specifically in the presence or absence of an ocean (Genda and Abe 2005; Schlichting et al. 2015; Lock and Stewart 2024). Owing to the different shock impedances between the rock, water and gas, the velocity of the ocean surface becomes higher than that of the rock surface without an ocean. As a result, the presence of an ocean enhances the loss efficiency of the planetary atmosphere significantly. For example, on an Earth-mass planet with a 1 bar H_2 atmosphere, in the absence of an ocean, the ground velocity would need to be greater than the escape velocity to completely remove the atmosphere. However, if there is a 3 km deep ocean, the atmosphere could be completely stripped away with a ground velocity of about 40% of the escape velocity (Lock and Stewart 2024). The effect of oceans in enhancing atmospheric loss becomes stronger as the ocean-to-atmosphere mass ratio increases. In comparison to the surface conditions, the effects of other parameters such as atmospheric composition and surface temperature are relatively minor. Quantifying the efficiency of atmospheric loss caused by giant impacts has been attempted by means of 3D SPH (smoothed particle hydrodynamics) simulations (e.g. Kegerreis et al. 2020). However, this remains challenging due to difficulties in resolving the crust, atmosphere and ocean accurately.

In the aftermath of giant impacts, the planetary surface becomes extremely hot through the propagation of the strong shock wave and the re-accretion of the ejected material. Consequently, a high-temperature (exceeding several thousand Kelvins) mixed atmosphere would form on the post-impact surface, consisting of the remaining volatile elements and the partially vaporized silicates. The extremely hot atmosphere may expand against the planet's gravity and escape hydrodynamically into space. Biersteker and Schlichting (2021) considered that thermal radiation from the lower atmosphere drives hydrodynamic escape and estimated the associated energy-limited mass loss rate. They found that planets with masses that are less than half of the Earth's mass are capable of losing their H-He dominated atmospheres, as long as the mean molar weight remains sufficiently low, even in the presence of vaporized silicate. As other heavier gas species increase, the mass loss rate decreases rapidly with increasing mean molecular weight. A more precise estimation of the mass loss rate would require hydrodynamic calculations that account for the detailed structure and energy budget of escaping atmospheres.

2.3 Observational Features of Escape

2.3.1 Present-Day Solar System

While there is evidence that the terrestrial planets have undergone significant thermal mass loss in the past (see Sect. 2.4), it only plays a minor role at the present day and is limited to the lightest element, hydrogen (Lammer et al. 2006; Jakosky et al. 2018). Instead, the dominating escape processes for the terrestrial planets in the Solar System at present-day are non-thermal processes, such as the escape of ionized species and photochemical escape. Below we will summarize some key observations of these escape mechanisms; for more details, see, e.g., Chappell (2015), Ramstad et al. (2018), Scherf and Lammer (2021), Gillmann et al. (2022), Kubyshkina et al. (2026, this collection).

Atmospheric escape at Venus is dominated by ion escape for oxygen and carbon, and by photochemical escape for hydrogen. Ions with a sufficient energy to gain escape velocity are produced either in Venus' exosphere and ionosphere via the Sun's XUV irradiation and are then accelerated by the solar wind or ionospheric electric fields (e.g., Hartle and Grebowsky 1990; Luhmann et al. 2004; Slapak et al. 2017). Escaping ions were, for instance, observed with the ion mass analyzer (IMA) of the ASPERA-4 instrument onboard Venus Express (VEX), see, e.g., Barabash et al. (2007), Fedorov et al. (2011), and Persson et al. (2018). Observations between 2006 and 2014 in the induced magnetotail of Venus yielded escape rates for O^+ and H^+ of $\sim 2.9 \times 10^{24}$ s^{-1} and $\sim 7.6 \times 10^{24}$ s^{-1}, respectively, for solar minimum and somewhat lower values for solar maximum due to an increase of the proton return flux toward the planet during solar maximum (see, Persson et al. 2018, for details). However, the ion mass analyzer onboard VEX was only able to distinguish H^+, He^+, and heavy ions (e.g., C^+ and O^+) from each other, implying that the derived O^+ escape rate prescribes the total ion escape of all heavy ions added together (Persson et al. 2018). Recently, however, measurements with the Mass Spectrum Analyzer onboard Bepi-Colombo while flying by Venus indicate the C^+ to O^+ ratio to be up to $\sim$0.3 (Hadid et al. 2024).

Whereas ion loss is the only significant source of escape into space for O, photochemical escape provides the dominant sink for hydrogen on Venus (Lammer et al. 2006; Chaffin et al. 2024, see also Sect. 5 for details). Energetic photochemical reactions for both species, however, produce hot coronae, i.e., exospheric suprathermal particles around Venus, that can be observed in Ly-α. Its hydrogen corona was already observed by Mariner 5 (Anderson 1976) and later by the Venera missions (Bertaux et al. 1978, 1982), the Pioneer Venus Orbiter (PVO) (Cravens et al. 1980) and VEX (Chaufray et al. 2012). Its structure can be approximated via a two component model consistent of a cold, thermal and a hot, non-thermal component (e.g., Chaufray et al. 2012) from which thermal and photochemical escape rates can be estimated, which are of the order of 10^{19} and 4×10^{25} s^{-1} (e.g., Lammer et al. 2006), respectively. Recently, Weichbold et al. (2025) analyzed ion cyclotron wave observations by VEX in Venus' exosphere and were able to derive photochemical escape rates for H and, for the first time, D. For hydrogen, their derived value of $\sim 4 \times 10^{25}$ s^{-1} is in agreement with Monte Carlo simulations (Lammer et al. 2006; Chaffin et al. 2024) and it highlights that photochemical escape is indeed the major source of H escape on Venus with loss rates being almost an order of magnitude higher than non-thermal H^+ escape (Persson et al. 2018). Oxygen, on the other hand, whose hot corona was for the first time observed with the UV spectrometer onboard PVO (Nagy et al. 1981), is too heavy to escape photochemically (see Sect. 5). The energy that oxygen obtains from the dissociative recombination of $O_2{}^+$ (i.e., $\leq$6.96 eV; e.g., Kim et al. 1998) is smaller than the relatively high escape energy at Venus' exobase (i.e., $\sim$8.6 eV as calculated through the gravitational potential); see also Sect. 5.

On Earth – the only terrestrial planet in the solar system that hosts both a collision-dominated atmosphere and an intrinsic magnetic field – atmospheric escape is dominated via ion outflow along the open field lines of its polar ovals. Observations of the so-called polar wind, whereby atmospheric ions are accelerated upwards from the ionosphere along the magnetic field lines due to the charge separation electric field present in the ionosphere (Chappell 2015), date back to the late 1960s and early 1970s when H^+, He^+, and O^+ were for the first time observed to flow upwards from the ionosphere into the magnetosphere (Shelley et al. 1972; Sharp et al. 1977; Chappell 2015). Various thermospheric, exospheric and magnetospheric missions collected data of the Earth's plasma environment since then (see, e.g., Dandouras et al. 2020, for an overview), and it was, for example, found through high-altitude spacecraft observations that only around 10% of the upflowing O^+ is indeed escaping via open field lines with the rest flowing back toward the Earth; a complex process that leads to a total upper limit for the O^+ escape rate of $\sim 5 \times 10^{25}$ (Seki et al. 2001). More recent observational studies found a positive correlation of the O^+ loss on the solar wind dynamic pressure (Haaland et al. 2012; Schillings et al. 2019), as well as a significant increase of the escape during geomagnetic storms (Haaland et al. 2012); extreme solar conditions therefore seem to be able to push O^+ outflow rates beyond 10^{26} (e.g., Haaland et al. 2012; Wei et al. 2012; Schillings et al. 2019). N^+ escape rates, on the other hand, are typically observed to be an order of magnitude lower than the O^+ escape rates (Lin et al. 2020).

Other escape channels at the Earth are typically negligible, except H escape, which predominantly stems from photochemical reactions in the thermosphere. As is the case for Venus and Mars, Earth's hydrogen corona can be mapped via Ly-α observations, e.g., with the Solar Wind Anisotropies instrument onboard the Solar and Heliospheric Observatory (SWAN/SOHO) from which the loss rate of H can be estimated. This was found to be in the order of 10^{26} s^{-1}, which – if it were constant through geological history – would remove around 1 meter of the terrestrial ocean into space over billion-year timescales (Baliukin et al. 2019). However, H escape toward the past has most likely been increasingly higher, specifically during the Archean and Hadean eons (e.g., Lammer et al. 2018). Another method to map Earth's extended H corona is to observe energetic neutral atoms (ENAs), e.g., with the Interstellar Boundary Explorer (IBEX) spacecraft, which are produced through charge exchange between exospheric hydrogen and shocked solar wind protons, predominantly at the subsolar magnetopause (Fuselier et al. 2010). This charge exchange process further generates X-rays planned to be observed by the Soft X-ray Imager (SXI) onboard the SMILE mission (Sembay et al. 2025).

For Mars – the smallest of the three planets with a collision-dominated atmosphere – atmospheric escape is more diverse. Whereas photochemical reactions are the dominant loss channels for nitrogen, oxygen, and likely carbon, it is thermal escape for H and sputtering for heavier species. For oxygen, photochemistry is primarily driven by the dissociative recombination of O_2^+ and CO_2^+ (Gronoff et al. 2020, see also Sect. 5). Theoretical models, however, predict that not all the oxygen atoms will gain sufficient energy to escape but will form a corona of hot oxygen surrounding the planet (Wallis 1978; Amerstorfer et al. 2017). This corona was observed by the Mars Atmosphere and Volatile Evolution mission by measuring the O I 130.4 nm triplet feature (Deighan et al. 2015; Chirakkil et al. 2024) with escape rates being derived to be in the order of 10^{25} (Deighan et al. 2015), i.e., comparable to O escape rates on Venus and Earth.

For N, the dominant production channels are the photodissociation of N_2 and the dissociative recombination of N_2^+ (e.g., Fox and Dalgarno 1980; Cui et al. 2019). Based on simultaneously modeling photochemical reactions and MAVEN observations of N_2 and N_2^+ profiles, the photochemical escape rate of nitrogen was derived to be slightly below 10^{25} s^{-1} (Cui et al. 2019). Also for H, photochemical reactions provide an important escape channel, but, based on Ly-α observations of the Martian H corona with HST, this is only as high as roughly 30% of the thermal H escape rate of $\sim 10^{26}$ s^{-1} (Bhattacharyya et al. 2023). Here, the radiative dissociation of HCO^+ provides the major photochemical loss reaction (Gregory et al. 2023).

Photochemical escape further played an important role during the Martian history. The radiative dissociation of N_2^+ is likely responsible for the strong atmospheric fractionation of $^{14}N/^{15}N$ (Fox and Hać 1997), C, and even O (e.g., Lillis et al. 2017b; Amerstorfer et al. 2017). Photochemical escape could have led to an integrated loss of CO_2 from Mars during the last 4 Gyr of about 200 mbar (Amerstorfer et al. 2017), making it, together with ion escape, the most important CO_2 loss mechanism (Lichtenegger et al. 2022). For the first 500 Myr of the Martian evolution, however, thermal escape was the dominant driver of atmospheric escape (Scherf and Lammer 2021).

Sputtering is another relevant loss process from the Martian atmosphere that was until recently only observed indirectly, e.g., via measuring the precipitation of planetary heavy pickup ions onto the atmosphere, which subsequently sputter other particles into space (e.g., Leblanc et al. 2015, 2018). Recently, however, first direct observations of sputtered argon at Mars were successfully attained with MAVEN by correlating Ar densities with the solar wind motional electric field, thereby deriving Ar sputter rates to be around 2×10^{23} s^{-1}, a value that is in agreement with the higher end of modeled sputtering rates (Lichtenegger et al. 2022). Although sputtering only contributes relatively minor loss rates compared to other species and escape channels, it is the dominant loss mechanism for species heavier than O and can provide important insights for reconstructing atmospheric losses on Mars over time since it preferentially removes lighter isotopes from the atmosphere, i.e., ^{36}Ar compared to ^{38}Ar in this specific case (Jakosky et al. 2018; Lichtenegger et al. 2022). A final important loss channel on Mars is heavy ion escape (i.e., C, N and O ions), which was measured by Mars Express (e.g., Lundin et al. 2013) and MAVEN (Brain et al. 2015), and can exceed $\sim 10^{25}$ s^{-1} during high solar activity (Ledvina et al. 2017). Observations have further shown that the plasma structure around Mars is dominated by tailward outflows of ions (Nilsson et al. 2012; Inui et al. 2019) and a permanent northern polar plume made of energetic ions that contributes more than 20% to the total heavy ion escape (Dong et al. 2015).

Besides the aforementioned planets, one may also mention Titan with its dense N_2-dominated atmosphere. The Ion and Neutral Mass Spectrometer onboard Cassini, for instance, observed a suprathermal corona around the satellite, through which suprathermal escape rates for N and CH_4 were estimated to be, again, in the order of 10^{25} s^{-1} (De La Haye et al. 2007). Sputtering, specifically induced by energetic particles in Saturn's magnetosphere, is another significant escape channel with loss rates in the order of 10^{25} s^{-1}, whereas ion escape and particularly thermal escape are comparatively insignificant, mostly due to the low XUV surface flux received from the distant Sun (see, e.g., Erkaev et al. 2021, for an overview on atmospheric escape at Titan).

As one can see from this summary, the loss rates from Venus, Earth, Mars, and even Titan are roughly on the same order of magnitude. This seems to be relatively surprising as it was initially thought that a planetary magnetic field would protect the atmosphere from escape by interaction with the stellar wind. Its protective role, therefore, remains highly debated (Ramstad et al. 2018; Ramstad and Barabash 2021; Way et al. 2023). While the diversion of energy from the stellar wind energy by a magnetic field protects the atmosphere from sputtering and ion pickup, the magnetosphere increases the interaction region between stellar wind and the planet, thus leading to a higher amount of transferred energy (Gunell et al. 2018). In addition, one can see that photochemical escape plays a crucial role for various species on all of these planets, a process whose efficiency is not necessarily diminished by an intrinsic magnetic field. Whether a magnetic field can provide shielding for present-day conditions and, even more so, for more intense solar/stellar plasma and radiation environments remains unknown.

2.3.2 Exoplanets

In the case of exoplanets, the outflow of gas from the atmosphere can in principle be seen through wavelength-dependent signatures in the transit spectrum of a planet (e.g., Dos Santos 2023). The first such observation was the detection of escaping H from the hot Jupiter HD 209458 b (Vidal-Madjar et al. 2003; Ehrenreich et al. 2008). Since then, outflow of H has been detected in a number of planets including sub-Neptune-sized planets such as HD 63433 (Zhang et al. 2022; Dos Santos 2023).

The escape of heavier elements such as carbon, nitrogen, and oxygen can be probed in the UV wavelength regime. However, these metal lines are typically very weak and have only been observed in hot Jupiters so far (e.g., Linsky et al. 2010; Schlawin et al. 2010; Dos Santos 2023). The UV spectroscopy capability of the upcoming HWO, however, will enable the study of atmospheric escape across a wide range of planets including cool sub-Neptunes (Dos Santos et al. 2025).

A promising observational probe of atmospheric escape is the helium triplet located at $1.083\,\mu$m. This line is observable both in transmission spectroscopy and at high spectral resolution with ground-based facilities (e.g., Allart et al. 2018; Vissapragada et al. 2020; Kirk et al. 2022; Zhang et al. 2023).

We can further study atmospheric escape by examining its impact on the exoplanet population as a whole. One of the most significant results of the Kepler mission is the detection of the so-called radius valley or radius gap, which refers to a lack of planets with radii between 1.5 to 2.0 $R_\oplus$ (e.g., Fulton et al. 2017a; Van Eylen et al. 2018; Fulton and Petigura 2018; Berger et al. 2020; Ho and Van Eylen 2023).

This bimodal distribution in planet size was actually predicted by theoretical models of photoevaporation previous to its detection (Owen and Wu 2013). According to photoevaporation models, planets below and above the gap are part of the same population of planets with Earth-like interiors that are initially surrounded by a large primordial atmosphere. After formation, these planets undergo significant thermal mass loss. Depending on their total mass, planets will either lose their entire atmosphere turning into super-Earths located below the radius gap or retain a fraction of the initial atmosphere, becoming sub-Neptunes located above the gap. Numerous studies have demonstrated that atmospheric escape processes described in Sect. 2.2.1 can explain the observed features of the radius gap, such as its dependence on the orbital period and stellar mass (e.g., Owen and Wu 2017; Jin and Mordasini 2018; Gupta and Schlichting 2019; Rogers et al. 2021).

However, the radius gap can also be explained by two distinct planet compositions. In this picture, planets below the radius gap have a composition similar to Earth, while planets above the radius gap can contain up to 50 wt.% water (e.g., Venturini et al. 2020; Luque and Pallé 2022; Burn et al. 2024). Although most models assume that super-Earths have undergone atmospheric escape, it is also possible that these planets formed without ever accreting a primordial atmosphere in the first place (Lee and Connors 2021; Lee et al. 2022; Nielsen et al. 2025).

One strategy for testing the two competing scenarios, atmospheric escape and water-rich formation, observationally involves multi-planet systems that straddle the radius gap. If the mass and radius are known for both planets, one can then test if the system architecture is consistent with predictions from atmospheric escape models or not (e.g., Owen and Campos Estrada 2020; Egger et al. 2024; Lockley et al. 2025) This will require a large sample of small-sized planets with precise mass and radius measurements (Lacedelli et al. 2024). The upcoming PLATO mission is expected to discover a vast number of multi-planet systems (Rauer et al. 2025). Thanks to the planned radial velocity follow-up observations to obtain mass measurements, the PLATO sample will thus allow a more detailed characterization of the radius valley. Planets situated directly within the radius valley such as TOI-544 b (Osborne et al. 2024) are of particular interest. Confirmation that the radius gap is caused by atmospheric escape implies that rocky planets typically accrete a primordial atmosphere. The potential influence of such an atmosphere on the long-term evolution of rocky planets, e.g., through interactions with the magma ocean, thus needs to be studied.

2.4 Effect of Atmospheric Loss on the Evolution of Rocky Planets

In the most extreme case, atmospheric escape can lead to the total erosion of the atmosphere, leaving behind a bare rock. This might be the case for close-in rocky planets around M-dwarfs (e.g. Van Looveren et al. 2025). Even in a less extreme scenario, atmospheric escape may drastically transform the composition of an accreted or outgassed atmosphere. Luger and Barnes (2015) suggested that it is possible to transform a sub-Neptune type planet into a rocky planet residing in the habitable zone. Tian et al. (2014a), Luger and Barnes (2015), Meadows (2017) suggested that planets orbiting early phase M-dwarfs or planets in a runaway greenhouse state could become strongly oxygen-rich over time, due to photodissociation and subsequent loss of hydrogen. Carone et al. (2025) extended these studies by including CO_2 in the magma ocean atmosphere, and found that the build-up of free O_2 in the atmosphere is, to some extent, possible by atmospheric erosion. Cherubim et al. (2025) show that the dissolution of water in the molten mantle shields the oxygen from escape (by limiting the amount of water in the atmosphere). Later water mantle outgassing can lead to oxidized secondary atmospheres (e.g. Luger and Barnes 2015; Meadows 2017). This suggested oxidation of the atmosphere by erosion of reducing gases (especially of hydrogen) also fits the observations from the solar system (see also further down), where Mars shows a thin but CO_2-dominated atmosphere, whereas theoretical predictions would suggest a more reduced outgassed atmosphere (Gaillard and Scaillet 2009).

For a high enough escape rate, hydrogen can drag along heavier elements (Zahnle and Kasting 1986; Hunten et al. 1987; Odert et al. 2018). This can lead to a loss of moderately volatile rock-forming elements on Mars-sized planetary embryos, altering their Fe/Mg and Si/Fe ratios compared to their host star (Benedikt et al. 2020). More importantly, atmospheric escape can modify the abundance of the radioactive isotope 40K, which is an important constraint on the tectonic evolution of a rocky planet (Benedikt et al. 2020; Erkaev et al. 2023).

For small, rocky planets on ultra-short orbits, the temperature on the dayside surface is hot enough to vaporize the planet (e.g., Kite et al. 2016; Zilinskas et al. 2022; Curry et al. 2024). The evaporated rocky material then escapes into space through thermally driven winds (Perez-Becker and Chiang 2013). The mass loss rates are high enough to result in disintegration lifetimes down to a few hundred Myr (Perez-Becker and Chiang 2013). To this date, four such planets have been found observed through asymmetric transit profiles and time-variable transit depths caused by comet-like tails formed by large dust grains: Kepler-1520 b (Rappaport et al. 2012), KOI-2700 b (Rappaport et al. 2014), K2-22 b (Sanchis-Ojeda et al. 2015), and BD+05 4868 Ab (Hon et al. 2025). These planets offer a unique opportunity to directly probe the interior of rocky planets (Curry et al. 2025).

The strength of a past atmospheric loss can also be estimated from the fractionation of different isotopic pairs in the remaining atmosphere, most prominently for the deuterium to hydrogen ratio. In the case of Venus and Mars, it implies high losses of hydrogen (be it from H_2 or CH_4 in the atmosphere, H_2O steam, or liquid, evaporated water oceans). Other isotopic fractionation patterns can be observed as well, for example for xenon, carbon, nitrogen and argon (Zahnle et al. 2019; Gillmann et al. 2011; Lammer et al. 2020). The $^{36}Ar/^{38}Ar$ and $^{20}Ne/^{22}Ne$ isotope ratios of the Earth and Venus are comparable to solar ratios (Porcelli and Pepin 2000; Porcelli et al. 2001; Yokochi and Marty 2004; Gillmann et al. 2009; Mukhopadhyay 2012; Odert et al. 2018; Williams and Mukhopadhyay 2019). These isotope ratios are seen as evidence that proto-Venus and proto-Earth have captured a H_2-dominated atmosphere (e.g., Mizuno et al. 1980). In order to reproduce the measured noble gas ratios, Lammer et al. (2021) find that proto-Earth must have grown to a mass of $0.5-0.6\,M_\oplus$ during the disk's lifetime, while Venus accreted most of its mass before the disk disperses. However, these isotope ratios can also be reproduced through implantation of solar wind onto accreted material (Podosek 2003; Moreira and Charnoz 2016; Péron et al. 2016). Nevertheless, the evolution of atmospheric composition is an important constraint on the formation timescale of terrestrial planets in the Solar System.

3 Interaction and Feedback Between Atmosphere, Surface, and Interior

Even though the atmosphere and mantle of a planet are not in direct contact anymore after the solidification of the primordial magma ocean, there is still interaction between the atmosphere and mantle. This is primarily facilitated by the transfer of volatile species between the different planetary reservoirs (mantle, crust, ocean, atmosphere). For example, volcanic outgassing from the mantle brings various gases into the atmosphere, while simultaneously depleting the mantle. Plate tectonics and crustal delamination can bring surface-bound volatiles back into the mantle (see 2.1.2).

These processes form a complex web of interactions which couple the planet's interior to its atmosphere (Fig. 5). Therefore, the evolution of the atmosphere can not be disentangled from the evolution of the interior. Furthermore, feedback processes arising from these

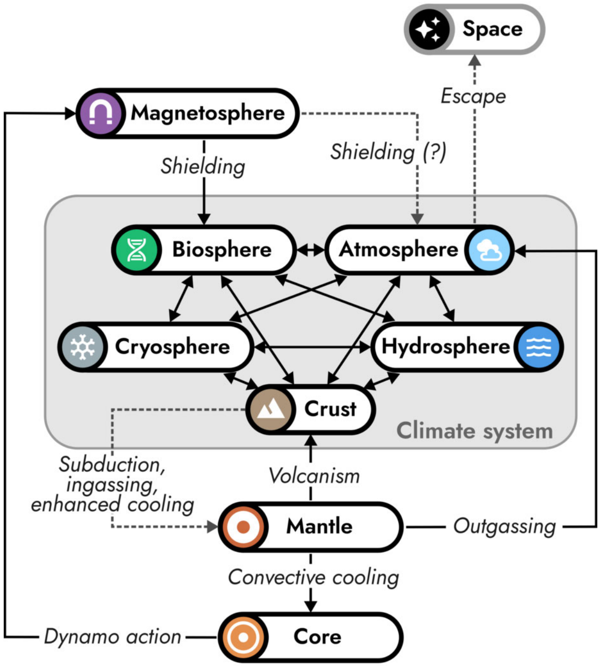

Fig. 5 Illustration of the interaction pathways between the interior, surface and atmosphere of a habitable planet. Figure adapted from Gillmann et al. (2022). Icons are modified from Pictogrammers, licensed under the Apache License 2.0 (https://www.apache.org/licenses/LICENSE-2.0)

interactions can drastically shape the trajectories a planet's atmosphere may take (see e.g., Noack et al. 2012; Krissansen-Totton et al. 2021a; Baumeister et al. 2023; Gillmann et al. 2022).

The fact that the interior, surface, and atmosphere are linked offers the potential to determine characteristics of exoplanet interiors by observing their atmospheric composition. A prerequisite for this is a comprehensive understanding of these processes, and how they and their interactions manifest themselves in the atmospheric composition.

Furthermore, the presence of climate feedback loops is critical in the context of planetary habitability. To sustain conditions suitable for the presence of liquid water in the long term, the climate must be stable against perturbations in temperature and composition of the atmosphere, for example from volcanic eruptions or the long-term increase in stellar luminosity. This stability is enabled by negative feedback loops, which counteract deviations from the equilibrium state. The most prominent example on Earth is the carbonate-silicate cycle, which regulates the CO_2 content in the atmosphere to a level which permits temperatures suitable for liquid water, thus preventing Earth from being permanently locked into a snowball or hothouse state. On the other hand, positive feedback cycles can exacerbate perturbations, thus acting to destabilize the climate. If these processes are strong enough, they may push a planet irreversibly toward uninhabitable conditions, as may have happened in the case of Venus.

The interactions and feedback loops of atmosphere, surface, and interior further enable us to distinguish between different types of surfaces based on the atmospheric spectrum of a planet (e.g., Byrne et al. 2024; Herbort and Sereinig 2025). Byrne et al. (2026, this collection) reviews our knowledge of Earth's interior, surface, and atmospheric composition through time. They then examine, to the best of our present abilities, the same for Mercury, Venus, Mars, Earth's moon and Jupiter's moon Io, and how they compare to each other. Finally, they consider exoplanetary worlds that may or may not have direct representation

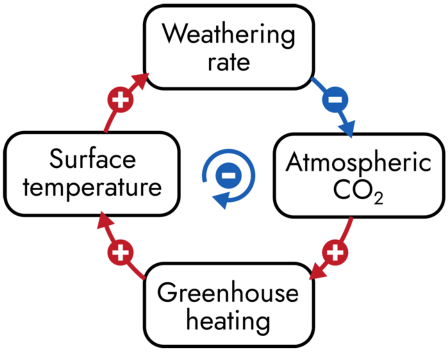

Fig. 6 Illustration of the negative feedback loop between CO_2 and silicate weathering that forms the backbone of the carbonate-silicate cycle. Red arrows with a plus mark positive feedbacks. Blue arrows with a minus mark negative feedbacks. After Catling and Kasting (2017)

within our solar system. In the future, it might even be possible to extract water/land ratios of temperate rocky exoplanets by observing their reflected light (see e.g, the discussion in Guimond et al. 2026, this collection).

3.1 The Carbonate-Silicate Cycle

The carbonate-silicate cycle (Fig. 6) is one of the most important long-term feedback cycles on Earth, acting as a "thermostat" (Catling and Kasting 2017) for Earth's climate by regulating the amount of CO_2 in the atmosphere (Walker et al. 1981). Atmospheric CO_2 forms carbonic acid in rain water, which can dissolve silicate minerals (continental weathering). The byproducts are washed into the ocean, where they can form carbonates through biotic and abiotic processes, which then precipitate as sediments on the sea floor. Plate tectonics transports these carbonate layers deep into the mantle. CO_2 is replenished in the atmosphere through volcanic outgassing or metamorphic decarbonation of carbonate rocks at high temperatures and pressures, closing the cycle. Importantly, the weathering processes involve liquid water. As the rate of surface weathering additionally depends on surface temperature and the atmospheric concentration of CO_2, this forms a negative feedback cycle, stabilizing the surface temperature and climate against perturbations on geological time scales and on a level that permits liquid water. Should the surface temperature fall below the freezing point of water, the water cycle slows down and with it the weathering rates, thus slowing down CO_2 removal from the atmosphere. CO_2 will continue to accumulate in the atmosphere due to volcanic outgassing, which eventually brings the surface temperature above freezing again. Likewise, a positive perturbation in atmospheric CO_2 increases the surface temperature, increasing weathering rates and therefore the draw-down of CO_2. In short, the carbonate-silicate cycle maintains a CO_2 level which enables liquid water.

Stagnant-lid planets lack the subducting plates to transport carbonates into the interior. However, as long as fresh rock is being created by volcanic activity, CO_2 weathering cycles can still work even in the absence of plate tectonics. Foley and Smye Astron (2018) propose a stagnant-lid carbon cycle where CO_2 is removed by the weathering of newly erupted basaltic rocks. Volcanic activity on stagnant-lid planets tends to be focused locally by hotspots from underlying mantle plumes. Thus, subsequent eruptions bury weathered crust which, through isostatic adjustment, sinks towards the convective mantle, where it may eventually be recycled by lithospheric delamination. With a sufficient level of ongoing volcanism, this process can stabilize the climate on stagnant-lid planets for several billion years (Foley and Smye Astron 2018; Foley 2019; Höning et al. 2019, 2021; Baumeister et al. 2023).

Fig. 7 Illustration of the negative feedback loop between surface temperature and outgoing IR flux (left loop) and the positive feedback loop caused by water vapor (right loop). After Catling and Kasting (2017)

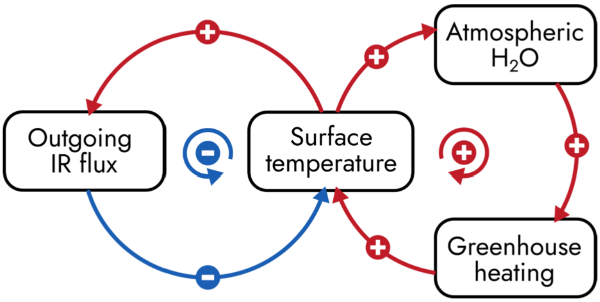

An important note to make here is that the conventional definition of the habitable zone (Kasting et al. 1993) implicitly assumes that some form of carbonate-silicate cycle is active to regulate the atmospheric CO_2 concentration. This property of the carbonate-silicate cycle allows a potential population-wide test of the habitable zone. Planets with an active carbonate-silicate cycle near the inner edge of the habitable zone should have low levels of CO_2 in their atmospheres, whereas planets toward the outer edge should have CO_2-rich atmospheres (Catling et al. 2018; Lehmer et al. 2020b). This could be tested statistically by observing several tens of Earth-like exoplanets (Lehmer et al. 2020b).

3.2 Water Vapor and the Runaway Greenhouse

Water plays a central role in many of the climate feedback cycles on Earth, in particular because it is a strong greenhouse gas, but also easily condensable under Earth's temperature and pressure conditions. As a result, water vapor enacts a positive feedback on the climate system (Fig. 7). The concentration of water vapor is a function of surface temperature according to the saturation pressure of water, where higher temperatures increase evaporation as more water vapor can be stored in the atmosphere. Due to the greenhouse effect of water vapor, this in turn raises the surface temperature further. As a result, water acts as an amplifier for climate perturbations. On Earth, this feedback loop is not strong enough to destabilize the climate system, as on short timescales, the surface temperature is moderated by the planet's outgoing infrared flux 7). As the surface temperature rises, infrared emission increases likewise, thus cooling the planet.

However, this stabilizing process only works to a certain point. If sufficient water vapor is in the atmosphere, the lower atmosphere becomes optically thick, putting a limit on the outgoing IR radiation flux. If the amount of absorbed stellar irradiation exceeds this critical flux, termed the Komabayashi-Ingersoll limit (Komabayasi 1967; Ingersoll 1969), the surface of the planet heats up uncontrollably in a runaway greenhouse effect, until the entire ocean is evaporated and the surface temperature approaches that of Venus (Komabayasi 1967; Ingersoll 1969; Kasting 1988; Nakajima et al. 1992). The critical outgoing IR flux puts a limit on the instellation a planet can receive and still retain liquid water on its surface, and is thus used to define the inner edge of the habitable zone. Depending on the study, the runaway greenhouse limit is reached at an effective stellar flux S_{eff} (in relation to today's solar flux at Earth's orbit) of 1.4 (Kasting 1988) to 1.05 (Kopparapu et al. 2013) for a planet with an Earth-like mass (for estimations for other surface gravities, see e.g., Pierrehumbert 2010b).

As soon as the water vapor reaches the stratosphere, photodissociation and subsequent escape of the hydrogen will rapidly desiccate the planet on timescales of tens to hundreds of millions of years (e.g., Kasting 1988) even before a runaway greenhouse is reached. This

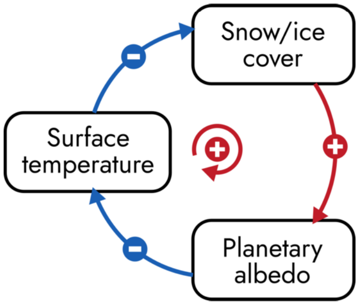

Fig. 8 Illustration of the positive ice/albedo feedback loop. After Catling and Kasting (2017)

'moist greenhouse' state (Kasting 1988) yields a more conservative estimate on the inner boundary of the habitable zone. Depending on the specifics and complexity of the climate models used, the moist greenhouse limit is somewhere between 1.05 and 1.2 S_{eff} (Kasting et al. 1993; Kopparapu et al. 2013; Leconte et al. 2013; Gómez-Leal et al. 2019).

The runaway greenhouse transition may be detectable in the exoplanet population (Schlecker et al. 2024). Planets undergoing runaway greenhouse conditions are expected, on average, to exhibit larger radii, which could allow one to map out the inner edge given a sample size of > 100, for example from the PLATO mission (Rauer et al. 2025).

Strictly speaking, this conventional definition of the habitable zone assumes that the planet is Earth-like, complete with Earth's important geological cycles and abundant surface water. In reality, many factors will influence this limit significantly. For example, Vladilo et al. (2013) find that higher atmospheric pressures broadens the habitable zone in both directions. Likewise, desert planets with limited surface water have significantly extended habitable zones (Abe et al. 2011). Toward the inner edge of the HZ, the dry stratospheres make these planets stable against a runaway greenhouse, while towards the outer edge, the lack of surface water and clouds available for freezing reduces the ice/albedo feedback (see next section).

3.3 The Ice/Albedo Feedback and Snowball Earths

Positive feedback loops can destabilize a planet's climate in both directions. While the water vapor feedback can drive a planet to extreme heating, and even a runaway greenhouse state, the ice-albedo feedback (Fig. 8) can drive a planet into extreme cooling and global glaciation (Budyko 1969). A decrease in temperature enhances snow and ice cover, which increases the planetary albedo, which lowers the absorbed stellar irradiation, thus cooling the surface further and promoting further ice growth. In extreme cases, this may trigger a 'Snowball Earth' state, where the surface becomes nearly entirely frozen with little exposed liquid surface water. On Earth, evidence suggests that global glaciation occurred at the end of the Proterozoic around 750 Myr ago (Hoffman et al. 1998; Hoffman and Schrag 2002; Maruyama and Santosh 2008).

To trigger a Snowball Earth, some process needs to cool the climate sufficiently so that the ice caps extend past $\approx 30^\circ$ latitude, at which point the feedback is strong enough to destabilize the climate (assuming a planet similar to Earth). At this point, the ice caps could rapidly grow and envelop the planet, although GCM simulations suggest that liquid water can remain in stable equatorial water belts (see e.g., Hyde et al. 2000; Abbot et al. 2011; Hoffman et al. 2017; Feulner et al. 2023).

In tidally locked aqua planets around M-dwarfs with low insolations it was initially discovered by Pierrehumbert (2010a) that an "eyeball" world would exist where there would only be open ocean at the substellar point, but that the planet would otherwise be frozen over. However, their model had the shortcoming that it did not include oceanic heat transport. It was later demonstrated that in fact the pattern of open ocean at the substellar point would more resemble a "lobster" shape than the more symmetric/circular "eyeball" (e.g. Hu and Yang 2014; Yang et al. 2014b; Del Genio et al. 2019b). Although the ice-albedo feedback (Fig. 8) is less pronounced around M-dwarfs given their blackbody radiation peaks more toward the IR where ice albedo is lower than in the visible, it still exists as shown in some studies (e.g. Del Genio et al. 2019b,a). Earlier work using 3D GCMs for tidally locked planets around M-dwarfs (e.g. Heath et al. 1999; Joshi 2003) showed that it might be possible to trap most of the planet's water inventory as ice sheets on the night side which led to the idea that these worlds would not be in the habitable zone, but later work using a full complexity model demonstrated otherwise (Yang et al. 2014b). The location of liquid water regions is further influenced by the existence and distribution of landmass (Macdonald et al. 2022).

3.4 Clouds and Climate

Clouds have an extremely important role in the climate of habitable worlds like Earth, but also in other terrestrial worlds in the Solar System such as Venus, Mars and Titan. On Earth, $\sim$67% of the planet is covered by clouds at any one time with $\sim$55% coverage over land and $\sim$72% over the ocean (King et al. 2013). They play multiple first-order roles in the climate such as providing precipitation, but also in the radiative budget. For example, low-level clouds tend to scatter sunlight (short wavelength photons) to space and have little greenhouse effect, whereas high-level clouds tend to trap more long wavelength photons scattered from the surface (See Fig. 9) and hence tend to have a greenhouse effect. Clouds have been invoked to solve the Earth's Faint Young Sun Paradox (Kasting 2010; Goldblatt and Zahnle 2011b; Feulner 2012; Güdel 2015) but different works give conflicting answers (Rondanelli and Lindzen 2010; Goldblatt et al. 2021; Goldblatt and Zahnle 2011a). High altitude cirrus type clouds (efficient at trapping longwave radiation) have been proposed as a possible solution for keeping ancient Mars' climate warm enough for surface liquid water (e.g. Urata and Toon 2013; Ramirez and Kasting 2017). However, they did not provide sufficient warming to fully resolve the issue. Venus' thick sulfuric acid clouds not only hide the surface of Venus from visible wavelength observations, but provide an extremely high albedo which has provided a featureless surface for Earth-based observers through the centuries. Until the dawn of the space age it was assumed that the clouds were in fact H_2O clouds as on Earth, and that beneath the clouds resided a hidden world filled with exotic life (e.g. O'Rourke et al. 2023). However, Hansen and Hovenier (1974) showed that in fact it was more likely they were 99% H_2SO_4 clouds, as turned out to be true. Clouds on Venus may have also played a highly important role in its early climate history. Work by Yang et al. (2014a), Way et al. (2016, 2018), Way and Del Genio (2020) showed that for slowly rotating worlds (like Venus) in a temperate state (unlike today's Venus where surface temperatures are $\sim$ 450 °C) a large substellar cloud deck could form. This substellar cloud deck would provide a wide area, high albedo surface reflecting back to space much of the planet's incident stellar radiation. The end result is a world that could have hosted surface liquid water for gigayears, even while its insolation could have ranged from 1.4 to 1.9 times that of modern Earth. This assumes that Venus had a temperate early period, which remains a matter of debate (e.g. Lebrun et al. 2013; Hamano et al. 2013; Turbet et al. 2021). Venus' thick atmosphere may also have influenced its retrograde rotation rate, but this is still up for discussion (Leconte et al. 2015; Ferraz-Mello 2026).

Fig. 9 Cloud effects on Earth's radiation budget

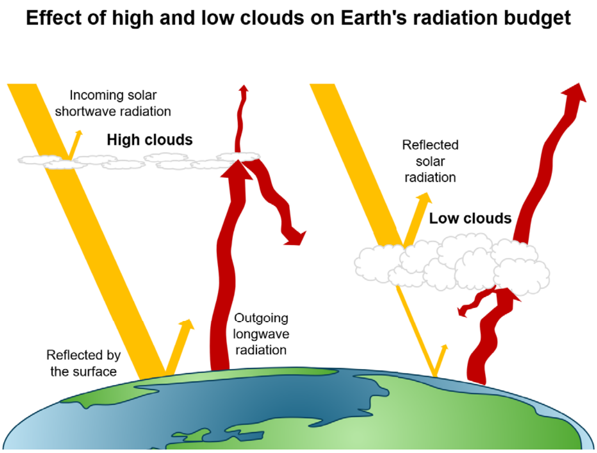

The effect of clouds and aerosols on exoplanetary atmospheres and their observables may currently be underestimated, although their importance has been recognised since their first detections (see Sect. 1.2) and initial modeling attempts (e.g., Marley et al. 2013).

Finally, many 1D climate models do not include clouds. This has important implications not only for the radiative budget, but also in terms of exoplanet atmosphere observations. Using a full-complexity 3D GCM Fauchez et al. (2019) has demonstrated that to fully characterize planetary spectra from climate models clouds must be included.

3.5 Volatile Cycles Underrepresented in the Literature

3.5.1 Nitrogen Cycle

N_2 is often assumed as an unreactive background gas in atmospheres of rocky planets, with its partial pressure, pN_2, remaining constant over geological timescales. This notion, however, does not necessarily hold because of various abiotic and, in the case of the Earth, biotic sources and sinks (e.g., Stüeken et al. 2016; Sproß et al. 2021). This is also highlighted by potential swings in the Earth's pN_2 and total pressure over time. Whereas pN_2 around 3.0 to 3.5 Gyr ago was likely below 1.1 bar, and potentially as low as 0.5 bar (Marty et al. 2013; Avice et al. 2018), the total pressure of Earth's atmosphere around 2.7 Gyr ago could have been below ∼300 mbar (Som et al. 2016; Rimmer et al. 2019), out of which a significant fraction was CO_2 (Kanzaki and Murakami 2015). During the Hadean and early Archean eons, the N_2 partial pressure could have been either around 50% higher than at present, based on an increased recycling efficiency of subducted N_2 over time (Barry and Hilton 2016; Mallik et al. 2018), or lower, presuming an increase in the N_2 degassing rate during the Archean eon (e.g., Mikhail and Sverjensky 2014; Aulbach and Stagno 2016).

High-energy processes such as lightning (Navarro-González et al. 1998, 2001), meteorite impacts (e.g., Heays et al. 2022), and cosmic rays (Tabataba-Vakili et al. 2016) can provide sufficient energy to break the triple bond of N_2 and to fix it into NH_x and/or NO_x. The first two of these processes were more effective on early Earth than at present (Navarro-González et al. 1998; Sproß et al. 2021), whereas N_2 fixation via cosmic rays and stellar energetic particles (SEP) can be a significant source of N_2 fixation on planets around M dwarfs (Grenfell et al. 2020; Scherf et al. 2024). However, SEPs have also been proposed as a means to break up N_2 while creating N_2O in early Earth's atmnosphere, possibly helping to solve the Faint

Young Sun Hypothesis (Airapetian et al. 2016; Kobayashi et al. 2026). On Earth, however, biological activity was likely the main cause of fluctuations in the N_2 partial pressure over time (Stüeken et al. 2016). Anaerobic biological nitrogen fixation (BNF), which fixes N_2 into bioavailable forms, originated some time before 3.2 Gyr ago (Stüeken et al. 2015, 2020) and could have significantly depleted Earth's atmospheric N_2 in-line with the low total surface pressure suggested for 2.7 Gyr ago. The first evidence for aerobic biological denitrification was found 2.3 Gyr ago during the Great Oxygenation Event (GOE), marking the onset of Earth's aerobic nitrogen cycle (Zerkle et al. 2017). Since denitrification releases N_2 back into the atmosphere, it counteracts BNF and has contributed to an increase of pN_2 during and after the GOE (Stüeken et al. 2016; Sproß et al. 2021).

For an abiotic world, the partial pressure of N_2 is expected to increase over geological timescales, at least to a certain extent, as a function of volcanic degassing, nitrogen recycling between the interior and the atmosphere, and abiotic fixation processes (Stüeken et al. 2016; Laneuville et al. 2018). The amount of N_2 in the atmosphere can hence allow constraints on surface and interior processes of a planet. As long as strong atmospheric losses can be ruled out, little N_2 in the atmosphere likely implies large abiotic fixation processes, whereas large amounts of atmospheric N_2 hint towards a lack of plate tectonics and/or a hydrological cycle, which both aid in recycling N_2 back into the mantle (Laneuville et al. 2018). However, to significantly deplete an N_2 atmosphere via abiotic fixation processes on a planet with an anoxic atmosphere in contact with liquid water, it must be >100 times larger than Earth's present-day abiotic fixation rate (Hu and Delgado Diaz 2019).

For Mars, isotopic signatures imply that most of its N_2 was lost into space early in its history (Kurokawa et al. 2018; Hu and Thomas 2022), leaving little traces on how the Martian geological evolution may have shaped its nitrogen cycle. For Venus, it is interesting to note that its atmosphere hosts about 3 bar of N_2. This is roughly the same amount of nitrogen presently assumed to be in Earth's bulk silicate mantle, crust, and atmosphere (Marty 2012; Li 2024), which suggests a well-degassed Venusian interior. However, ^{40}Ar abundances imply that Venus is less degassed than Earth (Kaula 1999; O'Rourke and Korenaga 2015). This is a mystery to be solved by future missions to Venus, but it may point toward a comparatively early degassing of (most of) its atmosphere and a subsequent lack of plate tectonics. During the magma ocean phase, or at a later point in its history, a runaway greenhouse phase on Venus led to the escape of hydrogen after photolysis of H_2O and a likely increase in the mantle's oxidation state via the left-behind oxygen (e.g., Gillmann et al. 2022). Since the degassing capacity of N_2 increases towards larger surface pressures (Gaillard and Scaillet 2014) and higher oxygen fugacities (Gaillard et al. 2022b), this indicates an efficient degassing of N_2 into Venus' atmosphere (Wordsworth 2016; Gaillard et al. 2022b), even during its present-day conditions (Gillmann et al. 2022). Little N_2 fixation and inefficient recycling due to the lack of plate tectonics and/or a hydrological cycle during the rest of Venus' history kept most of the N_2 in its atmosphere, compatible with the general abiotic nitrogen cycle scenarios outlined by Laneuville et al. (2018).

Finally, our solar system hosts three additional bodies with N_2-dominated atmospheres, i.e., Titan, Pluto, and Triton. All of these are icy bodies with large nitrogen reservoirs that were either accreted from cometary ammonia ices, complex refractory organics and/or directly from N_2 ices in the protosolar nebula (e.g., Scherf et al. 2020). Titan hosts a thick N_2-dominated atmosphere, which likely originated through the decomposition and degassing of ammonia ices and complex organics from its interior (Glein 2015; Erkaev et al. 2021). Pluto and Triton, on the other hand, host tenuous N_2-dominated atmospheres in evaporation pressure equilibrium with their surface, whose characteristics and evolution are poorly understood (e.g., Scherf et al. 2025). Their location in the outer solar system, their overall composition, and large accreted nitrogen reservoirs lead to completely different mechanisms dominating their nitrogen cycling compared to Venus, Earth, and Mars. However, planetary migration in exoplanetary systems could move such water- and nitrogen-rich bodies closer to their host stars, where they may end up as exotic ocean worlds with highly reducing CO_2 or N_2-dominated atmospheres, at least as long as their planetary mass is sufficiently high to hinder the hydrodynamic escape of nitrogen (Sproß et al. 2021). The gradual warming of a host star at the end of its main-sequence lifetime could have a similar effect; Titan, for instance, could enter a brief phase of liquid water-surface habitability in roughly 6 Gyr from now during the Sun's red giant phase (Lorenz et al. 1997; Sparrman et al. 2024). Such a scenario might in principle be distinguishable from a rocky exoplanet with a deep global ocean, since N_2 degassing, and hence the build-up of a thick N_2-dominated atmosphere, might be inhibited on water worlds (Krissansen-Totton et al. 2021b).

3.5.2 Sulfur Cycle

On modern Earth, sulfur cycles between the hydrosphere, atmosphere, biosphere, pedosphere, and upper lithosphere through geological, biological, and anthropogenic processes. At the same time a large, poorly constrained amount remains sequestered in the core and lower mantle, excluded from the active global cycle (Schoonen 2016). The largest reservoir is the upper lithosphere and marine sediments, which contains an estimated 10^{12} g of sulfur stored as gypsum, anhydrite, metal sulfides, or elemental sulfur (Brimblecombe 2003). From the lithosphere, sulfur can enter the atmosphere through volcanic degassing, but the atmosphere itself represents the smallest reservoir, holding sulfur primarily as gases such as H_2S, SO_2, DMS, and OCS, or as aerosols like H_2SO_4 and $(NH_4)_2SO_4$; additional inputs include dust particles, biogenic emissions, and biomass burning (Schoonen 2016). These atmospheric sulfur species are rapidly removed by precipitation and deposition, transferring sulfur into the hydrosphere and pedosphere. The hydrosphere, particularly the oceans, constitutes the second-largest reservoir and the site of the most active cycling, with sulfur present mainly as sulfate (Brimblecombe 2003). Inputs to this pool include weathering of sulfide- and sulfate-bearing rocks and atmospheric deposition, while losses occur through evaporation and microbial processes that reduce sulfate to sulfide or convert it into organosulfur compounds. In the biosphere and pedosphere, sulfur is found in both organic forms, such as amino acids, and inorganic forms, including sulfates, sulfides, and elemental sulfur (Brimblecombe 2003). Today, human activities strongly influence the sulfur cycle by releasing large amounts of SO_2 into the atmosphere and hydrosphere through the burning of sulfur-rich fossil fuels, with estimates suggesting that more than half of the sulfur transported to the oceans by rivers and about 75% of atmospheric sulfur emissions are anthropogenic in origin (Berner and Berner 2012).

Venus' atmosphere today contains about 200 ppm sulfur, primarily in the form of SO_2 and its oxidation product H_2SO_4 (Basilevsky and Head 2003). During planetary accretion and any early magma ocean stage, volatiles dissolved in the melt—including S, C, and H—would have been outgassed into the nascent atmosphere, and models suggest that this large-scale degassing delivered substantial sulfur, both as SO_2 and reduced sulfur gases, very early in Venus's history (Fegley 2003). After the magma ocean cooled, continuing volcanic activity provided the dominant source of sulfur to the atmosphere (Fegley 2003). Geological evidence indicates that Venus underwent major resurfacing episodes, as reflected in its relatively young surface age and widespread lava plains. If resurfacing occurred in pulses, each episode would have injected large SO_2 loads into the atmosphere, with significant consequences for cloud formation and atmospheric chemistry (Taylor and Grinspoon 2009). In the present atmosphere, intense ultraviolet radiation drives photolysis of CO_2 into CO and

O, and the resulting oxygen oxidizes SO_2 to SO_3, which ultimately hydrates to form H_2SO_4. Sulfuric acid then condenses into droplets and aerosols, forming the planet's extensive cloud decks (Marcq 2018). SO_2 also dissolves into cloud droplets, where interactions with salts or hydroxides can sequester sulfur temporarily from the gas phase (Rimmer et al. 2023). Unlike Earth, however, Venus lacks a rainout mechanism to remove H_2SO_4 from the atmosphere. Instead, laboratory experiments suggest that SO_2 can react directly with surface basalts to form secondary sulfates such as $CaSO_4$, $MgSO_4$, and Na_2SO_4, providing a significant near-surface sulfur sink (Radoman-Shaw et al. 2022; Renggli et al. 2019). Because Venus does not exhibit Earth-like plate tectonics, recycling of sulfur into the mantle is unlikely (Byrne et al. 2021; Gulcher Astron et al. 2020). Nevertheless, high resurfacing rates could permit burial and partial remobilization of sulfur-bearing basalts into magmatic systems, offering a possible, if incomplete, mechanism for closing the sulfur cycle.

Io, the innermost of Jupiter's Galilean moons, is the most volcanically active body in the solar system due to intense tidal heating driven by the gravitational interaction with Jupiter and its neighboring moons, particularly Europa (Geissler and McMillan 2008). During its early evolution, Io likely accreted volatiles such as hydrogen, carbon, and nitrogen, but these were lost over time as a result of its vigorous volcanism and interactions with Jupiter's magnetosphere. In particular, elastic scattering by high-energy protons in the magnetosphere caused the ejection of these lighter, reduced gases—such as H_2 and CO—from Io's exosphere into the surrounding plasma environment, gradually oxidizing the moon's surface chemistry and leaving sulfur predominantly in the form of SO_2 (Pollack and Yung 1980). Unlike the lighter volatiles, sulfur is heavier and more likely to remain near the surface, where it condenses and precipitates, leading to Io's desiccation and making it an archetype for a planetary body governed by sulfur-driven geochemical processes. Sulfur gases such as SO_2, S_2, and SO are either directly degassed from Io's volcanoes or produced through interactions between lava and surface SO_2 ice. These volcanic emissions often condense to form various sulfur ices, giving Io its characteristic multicolored surface with hues of white, yellow, orange, red, green, and black. Some volcanic plumes can reach altitudes of up to 500 km, and gases that escape Io's gravity contribute to a surrounding neutral torus. In this region, sulfur species are ionized through photochemical reactions to form the Io plasma torus, which primarily consists of ions such as S^+, O^+, SO^+, and $SO2^+$ (Thomas et al. 2004). These ions can then be accelerated within Jupiter's magnetosphere and transported to Jupiter's atmosphere or to other Galilean moons (Lodders and Fegley 2026). The ongoing degassing of volcanic vents, along with sublimation and sputtering of surface ices, sustains Io's tenuous atmosphere, which has a surface pressure ranging from 0.3 to 3 nbar on the day side and consists mostly of SO_2 (90%) along with minor constituents like S_2, S_2O, NaCl, and KCl, under average daytime temperatures around 130 K (Spencer et al. 2000). Additionally, SO_2 ice on the surface undergoes radiolysis, forming SO_3, and this ice is eventually buried and recycled back into Io's interior, where it is re-incorporated into volcanic activity—thereby closing Io's sulfur cycle.

Sulfur cycles as observed on Io have recently gained increased attention, due to tentative detections of SO_2 in the atmosphere of rocky planets (Bello-Arufe et al. 2025; Nicholls et al. 2026).

4 Effect of Life on the Atmosphere

4.1 Habitable Atmospheres

While the composition of the modern atmosphere of Earth is clearly linked to the existence of life (see above and in Figs. 2, 10), a habitable atmosphere does not necessarily need to be comprised of oxygen and nitrogen. As a matter of fact, since oxygen reacts easily and can therefore be very destructive, life first needed to adapt to the current oxygen-rich conditions before thriving in it (because of its reactive potential, it serves as an excellent energy source for life). While the exact atmospheric composition and redox state of the Hadean and Archean Earth remain unknown, we do know that free oxygen was mostly found at levels $<10^{-6}$ Present Atmospheric Level prior to the Great Oxygenation Event (explained in more detail in Sect. 4.2). Such reducing conditions are favorable for prebiotic chemistry (e.g., Luisi 2016; Lingam 2020), as demonstrated in the Urey-Miller experiment and follow-up experiments, to spontaneously create amino acids and other prebiotic molecules in reducing to moderately oxidizing atmospheres (Miller and Urey 1959). Macroscopic life, on the other hand, may be impossible without incorporating oxygen, and past bursts in growth of individual life forms are directly correlated with atmospheric oxygen levels (Payne et al. 2009; Vilović et al. 2023). We therefore need to distinguish between different habitable conditions — for the origin of life, as well as for the long-term evolution of macroscopic life. This implies, specifically, that an abiotically produced oxygen-rich atmosphere may not be favorable for the origin of life.

The atmosphere composition suitable for macroscopic, complex animal-like life has been suggested to lie in relatively narrow pressure limits for O_2 (Catling et al. 2005), CO_2 (Schwieterman et al. 2019), and N_2 (Ramirez and Levi 2018); see Fig. 4 in Lammer et al. (2024) for a review. These are mainly toxicity limits for CO_2 and N_2 that may, in principle, vary for other inhabited planets based on the specific evolutionary pathways taken (Scherf et al. 2024). O, on the other hand, provides physical limits that can be expected to be valid for any macroscopic animal-like life (Catling et al. 2005). Oxygen provides by far the highest free energy of all elements that can considerably accumulate in an atmosphere, and aerobic metabolism supplies about an order of magnitude more energy than anaerobic metabolism (see in-depth discussion in Catling et al. 2005). Anaerobic organisms are therefore highly restricted in their growth and size, whereas aerobic macroscopic life is either limited in its physical size by oxygen diffusion (and hence O_2 partial pressure), or has to evolve a circulatory system that transports oxygen effectively through the entire body. An O_2 mixing ratio beyond $\sim$30%, on the other hand, leads to uncontrollable flammability, (e.g., Belcher et al. 2010; Balbi and Frank 2024) potentially serving as a regulatory factor for the O_2 mixing ratio on an inhabited planet (Belcher et al. 2010, 2021). Therefore, we need to keep in mind that the variety of habitable atmospheres might be much more restricted for macroscopic than for microscopic life. In addition, we highlight that "habitable" does not necessarily mean "inhabited" (see review by Cockell et al. 2016).

4.2 Inhabited Atmospheres Like Earth

We start first with what we know best, Earth. Although the dates for the rise of life on Earth are debated (e.g. Westall et al. 2023, Sect. 2.2.3), it is clear that some of the first life forms to influence the atmosphere were methanogens in the Archean (3-8–2.5 Ga), which used H_2 and CO_2 to produce CH_4 via the reaction $CO_2+4H_2 \rightarrow CH_4+2H_2O$. Given the lack of O_2 in this epoch, the longer residence lifetime of CH_4 (compared to today) would imply substantial build-up of this powerful greenhouse gas. It has long been speculated that it could have played a role in the Faint Young Sun Paradox given that Earth's insolation was 20–25% less in the Archean than today, and a modern atmospheric composition at that time would otherwise produce a snowball Earth that is not supported by proxy data (e.g. Wilde et al. 2001; Valley et al. 2002). At the same time, it is clear that CO_2 partial pressures were also higher (e.g. Feulner et al. 2023). However, one cannot have too much of a good thing, if the CH_4 to CO_2 ratio is $\sim$0.1 or higher hydrocarbon hazes (e.g., C_5H_4, C_4H_2, etc.) can form,

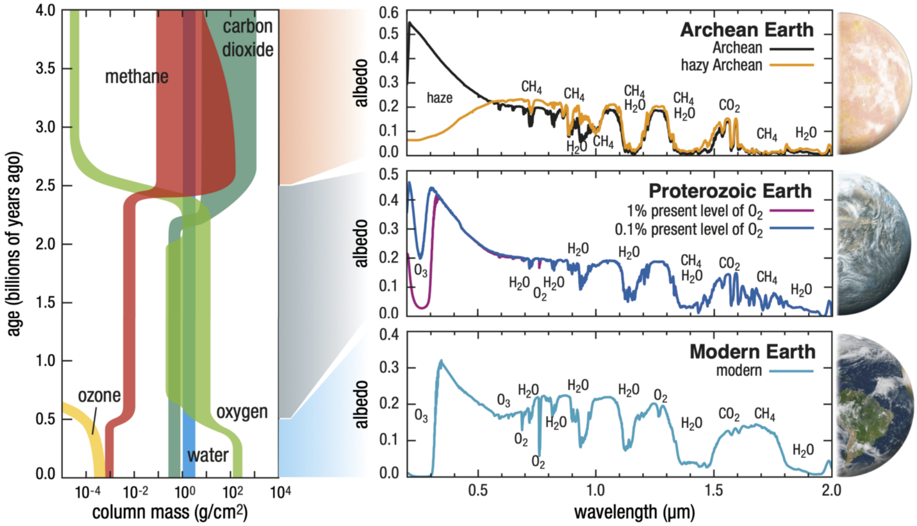

Fig. 10 Hypothetical transmission spectra of Earth through time as seen with the proposed LUVOIR/HWO telescope (The LUVOIR Team 2019). Credit: G. Arney, S. Domagal-Goldman, T. B. Griswold (NASA GSFC)

which exert a cooling effect on the atmosphere (e.g. Haqq-Misra et al. 2008; Arney et al. 2018). CH_4 in particular may be observable in planetary transmission spectra from JWST or LUVOIR/HWO (see Fig. 10), but clouds and hydrocarbon hazes make the detection of CH_4 and other species more challenging (e.g. Fauchez et al. 2019). However, CH_4 may also be produced abiotically via processes in the upper mantle and crust (e.g. Des Marais et al. 2002), motivating the need to rule out the detection of CO — a so-called anti-biosignature — to strengthen the case for CH_4 as a biosignature (Krissansen-Totton et al. 2022; Thompson et al. 2022).

As we move forward in Earth's history into the Proterozoic (2.5 Ga–541 Ma) at around 2.5 Ga we have the Great Oxygenation Event (GOE) which is believed to have been driven by the rise of cyanobacteria (e.g. Kasting and Catling 2003; Lyons et al. 2014). For many years it was assumed that O_2 was an excellent biosignature (e.g. Des Marais et al. 2002), but it was later realized that it is in fact an ambiguous one. For example, it is possible to create large quantities of O_2 abiotically via photolysis of H_2O coupled with high rates of atmospheric escape producing 100 s if not 1000 s of bars of O_2 possibly in a runaway or post-runaway greenhouse state (e.g. Luger and Barnes 2015; Meadows 2017). But there are other mechanisms for producing O_2 and even O_3 abiotically (e.g. Schwieterman et al. 2018). Schwieterman et al. (2018) provides an in-depth review of exoplanet biosignature gases (also see Sect. 5). Other work by Léger et al. (2011) showed that abiotic build-up of O_2 on a habitable planet was unlikely, but later work by Narita et al. (2015) maintained that it was still possible. Earth provides three main epochs in which its atmosphere has changed sufficiently to be distinguishable if observed as an exoplanet, in the Archean, Proterozoic, and Modern epochs as can be seen in Fig. 10.

5 Role of Photochemistry

The incident near-UV to X-ray flux from the host star is an important driver of chemistry in planetary atmospheres, responsible for various photodissociation and photoionization reactions (e.g., Yung and Demore 1999; Bauer and Lammer 2004). The far-UV (920-1700 Å) is absorbed at pressure levels above about 0.1 mbar, that is, in the mesosphere and the lower thermosphere in the case of the Earth, whereas the near-UV (1700-3200 Å) can reach further down to the stratosphere and troposphere (see Fig. 11, panel c). Various molecules such as CH_4, O_2, H_2O, CO_2, and N_2O have large parts of their photodissociation cross-sections in the far-UV, with the latter three of them expanding toward the near-UV (e.g., Loyd et al. 2016; Linsky 2025), as can be seen in panels (a) and (b) of Fig. 11. These UV photons drive oxygen photochemistry via the dissociation of molecules such as H_2O, O_2 and CO_2, and subsequent three-body reactions, for example, $O + O_2 + M \rightarrow O_3 + M$, where M is an atmospheric molecule needed to ensure momentum balance, can then further produce ozone (e.g., Bauer and Lammer 2004). Low-mass M dwarfs are specifically active in the far-UV (e.g., France et al. 2016; Loyd et al. 2016) and it was suggested that habitable zone planets orbiting these stars can therefore build up atmospheres with high O_2 and O_3 mixing ratios produced purely by photochemistry (e.g., Gao et al. 2015; Harman et al. 2015). More recent studies indicate that these results are sensitive to various model assumptions, such as the implemented lightning rates and the related production of NO_x species (Harman et al. 2018), the chosen photodissociation cross-sections (Ranjan et al. 2020), and the pressure range of the upper model boundary (Ranjan et al. 2023). The abiotic build-up of photochemically produced O_2 may hence be less efficient as recently assumed, since CO can efficiently recombine to CO_2 via OH as a catalyst under properly chosen model conditions (Harman et al. 2018; Ranjan et al. 2023). Still, Ranjan et al. (2023) point out that an abiotic build-up of O_3 remains feasible in these photochemical models around M dwarfs.

However, photochemical models often do not include the thermosphere, that is, the region in the atmosphere above the mesosphere where the XUV flux – the extreme-UV (100-920 Å) and the X-ray part of the spectrum (10-100 Å) – is predominantly absorbed. In the Earth's atmosphere, this happens at a relatively broad range of pressure levels between ~ 0.1 mbar in the upper mesosphere and $\sim 10^{-6}$ mbar in the thermosphere (e.g., Bauer and Lammer 2004). The absorbed XUV flux (or, more broadly, the absorbed wavelength range below the Lyman-α line at 1215 Å) in the upper atmosphere is an important driver for photodissociation of, e.g., H_2, CO, N_2, and CO_2 (Loyd et al. 2016; Linsky 2025), as can be seen in panel (b) of Fig. 11. In addition, it is primarily responsible for photoionization, the corresponding formation of an ionosphere, and thermospheric heating (Bauer and Lammer 2004). Because of the latter, highly irradiated atmospheres, such as planets in the HZ of M dwarfs (e.g., Van Looveren et al. 2024; Scherf et al. 2024), can have significantly expanded atmospheres and strong thermal escape due to the large amounts of energy deposited into the thermosphere. High-energy photons in the thermosphere can also dissociate molecules that cool the atmosphere, such as CO_2 (Tian et al. 2009; Johnstone et al. 2021b). As the altitude at which the XUV flux is typically absorbed increases for expanding atmospheres, it is important to note that thermal escape calculated via the energy-limited escape formulation (see Equation (3)) depends on $R_{\mathrm{XUV}}^2 R_{\mathrm{pl}}$, and not, as often simplified, on R_{pl}^3 (e.g., Erkaev et al. 2016). Estimating thermal losses via the latter simplification can, therefore, lead to a significant underestimation of atmospheric escape rates.

Since the XUV flux absorbed in the thermosphere drives photodissociation, photoionization, and atmospheric escape, one has to take account of the upper atmosphere (i.e., the thermosphere above $\sim$80 km) for evaluating whether O_2 and O_3 may constitute a false-positive biosignature (e.g., Meadows et al. 2018; Schwieterman and Leung 2024). As thermal escape preferentially removes the lighter species from the atmosphere, the photodissociation of H_2O, mostly via absorption at the Lyman-α line (see Fig. 11), can lead to an accumulation of O_2 compared to H (Tian et al. 2014b; Luger and Barnes 2015; Wordsworth and

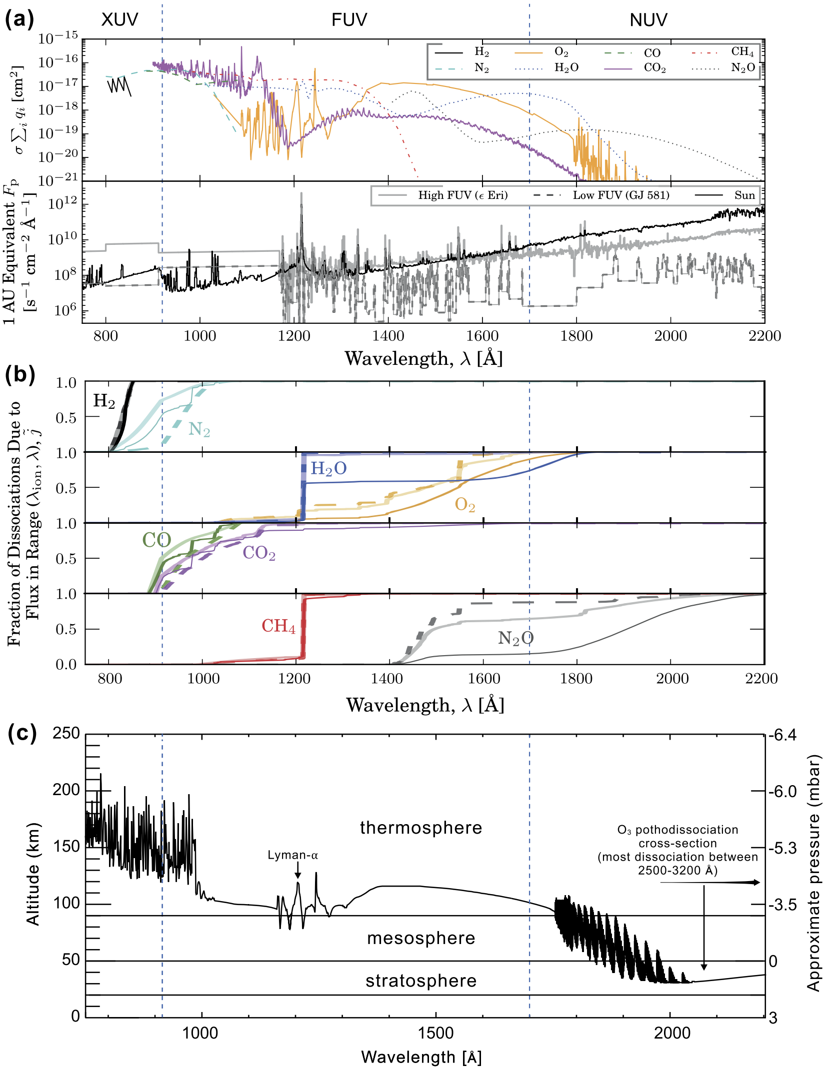

Fig. 11 a) top panel: photodissociation cross-sections of various molecules. bottom panel: spectral energy distribution of the Sun, the most active (ϵ Eri; with ~0.85 $M_\odot$ and an age of ~ 660 Myr) and the least active (GJ 581; with ~0.3 $M_\odot$ and an age of ~ 9.5 Gyr) star of the MUSCLES survey (France et al. 2016; Loyd et al. 2016) defined by the ratio of the FUV(far ultraviolet) to bolometric flux. The panel shows the photon flux density scaled to a bolometric flux equivalent to Earth's insolation. (b) Cumulative photodissociation spectra of the same molecules based on the curves in panel (a). The three curves per molecule correspond to the three aforementioned reference stars. (c) Absorption altitudes and approximate pressure levels of unit optical depth (i.e., about 63% of the flux is absorbed above this altitude) of the same wavelength range as depicted in panels (a) and (b) for the Earth's present atmosphere; note that the absorption altitudes differ for different atmospheric compositions. For the absorption altitudes, see, e.g., Meier et al. (1997) and Woods et al. (2000). This panel also schematically depicts the wavelengths at which O_3 photodissociates. However, most of the photodissociation of O_3 for the Sun and ϵ Eri takes place between 2500 and 3200 Å (Loyd et al. 2016, see also their Fig. 10). The vertical blue dashed lines depict the EUV (extreme ultraviolet), FUV (far ultraviolet), and NUV (near ultraviolet) wavelength ranges. Subfigures (a) and (b) are adopted from Loyd et al. (2016); the data of the absorption altitudes in (c) is taken from Woods et al. (2000), their Fig. 2

Pierrehumbert 2014; Wordsworth et al. 2018; Johnstone 2020). The high XUV activity of M dwarfs their habitable zones (e.g., Johnstone et al. 2021a) favors such scenarios, but highly active young K and G stars can also lead to an accumulation of O_2 on planets within their HZs (Johnstone 2020). In addition, one should also note that CO, which drives the recombination of CO_2 and hence the decrease of abiotically produced O_2 (Ranjan et al. 2023), is dissociated in the thermosphere as most of its photodissociation cross-section is in the XUV (Loyd et al. 2016).

Another relevant photochemical process in the upper atmosphere is the production of suprathermal atoms. This is an important source of non-thermal escape in terrestrial atmospheres (see Sect. 2.3.1, specifically for Mars) since the related photochemical reactions usually include the excitation of atoms above energy levels needed for gaining escape velocity (Bauer and Lammer 2004). These reactions comprise radiative recombination reactions, which can be expressed as

$$\mathrm{X}^+ + \mathrm{e} \rightarrow \mathrm{X}^* + \Delta\mathrm{E}, \tag{4}$$

where X is the initially ionized species, e is a photoelectron, and $*$ denotes the excited state of species X. They also include dissociative recombination reactions in the form of

$$\mathrm{XY}^+ + \mathrm{e} \rightarrow \mathrm{XY}^* \rightarrow \mathrm{X}^* + \mathrm{Y} + \Delta\mathrm{E}, \tag{5}$$

where XY is the molecule, X and Y are its dissociation products, and $+$ and $*$ again refer to the ionized and excited states, respectively. In both reaction pathways, the excess energy ΔE goes into the kinetic energy of the neutralized particles (Bauer and Lammer 2004). Dissociative recombination coefficients (in the order of 10^{-7} cm^3 s^{-1}) are typically orders of magnitude larger than radiative recombination coefficients (in the order of 10^{-12} cm^3 s^{-1}), making dissociative recombination one of the most important photochemical loss processes in planetary atmospheres (e.g., Biondi 1969; Bauer and Lammer 2004); see Sect. 2.3.1 for a discussion on the role of photochemical escape on Venus and Mars.

Photochemistry in the upper atmosphere also depends on atmospheric composition. For hydrogen-rich atmospheres, lower atmospheric layers are dominated by molecules such as H_2, H_2O, and CH_4 (e.g., Hu et al. 2012; Madhusudhan et al. 2016). There, the radical OH is much less abundant by orders of magnitude than atomic H. OH, which forms from the dissociation of H_2O, quickly reacts with H_2 to reform H_2O, a process that assures a long lifetime of CH_4 and CO (Hu et al. 2012). In the thermosphere, H_2 becomes increasingly photodissociated, and H becomes ionized. In H-He-dominated atmospheres, most of the absorbed energy from the incident XUV flux feeds the photo-dissociation and -ionization of H_2, and H and He, respectively, but the excess energy heats the atmosphere and drives atmospheric expansion and escape (e.g., Shematovich et al. 2014; Erkaev et al. 2016; Salz et al. 2016; Linsky 2025).

Similar to hydrogen-rich atmospheres, the lifetimes of CH_4 and CO are long in CO_2- and N_2-dominated atmospheres and mostly depend on the availability of OH (Hu et al. 2012). In reduced N_2-dominated atmospheres, a rich hydrocarbon chemistry can take place that forms hazes and aerosols, for which CH radicals produced from the photodissociation of CH_4 via far-UV irradiation play an important role (e.g, Trainer et al. 2012; Carrasco et al. 2022). This can be observed today at Titan, (e.g., Lavvas et al. 2008), Pluto and Triton (e.g., Luspay-Kuti and Mandt 2025), and a photochemically produced hydrocarbon haze layer could have also been present on the Archean Earth (e.g., Pavlov et al. 2001). There, such a layer may have formed for CH_4 and CO_2 abundances of $CH_4/CO_2 \geq 0.1$ (e.g., Trainer et al. 2004; Mak et al. 2023), although with a different chemical composition as on Titan (Mak et al. 2023).

Hazy atmospheres, similar to the Earth's prior to the Great Oxygenation event, as, e.g., recently simulated for TRAPPIST-1e (Mak et al. 2024), may also exist on exoplanets and often serve as example atmospheres of habitats with primitive pre-photosynthesizing life (e.g, Eager-Nash et al. 2024). However, one has to account for the incident XUV flux and the related thermal stability of these atmospheres. It is unlikely that secondary, Earth-like atmospheres are thermally stable on planets orbiting in the HZ of low-mass M dwarfs such as TRAPPIST-1e (Van Looveren et al. 2024; Scherf et al. 2024). Simulating the photochemistry of specific atmospheres on these planets should, therefore, either include a proper treatment of their thermospheres that also investigates their thermal stability, or the results must be viewed cautiously. If the assumed atmosphere cannot exist because of the high incident XUV flux, neither simulating their photochemistry nor their climates has a practical physical sense.

6 Summary

This review highlights that the composition of the atmosphere of a rocky exoplanet is not static in time but evolves throughout the lifetime of the planet through interactions with the planet's interior, stellar irradiation, and, potentially, biological activity.

In order for a rocky planet to retain an atmosphere in the first place, the volatile source flux must exceed the combined loss of volatiles via escape to space and sequestration into the planetary interior. There are two main ways how a rocky planet can gain an atmosphere. The first is the direct capture of a primordial atmosphere during formation, and the second is through outgassing of volatiles that are initially stored in the interior of the planet. These secondary atmospheres are further divided in atmospheres formed by the outgassing of volatiles during the solidification of the magma ocean and volcanic outgassing, which can act over Gyr timescales.

In the first few 100 s Myr, the most dominating escape mechanism is hydrodynamic thermal escape. As the planet evolves, the dominating escape process shifts to non-thermal escape processes, such as photochemical escape and stellar-wind escape. The biggest difference between the two escape processes is that thermal escape is in general more efficient at removing lighter species especially for planets that experience XUV fluxes similar to ones of the terrestrial planets in the Solar System, while non-thermal escape processes can also remove heavier species. Rocky planets likely undergo episodic atmospheric replenishment after significant mass-loss events throughout their lifetime.

The volatile mixtures degassed into the atmosphere further undergo significant transformations through selective loss to space, photochemical reactions in the upper atmosphere, and fluid-rock interactions in the lower atmosphere. These processes can drastically alter the composition of the volcanic atmosphere compared to the initial composition after outgassing.

The interaction between the interior and the atmosphere continues throughout an active planet's lifetime. On modern Earth the carbonate-silicate cycle in concert with subductive plate tectonics provides a means to stabilize the climate over long time-scales providing long-term habitability. However, even on a planet with a stagnant lid there are means to provide volatile cycling over shorter timescales of order 1 Gyr. With volatile cycling a planet can end up in a moist or runaway greenhouse state (like Venus) or conversely a snowball state via the ice/albedo feedback as seen in Earth's distant past over short periods of time. Clouds play a key role in the radiative budget of a planet, and may even provide a means to stabilize the climate of a planet inside the conservative habitable zone via the cloud-albedo feedback seen in simulations of slowly rotating worlds. In addition to conventional volatile cycling, Nitrogen and Sulfur cycling may also take place. Venus has more than three times Earth's atmospheric nitrogen budget, which is likely tied to its distinct outgassing history from Earth and a long-term lack of plate tectonics (see Sect. 3.5.1 above).

The effect of life on an atmosphere and the search for it via unambiguous biosignatures remains one of the most sought after goals in exoplanetary science. We know that Earth has exhibited biosignature gases such as CH_4 since the early Archean and the rise of microscopic life. CH_4 could have also played a critical role in resolving the Faint Young Sun Paradox: the fact that the sun was 25% less luminous $\sim$ 4Gyr ago and was not in a snowball state. Earth's great oxygenation event, driven by cyanobacteria, completely transformed the atmosphere and eventually gave rise to diverse forms of macroscopic life. Yet CH_4 and O_2 are in fact not unambiguous biosignature gases. For this reason the search of unambiguous biosignature gases remains an active area of research.

The characterization of a large sample of rocky exoplanet atmospheres with current and upcoming telescopes will therefore allow us to deepen our understanding of rocky exoplanets and their interior. It is especially important to probe planets across a variety of ages and environments. However, interpreting the observations of rocky planet atmospheres necessitates the understanding of the interdependent nature of diverse planetary and atmospheric processes. This will require not just advancements in instrumentation and observational techniques, but, crucially, the development of numerical models capable of simulating the co-evolution of the atmosphere and interior of rocky planets as a single system. The development of such models further requires robust knowledge of the physiochemical properties, such as solubility and partitioning coefficients, of key volatiles across a wide range of pressures, temperatures and redox states. Furthermore, aerosols remain a major uncertainty in understanding the atmospheres of rocky exoplanets, demanding improvements in microphysical modelling and the acquisition of new laboratory data. Most importantly, we need to foster strong multidisciplinary collaborations to truly understand and characterize rocky exoplanets.

Acknowledgements The authors thank the anonymous reviewer for their insightful comments and the International Space Science Institute and the organizers for hosting and managing the workshop "The Geoscience of (Exo)planets: Going beyond habitability", from which this article originated. We would also like to thank A. Mandell, J. Lustig-Yaeger and R. Hu for useful discussions and comments. MS thanks the Austrian Science Fund (FWF) for the support of the VeReDo research project, grant I6857-N. This project was funded by the European Union (ERC, DIVERSE, 101087755). Views and opinions expressed are however those of the author(s) only and do not necessarily reflect those of the European Union or the European Research Council Executive Agency. Neither the European Union nor the granting authority can be held responsible for them.

Funding Information Open access funding provided by Swiss Federal Institute of Technology Zurich.

Declarations

Competing Interests The authors declare that there are no competing interests.

References

Abbot DS, Voigt A, Koll D (2011) The Jormungand global climate state and implications for Neoproterozoic glaciations. J Geophys Res 116(D18):D18103. https://doi.org/10.1029/2011JD015927

Abe T, Whalen BA, Yau AW, et al (1993) EXOS D (Akebono) suprathermal mass spectrometer observations of the polar wind. J Geophys Res 98(A7):11191–11204. https://doi.org/10.1029/92JA01971

Abe Y, Abe-Ouchi A, Sleep NH, et al (2011) Habitable zone limits for dry planets. Astrobiology 11(5):443–460. https://doi.org/10.1089/ast.2010.0545

Airapetian V, Glocer A, Gronoff G, et al (2016) Prebiotic chemistry and atmospheric warming of early Earth by an active young sun. Nat Geosci 9(6):452–455

Alcott LJ, Mills BJ, Poulton SW (2019) Stepwise Earth oxygenation is an inherent property of global biogeochemical cycling. Science 366(6471):1333–1337

Alibert Y (2017) Maximum mass of planetary embryos that formed in core-accretion models. Astron Astrophys 606:A69. https://doi.org/10.1051/0004-6361/201630051

Allart R, Bourrier V, Lovis C, et al (2018) Spectrally resolved helium absorption from the extended atmosphere of a warm Neptune-mass exoplanet. Science 362(6421):1384–1387. https://doi.org/10.1126/science.aat5879

Amerstorfer UV, Gröller H, Lichtenegger H, et al (2017) Escape and evolution of Mars's CO_2 atmosphere: influence of suprathermal atoms. J Geophys Res Planets 122(6):1321–1337. https://doi.org/10.1002/2016JE005175

Anderson DE (1976) The Mariner 5 ultraviolet photometer experiment: analysis of hydrogen Lyman alpha data. J Geophys Res 81(7):1213. https://doi.org/10.1029/JA081i007p01213

Armitage PJ (2011) Dynamics of protoplanetary disks. Annu Rev Astron Astrophys 49(1):195–236. https://doi.org/10.1146/annurev-astro-081710-102521

Arney G, Domagal-Goldman SD, Meadows VS (2018) Organic haze as a biosignature in anoxic Earth-like atmospheres. Astrobiology 18:311–329

August PC, Buchhave LA, Diamond-Lowe H, et al (2025) Hot rocks survey I: a possible shallow eclipse for LHS 1478 b. Astron Astrophys 695:A171. https://doi.org/10.1051/0004-6361/202452611

Aulbach S, Stagno V (2016) Evidence for a reducing Archean ambient mantle and its effects on the carbon cycle. Geology 44(9):751–754. https://doi.org/10.1130/G38070.1

Avice G, Marty B, Burgess R, et al (2018) Evolution of atmospheric xenon and other noble gases inferred from Archean to Paleoproterozoic rocks. Geochim Cosmochim Acta 232:82–100. https://doi.org/10.1016/j.gca.2018.04.018

Balbi A, Frank A (2024) The oxygen bottleneck for technospheres. Nat Astron 8(1):39–43

Baliukin II, Bertaux JL, Quémerais E, et al (2019) Swan/soho lyman-α mapping: The hydrogen geocorona extends well beyond the moon. J Geophys Res Space Phys 124(2):861–885. https://doi.org/10.1029/2018JA026136

Barabash S, Fedorov A, Sauvaud JJ, et al (2007) The loss of ions from Venus through the plasma wake. Nature 450(7170):650–653. https://doi.org/10.1038/nature06434

Barry PH, Hilton DR (2016) Release of subducted sedimentary nitrogen throughout Earth's mantle. Geochem Perspect Lett 2(2):148–159. https://doi.org/10.7185/geochemlet.1615

Basilevsky AT, Head JW (2003) The surface of Venus. Rep Prog Phys 66(10):1699–1734. https://doi.org/10.1088/0034-4885/66/10/R04

Bauer SJ, Lammer H (2004) Planetary aeronomy: physics of Earth and space environments. Springer, Berlin. https://doi.org/10.1007/978-3-662-09362-7

Baumeister P, Tosi N, Brachmann C, et al (2023) Redox state and interior structure control on the long-term habitability of stagnant-lid planets. Astron Astrophys 675:A122. https://doi.org/10.1051/0004-6361/202245791

Baumeister P, Miozzi F, Guimond CM, et al (2025) Fundamentals of interior modelling and challenges in the interpretation of observed rocky exoplanets. Space Sci Rev 221(8):123. https://doi.org/10.1007/s11214-025-01248-5

Beatty TG, Welbanks L, Schlawin E, et al (2024) Sulfur dioxide and other molecular species in the atmosphere of the sub-Neptune GJ 3470 b. Astrophys J Lett 970(1):L10. https://doi.org/10.3847/2041-8213/ad55e9

Belcher CM, Yearsley JM, Hadden RM, et al (2010) Baseline intrinsic flammability of Earth's ecosystems estimated from paleoatmospheric oxygen over the past 350 million years. Proc Natl Acad Sci USA 107(52):22448–22453. https://doi.org/10.1073/pnas.1011974107

Belcher C, Mills B, Vitali R, et al (2021) The rise of angiosperms strengthened fire feedbacks and improved the regulation of atmospheric oxygen. Nat Commun 12. https://doi.org/10.1038/s41467-020-20772-2

Bello-Arufe A, Damiano M, Bennett KA, et al (2025) Evidence for a volcanic atmosphere on the sub-Earth l 98-59 b. Astrophys J Lett 980(2):L26

Belu A, Selsis F, Morales JC, et al (2011) Primary and secondary eclipse spectroscopy with JWST: exploring the exoplanet parameter space. Astron Astrophys 525:A83
Benedikt MR, Scherf M, Lammer H, et al (2020) Escape of rock-forming volatile elements and noble gases from planetary embryos. Icarus 347:113772. https://doi.org/10.1016/j.icarus.2020.113772
Benneke B, Roy PA, Coulombe LP, et al (2024) JWST reveals CH_4, CO_2, and H_2O in a metal-rich miscible atmosphere on a two-Earth-radius exoplanet. arXiv e-prints arXiv:2403.03325 [astro-ph]
Berdyugina SV, Berdyugin AV, Fluri DM, et al (2008) First detection of polarized scattered light from an exoplanetary atmosphere. Astrophys J Lett 673(1):L83. https://doi.org/10.1086/527320
Berdyugina SV, Berdyugin AV, Fluri DM, et al (2011) Polarized reflected light from the exoplanet HD189733b: first multicolor observations and confirmation of detection. Astrophys J Lett 728(1):L6. https://doi.org/10.1088/2041-8205/728/1/L6
Berger TA, Huber D, Gaidos E, et al (2020) The Gaia-Kepler stellar properties catalog. II. Planet radius demographics as a function of stellar mass and age. Astron J 160(3):108. https://doi.org/10.3847/1538-3881/aba18a
Berner EK, Berner RA (2012) Global environment: water, air, and geochemical cycles. Princeton University Press, Princeton
Bertaux JL, Blamont J, Marcelin M, et al (1978) Lyman-alpha observations of Venera-9 and 10 I. The non-thermal hydrogen population in the exosphere of Venus. Planet Space Sci 26(9):817–831. https://doi.org/10.1016/0032-0633(78)90105-8
Bertaux JL, Lepine VM, Kurt VG, et al (1982) Altitude profile of H in the atmosphere of Venus from Lyman α observations of Venera 11 and Venera 12 and origin of the hot exospheric component. Icarus 52(2):221–244. https://doi.org/10.1016/0019-1035(82)90110-5
Bhattacharyya D, Clarke JT, Mayyasi M, et al (2023) Evidence of non-thermal hydrogen in the exosphere of Mars resulting in enhanced water loss. J Geophys Res Planets 128(8):e2023JE007801. https://doi.org/10.1029/2023JE007801
Biersteker JB, Schlichting HE (2021) Losing oceans: the effects of composition on the thermal component of impact-driven atmospheric loss. Mon Not R Astron Soc 501(1):587–595
Biondi MA (1969) Atmospheric electron–ion and ion–ion recombination processes. Can J Chem 47(10):1711–1719. https://doi.org/10.1139/v69-282
Bond DP, Grasby SE (2017) On the causes of mass extinctions. Palaeogeogr Palaeoclimatol Palaeoecol 478:3–29
Bonomo A, Dumusque X, Massa A, et al (2023) Cold Jupiters and improved masses in 38 Kepler and K2 small planet systems from 3661 HARPS-N radial velocities: no excess of cold Jupiters in small planet systems. Astron Astrophys 677:A33. https://doi.org/10.1051/0004-6361/202346211
Bower DJ, Kitzmann D, Wolf AS, et al (2019) Linking the evolution of terrestrial interiors and an early outgassed atmosphere to astrophysical observations. Astron Astrophys 631:A103
Bower DJ, Hakim K, Sossi PA, et al (2022) Retention of water in terrestrial magma oceans and carbon-rich early atmospheres. Planet Sci J 3(4):93. https://doi.org/10.3847/PSJ/ac5fb1
Brachmann C, Noack L, Baumeister PA, et al (2025) Distinct types of chon atmospheres and surface pressures depending on melt redox state and outgassing efficiency. Icarus 429:116450
Brain DA, McFadden JP, Halekas JS, et al (2015) The spatial distribution of planetary ion fluxes near Mars observed by maven. Geophys Res Lett 42(21):9142–9148. https://doi.org/10.1002/2015GL065293
Brimblecombe P (2003) The global sulfur cycle. In: Treatise on geochemistry. Vol 8: Biogeochemistry. Elsevier, Amsterdam, pp 645–682. https://doi.org/10.1016/B0-08-043751-6/08134-2
Brouwers MG, Vazan A, Ormel CW (2018) How cores grow by pebble accretion. I. Direct core growth. Astron Astrophys 611:A65. https://doi.org/10.1051/0004-6361/201731824
Budyko MI (1969) The effect of solar radiation variations on the climate of the Earth. Tellus A: dynamic meteorology and. Oceanography 21(5):611. https://doi.org/10.3402/tellusa.v21i5.10109
Burgisser A, Scaillet B (2007) Redox evolution of a degassing magma rising to the surface. Nature 445(7124):194–197
Burn R, Mordasini C, Mishra L, et al (2024) A radius valley between migrated steam worlds and evaporated rocky cores. Nat Astron 8:463–471. https://doi.org/10.1038/s41550-023-02183-7
Byrne PK, Jozwiak LA, Treiman AH, et al (2021) Venus resurfacing: constraints from crater densities, geomorphology, and stratigraphy. Nat Astron 5:1–9. https://doi.org/10.1038/s41550-021-01372-2
Byrne X, Shorttle O, Jordan S, et al (2024) Atmospheres as a window to rocky exoplanet surfaces. Mon Not R Astron Soc 527(4):10748–10759. https://doi.org/10.1093/mnras/stad3914. arXiv:2312.11133 [astro-ph.EP]
Byrne PK, Guimond CM, Cawood PA, et al (2026) What the solar system can teach us about rocky exoplanets. Space Sci Rev. 222
Carone L, Barnes R, Noack L, et al (2025) From co2-to h2o-dominated atmospheres and back-how mixed outgassing changes the volatile distribution in magma oceans around m dwarf stars. Astron Astrophys 693:A303

Carrasco N, Bourgalais J, Vettier L, et al (2022) A missing link in the nitrogen-rich organic chain on Titan. Astron Astrophys 663:A165. https://doi.org/10.1051/0004-6361/202141025
Catling DC, Kasting JF (2017) Atmospheric evolution on inhabited and lifeless worlds, 1st edn. Cambridge University Press, Cambridge
Catling DC, Zahnle KJ (2020) The archean atmosphere. Sci Adv 6(9):eaax1420
Catling DC, Glein CR, Zahnle KJ, et al (2005) Why O_2 is required by complex life on habitable planets and the concept of planetary "oxygenation time". Astrobiology 5(3):415–438. https://doi.org/10.1089/ast.2005.5.415
Catling DC, Krissansen-Totton J, Kiang NY, et al (2018) Exoplanet biosignatures: a framework for their assessment. Astrobiology 18(6):709–738. https://doi.org/10.1089/ast.2017.1737
Chaffin M, Cangi E, Gregory B, et al (2024) Venus water loss is dominated by hco dissociative recombination. Nature 629:1–4. https://doi.org/10.1038/s41586-024-07261-y
Chamberlain JW (1963) Planetary coronae and atmospheric evaporation. Planet Space Sci 11(8):901–960. https://doi.org/10.1016/0032-0633(63)90122-3
Chappell CR (2015) The role of the ionosphere in providing plasma to the terrestrial magnetosphere—an historical overview. Space Sci Rev 192(1–4):5–25. https://doi.org/10.1007/s11214-015-0168-5
Charbonneau D, Brown TM, Noyes RW, et al (2002) Detection of an extrasolar planet atmosphere. Astrophys J 568(1):377–384. https://doi.org/10.1086/338770
Charnay B, Le Hir G, Fluteau F, et al (2017) A warm or a cold early Earth? New insights from a 3-d climate-carbon model. Earth Planet Sci Lett 474:97–109
Chaufray JY, Bertaux JL, Quémerais E, et al (2012) Hydrogen density in the dayside Venusian exosphere derived from Lyman-α observations by SPICAV on Venus Express. Icarus 217(2):767–778. https://doi.org/10.1016/j.icarus.2011.09.027
Chen GQ, Ahrens TJ (1997) Erosion of terrestrial planet atmosphere by surface motion after a large impact. Phys Earth Planet Inter 100(1–4):21–26
Chen J, Kipping D (2016) Probabilistic forecasting of the masses and radii of other worlds. Astrophys J 834(1):17
Cherubim C, Wordsworth R, Bower DJ, et al (2025) An oxidation gradient straddling the small planet radius valley. Astrophys J 983(2):97. https://doi.org/10.3847/1538-4357/adbca9
Chirakkil K, Deighan J, Chaffin MS, et al (2024) EMM EMUS observations of hot oxygen corona at Mars: radial distribution and temporal variability. J Geophys Res Space Phys 129(3):e2023JA032342. https://doi.org/10.1029/2023JA032342
Chyba CF (1990) Impact delivery and erosion of planetary oceans in the early inner Solar System. Nature 343(6254):129–133. https://doi.org/10.1038/343129a0
Cockell CS, Bush T, Bryce C, et al (2016) Habitability: a review. Astrobiology 16(1):89–117. https://doi.org/10.1089/ast.2015.1295
Cravens TE, Gombosi T, Nagy AF (1980) Hot hydrogen in the exosphere of Venus. Nature 283(5743):178–180. https://doi.org/10.1038/283178a0
Cui J, Wu X-S, Gu H, et al (2019) Photochemical escape of atomic C and n on Mars: clues from a multi-instrument maven dataset. Astron Astrophys 621:A23. https://doi.org/10.1051/0004-6361/201833749
Curry SM, Luhmann J, Ma Y, et al (2015) Comparative pick-up ion distributions at Mars and Venus: consequences for atmospheric deposition and escape. Planet Space Sci 115:35–47. https://doi.org/10.1016/j.pss.2015.03.026
Curry A, Booth R, Owen JE, et al (2024) The evolution of catastrophically evaporating rocky planets. Mon Not R Astron Soc 528(3):4314–4336. https://doi.org/10.1093/mnras/stae191
Curry SM, Hara T, Luhmann JG, et al (2025) First direct observations of atmospheric sputtering at Mars. Sci Adv 11(22):eadt1538. https://doi.org/10.1126/sciadv.adt1538
Daly RT, Schultz PH (2018) The delivery of water by impacts from planetary accretion to present. Sci Adv 4(4):eaar2632
Dandouras I, Blanc M, Fossati L, et al (2020) Future missions related to the determination of the elemental and isotopic composition of Earth, Moon and the terrestrial planets. Space Sci Rev 216(8):121. https://doi.org/10.1007/s11214-020-00736-0
De La Haye V, Waite Jr JH, Johnson RE, et al (2007) Cassini ion and Neutral Mass Spectrometer data in Titan's upper atmosphere and exosphere: Observation of a suprathermal corona. J Geophys Res Space Phys 112(A7). https://doi.org/10.1029/2006JA012222
Deighan J, Chaffin MS, Chaufray JY, et al (2015) MAVEN IUVS observation of the hot oxygen corona at Mars. Geophys Res Lett 42(21):9009–9014. https://doi.org/10.1002/2015GL065487
Del Genio AD, Kiang NY, Way MJ, et al (2019a) Albedos, equilibrium temperatures, and surface temperatures of habitable planets. Astrophys J 884(1):75
Del Genio AD, Way MJ, Amundsen DS, et al (2019b) Habitable climate scenarios for Proxima Centauri b with a dynamic ocean. Astrobiology 19(1):99–125

Demangeon ODS, Zapatero Osorio MR, Alibert Y, et al (2021) Warm terrestrial planet with half the mass of Venus transiting a nearby star. Astron Astrophys 653:A41. https://doi.org/10.1051/0004-6361/202140728

Deming D, Seager S, Richardson LJ, et al (2005) Infrared radiation from an extrasolar planet. Nature 434(7034):740–743. https://doi.org/10.1038/nature03507. arXiv:astro-ph/0503554 [astro-ph]

Demory BO, de Wit J, Lewis N, et al (2013) Inference of inhomogeneous clouds in an exoplanet atmosphere. Astrophys J Lett 776(2):L25. https://doi.org/10.1088/2041-8205/776/2/L25

Des Marais DJ, Harwit MO, Jucks KW, et al (2002) Remote sensing of planetary properties and biosignatures on extrasolar terrestrial planets. Astrobiology 2(2):153–181

Dong Y, Fang X, Brain DA, et al (2015) Strong plume fluxes at Mars observed by MAVEN: an important planetary ion escape channel. Geophys Res Lett 42(21):8942–8950. https://doi.org/10.1002/2015GL065346

Dos Santos LA (2023) Observations of planetary winds and outflows. In: Vidotto AA, Fossati L, Vink JS (eds) Winds of stars and exoplanets, pp 56–71. https://doi.org/10.1017/S1743921322004239. arXiv:2211.16243

Dos Santos LA, Lopez ED, Fossati L, et al (2025) Exoplanet Atmospheric Escape Observations with the Habitable Worlds Observatory. https://doi.org/10.48550/arXiv.2507.07124. arXiv e-prints. arXiv:2507.07124

Doyle AE, Young ED, Klein B, et al (2019) Oxygen fugacities of extrasolar rocks: evidence for an Earth-like geochemistry of exoplanets. Science 366(6463):356–359

Drążkowska J, Bitsch B, Lambrechts M, et al (2023) Planet formation theory in the era of ALMA and Kepler: from pebbles to exoplanets. In: Inutsuka S, Aikawa Y, Muto T, et al (eds) Protostars and planets VII, p 717. https://doi.org/10.48550/arXiv.2203.09759

Ducrot E, Lagage PO, Min M, et al (2025) Combined analysis of the 12.8 and 15 μm jwst/miri eclipse observations of trappist-1 b. Nat Astron 9(3):358–369

Eager-Nash JK, Daines SJ, McDermott JW, et al (2024) Simulating biosignatures from pre-oxygen photosynthesizing life on TRAPPIST-1e. Mon Not R Astron Soc 531(1):468–494. https://doi.org/10.1093/mnras/stae1142

Egger JA, Osborn HP, Kubyshkina D, et al (2024) Unveiling the internal structure and formation history of the three planets transiting HIP 29442 (TOI-469) with CHEOPS. Astron Astrophys 688:A223. https://doi.org/10.1051/0004-6361/202450472

Ehrenreich D, Lecavelier Des Etangs A, Hébrard G, et al (2008) New observations of the extended hydrogen exosphere of the extrasolar planet HD 209458b. Astron Astrophys 483(3):933–937. https://doi.org/10.1051/0004-6361:200809460. arXiv:0803.1831 [astro-ph]

Elkins-Tanton L (2008) Linked magma ocean solidification and atmospheric growth for Earth and Mars. Earth Planet Sci Lett 271(1–4):181–191

Elkins-Tanton LT (2012) Magma oceans in the inner Solar System. Annu Rev Earth Planet Sci 40(1):113–139

Erkaev NV, Kulikov YN, Lammer H, et al (2007) Roche lobe effects on the atmospheric loss from "Hot Jupiters". Astron Astrophys 472(1):329–334. https://doi.org/10.1051/0004-6361:20066929

Erkaev NV, Lammer H, Odert P, et al (2016) EUV-driven mass-loss of protoplanetary cores with hydrogen-dominated atmospheres: the influences of ionization and orbital distance. Mon Not R Astron Soc 460(2):1300–1309. https://doi.org/10.1093/mnras/stw935. arXiv:1601.00452 [astro-ph.EP]

Erkaev NV, Scherf M, Thaller SE, et al (2021) Escape and evolution of Titan's N_2 atmosphere constrained by $^{14}N/^{15}N$ isotope ratios. Mon Not R Astron Soc 500(2):2020–2035. https://doi.org/10.1093/mnras/staa3151

Erkaev NV, Scherf M, Herbort O, et al (2023) Modification of the radioactive heat budget of Earth-like exoplanets by the loss of primordial atmospheres. Mon Not R Astron Soc 518(3):3703–3721. https://doi.org/10.1093/mnras/stac3168

Evans TM, Pont F, Sing DK, et al (2013) The deep blue color of HD 189733b: albedo measurements with Hubble Space Telescope/space telescope imaging spectrograph at visible wavelengths. Astrophys J Lett 772(2):L16. https://doi.org/10.1088/2041-8205/772/2/L16

Fauchez TJ, Turbet M, Villanueva GL, et al (2019) Impact of clouds and hazes on the simulated jwst transmission spectra of habitable zone planets in the trappist-1 system. Astrophys J 887(2):194

Fedorov A, Barabash S, Sauvaud JA, et al (2011) Measurements of the ion escape rates from Venus for solar minimum. J Geophys Res Space Phys 116(A7):A07220. https://doi.org/10.1029/2011JA016427

Fegley B (2003) Venus. In: Holland HD, Turekian KK (eds) Treatise on geochemistry, vol 1. Elsevier, Oxford, pp 487–507. https://doi.org/10.1016/B0-08-043751-6/01038-4

Ferraz-Mello S (2026) Exoplanet synchronization in the habitable zone: learning from Venus' retrograde rotation. Astron J 171(4):206. https://doi.org/10.3847/1538-3881/ae43e4. arXiv:2512.06526 [astro-ph.EP]

Feulner G (2012) The faint young sun problem. Rev Geophys 50(2)

Feulner G, Bukenberger M, Petri S (2023) Tracing the snowball bifurcation of aquaplanets through time reveals a fundamental shift in critical-state dynamics. Earth Syst Dyn 14(3):533–547

Foley BJ (2019) Habitability of Earth-like stagnant lid planets: climate evolution and recovery from snowball states. Astrophys J 875(1):72. https://doi.org/10.3847/1538-4357/ab0f31

Foley BJ, Smye Astron J (2018) Carbon cycling and habitability of Earth-sized stagnant lid planets. Astrobiology 18(7):873–896. https://doi.org/10.1089/ast.2017.1695

Fossati L, Erkaev NV, Lammer H, et al (2017) Aeronomical constraints to the minimum mass and maximum radius of hot low-mass planets. Astron Astrophys 598:A90. https://doi.org/10.1051/0004-6361/201629716

Fox J, Dalgarno A (1980) The production of nitrogen atoms on Mars and their escape. Planet Space Sci 28(1):41–46. https://doi.org/10.1016/0032-0633(80)90102-6

Fox JL, Hać A (1997) The $^{15}N/^{14}N$ isotope fractionation in dissociative recombination of N_2^+. J Geophys Res 102(E4):9191–9204. https://doi.org/10.1029/97JE00086

France K, Loyd ROP, Youngblood A, et al (2016) The MUSCLES treasury survey. I. Motivation and overview. Astrophys J 820(2):89. https://doi.org/10.3847/0004-637X/820/2/89

Frost DJ, Liebske C, Langenhorst F, et al (2004) Experimental evidence for the existence of iron-rich metal in the Earth's lower mantle. Nature 428(6981):409–412. https://doi.org/10.1038/nature02413

Fulton BJ, Petigura EA (2018) The California-Kepler survey. VII. Precise planet radii leveraging Gaia DR2 reveal the stellar mass dependence of the planet radius gap. Astron J 156(6):264. https://doi.org/10.3847/1538-3881/aae828

Fulton BJ, Petigura EA, Howard AW, et al (2017a) The California-Kepler survey. III. A gap in the radius distribution of small planets. Astron J 154(3):109. https://doi.org/10.3847/1538-3881/aa80eb. arXiv:1703.10375 [astro-ph.EP]

Fulton BJ, Petigura EA, Howard AW, et al (2017b) The California-Kepler survey. III. A gap in the radius distribution of small planets. Astron J 154(3):109

Fung J, Lee EJ (2018) Inner super-earths, outer gas giants: how pebble isolation and migration feedback keep jupiters cold. Astrophys J 859(2):126. https://doi.org/10.3847/1538-4357/aabaf7

Fuselier SA, Funsten HO, Heirtzler D, et al (2010) Energetic neutral atoms from the Earth's subsolar magnetopause. Geophys Res Lett 37(13):L13101. https://doi.org/10.1029/2010GL044140

Gaillard F, Scaillet B (2009) The sulfur content of volcanic gases on Mars. Earth Planet Sci Lett 279(1–2):34–43

Gaillard F, Scaillet B (2014) A theoretical framework for volcanic degassing chemistry in a comparative planetology perspective and implications for planetary atmospheres. Earth Planet Sci Lett 403:307–316

Gaillard F, Scaillet B, Arndt NT (2011) Atmospheric oxygenation caused by a change in volcanic degassing pressure. Nature 478(7368):229–232

Gaillard F, Bouhifd MA, Füri E, et al (2021) The diverse planetary ingassing/outgassing paths produced over billions of years of magmatic activity. Space Sci Rev 217(1):22. https://doi.org/10.1007/s11214-021-00802-1

Gaillard F, Bernadou F, Roskosz M, et al (2022a) Redox controls during magma ocean degassing. Earth Planet Sci Lett 577:117255. https://doi.org/10.1016/j.epsl.2021.117255

Gaillard F, Malavergne V, Bouhifd MA, et al (2022b) A speciation model linking the fate of carbon and hydrogen during core–magma ocean equilibration. Earth Planet Sci Lett 577:117266

Gao P, Hu R, Robinson TD, et al (2015) Stability of CO2 atmospheres on desiccated M dwarf exoplanets. Astrophys J 806(2):249. https://doi.org/10.1088/0004-637X/806/2/249

Gao P, Wakeford HR, Moran SE, et al (2021) Aerosols in exoplanet atmospheres. J Geophys Res Planets 126(4):e06655. https://doi.org/10.1029/2020JE006655

Geissler P, McMillan M (2008) Galileo observations of volcanic plumes on io. Icarus 197(2):505–518

Genda H, Abe Y (2005) Enhanced atmospheric loss on protoplanets at the giant impact phase in the presence of oceans. Nature 433(7028):842–844

Giggenbach WF (1996) Chemical composition of volcanic gases. In: Scarpa R, Tilling RI (eds) Monitoring and mitigation of volcano hazards. Springer, Berlin, pp 221–256. https://doi.org/10.1007/978-3-642-80087-0_7

Gillmann C, Chassefière E, Lognonné P (2009) A consistent picture of early hydrodynamic escape of Venus atmosphere explaining present Ne and Ar isotopic ratios and low oxygen atmospheric content. Earth Planet Sci Lett 286(3–4):503–513. https://doi.org/10.1016/j.epsl.2009.07.016

Gillmann C, Lognonné P, Moreira M (2011) Volatiles in the atmosphere of Mars: the effects of volcanism and escape constrained by isotopic data. Earth Planet Sci Lett 303(3–4):299–309

Gillmann C, Way MJ, Avice G, et al (2022) The long-term evolution of the atmosphere of Venus: processes and feedback mechanisms. Space Sci Rev 218(7):56. https://doi.org/10.1007/s11214-022-00924-0

Ginzburg S, Chiang E (2019) The end of runaway: how gap opening limits the final masses of gas giants. Mon Not R Astron Soc 487(1):681–690. https://doi.org/10.1093/mnras/stz1322

Ginzburg S, Schlichting HE, Sari R (2016) Super-Earth atmospheres: self-consistent gas accretion and retention. Astrophys J 825(1):29. https://doi.org/10.3847/0004-637X/825/1/29

Ginzburg S, Schlichting HE, Sari R (2018) Core-powered mass-loss and the radius distribution of small exoplanets. Mon Not R Astron Soc 476(1):759–765. https://doi.org/10.1093/mnras/sty290
Glein CR (2015) Noble gases, nitrogen, and methane from the deep interior to the atmosphere of Titan. Icarus 250:570–586. https://doi.org/10.1016/j.icarus.2015.01.001
Goldblatt C, Zahnle KJ (2011a) Clouds and the faint young sun paradox. Clim Past 7(1):203–220
Goldblatt C, Zahnle KJ (2011b) Faint young sun paradox remains. Nature 474(7349):E1–E1
Goldblatt C, McDonald VL, McCusker KE (2021) Earth's long-term climate stabilized by clouds. Nat Geosci 14(3):143–150
Gómez-Leal I, Kaltenegger L, Lucarini V, et al (2019) Climate sensitivity to ozone and its relevance on the habitability of Earth-like planets. Icarus 321:608–618. https://doi.org/10.1016/j.icarus.2018.11.019
Greene TP, Bell TJ, Ducrot E, et al (2023) Thermal emission from the Earth-sized exoplanet TRAPPIST-1 b using JWST. Nature 618(7963):39–42. https://doi.org/10.1038/s41586-023-05951-7
Gregory BS, Elliott RD, Deighan J, et al (2023) HCO^+ dissociative recombination: a significant driver of nonthermal hydrogen loss at Mars. J Geophys Res Planets 128(1):e2022JE007576. https://doi.org/10.1029/2022JE007576
Grenfell JL, Leconte J, Forget F, et al (2020) Possible atmospheric diversity of low mass exoplanets - some central aspects. Space Sci Rev 216(5):98. https://doi.org/10.1007/s11214-020-00716-4
Gronoff G, Arras P, Baraka S, et al (2020) Atmospheric escape processes and planetary atmospheric evolution. J Geophys Res Space Phys 125(8):e27639. https://doi.org/10.1029/2019JA02763910.1002/essoar.10502458.1
Güdel M (2015) Faint young sun paradox Springer, Berlin. https://doi.org/10.1007/978-3-662-44185-5_1700
Guimond CM, Spohn T, Berdyugina S, et al (2026) Water versus land on temperate rocky planets. Space Sci Rev 222(1):8. https://doi.org/10.1007/s11214-025-01264-5. arXiv:2512.09785 [astro-ph.EP]
Gulcher Astron J, Gerya T, Fournier AM, et al (2020) Consequences of stagnant lid convection on the volatile cycles of terrestrial planets. Nat Geosci 13:548–554. https://doi.org/10.1038/s41561-020-0592-3
Gunell H, Maggiolo R, Nilsson H, et al (2018) Why an intrinsic magnetic field does not protect a planet against atmospheric escape. Astron Astrophys 614:L3. https://doi.org/10.1051/0004-6361/201832934
Gupta A, Schlichting HE (2019) Sculpting the valley in the radius distribution of small exoplanets as a by-product of planet formation: the core-powered mass-loss mechanism. Mon Not R Astron Soc 487(1):24–33. https://doi.org/10.1093/mnras/stz1230
Guzewich SD, Way MJ, Aleinov I, et al (2021) 3d simulations of the early Martian hydrological cycle mediated by a h2-co2 greenhouse. J Geophys Res Planets 126(7):e2021JE006825
Haaland S, Eriksson A, Engwall E, et al (2012) Estimating the capture and loss of cold plasma from ionospheric outflow. J Geophys Res Space Phys 117(A7):A07311. https://doi.org/10.1029/2012JA017679
Haberle RM, Zahnle K, Barlow NG, et al (2019) Impact degassing of H_2 on early Mars and its effect on the climate system. Geophys Res Lett 46(22):13355–13362
Hadid LZ, Delcourt D, Saito Y, et al (2024) BepiColombo observations of cold oxygen and carbon ions in the flank of the induced magnetosphere of Venus. Nat Astron 8:716–724. https://doi.org/10.1038/s41550-024-02247-2
Hamano K, Abe Y, Genda H (2013) Emergence of two types of terrestrial planet on solidification of magma ocean. Nature 497(7451):607–610
Hansen JE, Hovenier J (1974) Interpretation of the polarization of Venus. J Atmos Sci 31(4):1137–1160
Haqq-Misra JD, Domagal-Goldman SD, Kasting P, et al (2008) A revised, hazy methane greenhouse for the archean Earth. Astrobiology 8(6):1127–1137
Harman C, Schwieterman E, Schottelkotte J, et al (2015) Abiotic O2 levels on planets around F, G, K, and M stars: possible false positives for life? Astrophys J 812:137. https://doi.org/10.1088/0004-637X/812/2/137
Harman CE, Felton R, Hu R, et al (2018) Abiotic O_2 levels on planets around F, G, K, and M stars: effects of lightning-produced catalysts in eliminating oxygen false positives. Astrophys J 866(1):56. https://doi.org/10.3847/1538-4357/aadd9b
Harper CL, Jacobsen SB (1996) Noble gases and Earth's accretion. Science 273(5283):1814–1818. https://doi.org/10.1126/science.273.5283.1814
Hartle RE, Grebowsky JM (1990) Upward ion flow in ionospheric holes on Venus. J Geophys Res 95(A1):31–37. https://doi.org/10.1029/JA095iA01p00031
Hashimoto GL, Abe Y, Sugita S (2007) The chemical composition of the early terrestrial atmosphere: formation of a reducing atmosphere from CI-like material. J Geophys Res Planets 112:E5
Hayashi C, Nakazawa K, Mizuno H (1979) Earth's melting due to the blanketing effect of the primordial dense atmosphere. Earth Planet Sci Lett 43(1):22–28
Heath MJ, Doyle LR, Joshi MM, et al (1999) Habitability of planets around red dwarf stars. Orig Life Evol Biosph 29(4):405–424. https://doi.org/10.1023/A:1006596718708

Heays A.N., Kaiserová T, Rimmer PB, et al (2022) Nitrogen oxide production in laser-induced breakdown simulating impacts on the Hadean atmosphere. J Geophys Res Planets 127(3):e06842. https://doi.org/10.1029/2021JE006842

Herbort O, Sereinig L (2025) The atmospheres of rocky exoplanets: III. Using atmospheric spectra to constrain surface rock composition. Astron Astrophys 699:A67. https://doi.org/10.1051/0004-6361/202453069. arXiv:2505.08883 [astro-ph.EP]

Hier-Majumder S, Hirschmann MM (2017) The origin of volatiles in the Earth's mantle. Geochem Geophys Geosyst 18(8):3078–3092. https://doi.org/10.1002/2017GC006937

Ho CSK, Van Eylen V (2023) A deep radius valley revealed by Kepler short cadence observations. Mon Not R Astron Soc 519(3):4056–4073. https://doi.org/10.1093/mnras/stac3802

Hoffman PF, Schrag DP (2002) The snowball Earth hypothesis: testing the limits of global change. Terra Nova 14(3):129–155. https://doi.org/10.1046/j.1365-3121.2002.00408.x

Hoffman PF, Kaufman Astron J, Halverson GP, et al (1998) A neoproterozoic snowball Earth. Science 281(5381):1342–1346. https://doi.org/10.1126/science.281.5381.1342

Hoffman PF, Abbot DS, Ashkenazy Y, et al (2017) Snowball Earth climate dynamics and Cryogenian geology-geobiology. Sci Adv 3(11):e1600983. https://doi.org/10.1126/sciadv.1600983

Hon M, Rappaport S, Shporer A, et al (2025) A disintegrating rocky planet with prominent comet-like tails around a bright star. Astrophys J Lett 984(1):L3. https://doi.org/10.3847/2041-8213/adbf21

Höning D, Tosi N, Spohn T (2019) Carbon cycling and interior evolution of water-covered plate tectonics and stagnant-lid planets. Astron Astrophys 627:A48. https://doi.org/10.1051/0004-6361/201935091

Höning D, Baumeister P, Grenfell JL, et al (2021) Early Habitability and Crustal Decarbonation of a Stagnant-Lid Venus. J Geophys Res Planets 126(10). https://doi.org/10.1029/2021JE006895

Hori Y, Ikoma M (2011) Gas giant formation with small cores triggered by envelope pollution by icy planetesimals. Mon Not R Astron Soc 416(2):1419–1429. https://doi.org/10.1111/j.1365-2966.2011.19140.x

Hu R, Delgado Diaz H (2019) Stability of nitrogen in planetary atmospheres in contact with liquid water. Astrophys J 886(2):126. https://doi.org/10.3847/1538-4357/ab4cea

Hu R, Thomas TB (2022) A nitrogen-rich atmosphere on ancient Mars consistent with isotopic evolution models. Nat Geosci 15(2):106–111. https://doi.org/10.1038/s41561-021-00886-y

Hu Y, Yang J (2014) Role of ocean heat transport in climates of tidally locked exoplanets around m dwarf stars. Proc Natl Acad Sci USA 111(2):629–634

Hu R, Seager S, Bains W (2012) Photochemistry in terrestrial exoplanet atmospheres. I. Photochemistry model and benchmark cases. Astrophys J 761(2):166. https://doi.org/10.1088/0004-637X/761/2/166. arXiv:1210.6885 [astro-ph.EP]

Hu R, Bello-Arufe A, Zhang M, et al (2024) A secondary atmosphere on the rocky exoplanet 55 Cancri e. Nature 630:609–612. https://doi.org/10.1038/s41586-024-07432-x

Hunten DM, Pepin RO, Walker JCG (1987) Mass fractionation in hydrodynamic escape. Icarus 69(3):532–549. https://doi.org/10.1016/0019-1035(87)90022-4

Hyde WT, Crowley TJ, Baum SK, et al (2000) Neoproterozoic 'snowball Earth' simulations with a coupled climate/ice-sheet model. Nature 405(6785):425–429. https://doi.org/10.1038/35013005

Ikoma M, Genda H (2006) Constraints on the mass of a habitable planet with water of nebular origin. Astrophys J 648(1):696–706. https://doi.org/10.1086/505780

Ikoma M, Hori Y (2012) In situ accretion of hydrogen-rich atmospheres on short-period super-earths: implications for the Kepler-11 planets. Astrophys J 753(1):66. https://doi.org/10.1088/0004-637X/753/1/66. arXiv:1204.5302 [astro-ph.EP]

Ikoma M, Nakazawa K, Emori H (2000) Formation of giant planets: dependences on core accretion rate and grain opacity. Astrophys J 537(2):1013–1025. https://doi.org/10.1086/309050

Ikoma M, Elkins-Tanton L, Hamano K, et al (2018) Water partitioning in planetary embryos and protoplanets with magma oceans. Space Sci Rev 214(4):76. https://doi.org/10.1007/s11214-018-0508-3

Ingersoll AP (1969) The runaway greenhouse: a history of water on Venus. J Atmos Sci 26(6):1191–1198. https://doi.org/10.1175/1520-0469(1969)026<1191:TRGAHO>2.0.CO;2

Inui S, Seki K, Sakai S, et al (2019) Statistical study of heavy ion outflows from Mars observed in the Martian-induced magnetotail by MAVEN. J Geophys Res Space Phys 124(7):5482–5497. https://doi.org/10.1029/2018JA026452

Jackson AP, Davis TA, Wheatley PJ (2012) The coronal X-ray-age relation and its implications for the evaporation of exoplanets. Mon Not R Astron Soc 422(3):2024–2043. https://doi.org/10.1111/j.1365-2966.2012.20657.x

Jakosky BM, Brain D, Chaffin M, et al (2018) Loss of the Martian atmosphere to space: present-day loss rates determined from MAVEN observations and integrated loss through time. Icarus 315:146–157. https://doi.org/10.1016/j.icarus.2018.05.030

Jaziri AY, Sohier O, Venot O, et al (2025) Unraveling the non-equilibrium chemistry of the temperate sub-Neptune K2-18 b. Astron Astrophys 701:A33. https://doi.org/10.1051/0004-6361/202555496

Jeans JH (1955) The dynamical theory of gases. Dover, New York
Jin S, Mordasini C (2018) Compositional imprints in density-distance-time: a rocky composition for close-in low-mass exoplanets from the location of the valley of evaporation. Astrophys J 853(2):163. https://doi.org/10.3847/1538-4357/aa9f1e. arXiv:1706.00251 [astro-ph.EP]
Johansen A, Ronnet T, Bizzarro M, et al (2021) A pebble accretion model for the formation of the terrestrial planets in the Solar System. Sci Adv 7(8):eabc0444. https://doi.org/10.1126/sciadv.abc0444
Johnstone CP (2020) Hydrodynamic escape of water vapor atmospheres near very active stars. Astrophys J 890(1):79. https://doi.org/10.3847/1538-4357/ab6224
Johnstone CP, Güdel M, Lammer H, et al (2018) Upper atmospheres of terrestrial planets: carbon dioxide cooling and the Earth's thermospheric evolution. Astron Astrophys 617:A107. https://doi.org/10.1051/0004-6361/201832776. arXiv:1806.06897 [astro-ph.EP]
Johnstone CP, Bartel M, Güdel M (2021a) The active lives of stars: a complete description of the rotation and XUV evolution of F, G, K, and M dwarfs. Astron Astrophys 649:A96. https://doi.org/10.1051/0004-6361/202038407
Johnstone CP, Lammer H, Kislyakova KG, et al (2021b) The young Sun's XUV-activity as a constraint for lower CO_2-limits in the Earth's Archean atmosphere. Earth Planet Sci Lett 576:117197. https://doi.org/10.1016/j.epsl.2021.117197
Joshi M (2003) Climate model studies of synchronously rotating planets. Astrobiology 3(2):415–427
Kamada A, Kuroda T, Kasaba Y, et al (2020) A coupled atmosphere–hydrosphere global climate model of early Mars: a 'cool and wet'scenario for the formation of water channels. Icarus 338:113567
Kanzaki Y, Murakami T (2015) Estimates of atmospheric CO_2 in the Neoarchean-Paleoproterozoic from paleosols. Geochim Cosmochim Acta 159:190–219. https://doi.org/10.1016/j.gca.2015.03.011
Kasting JF (1988) Runaway and moist greenhouse atmospheres and the evolution of Earth and Venus. Icarus 74(3):472–494. https://doi.org/10.1016/0019-1035(88)90116-9
Kasting JF (2010) Faint young sun redux. Nature 464(7289):687–689
Kasting JF, Catling D (2003) Evolution of a habitable planet. Annu Rev Astron Astrophys 41(1):429–463
Kasting JF, Whitmire DP, Reynolds RT (1993) Habitable zones around main sequence stars. Icarus 101(1):108–128. https://doi.org/10.1006/icar.1993.1010
Katyal N, Ortenzi G, Lee Grenfell J (2020) Effect of mantle oxidation state and escape upon the evolution of Earth's magma ocean atmosphere. Astron Astrophys 643:A81. https://doi.org/10.1051/0004-6361/202038779
Kaula WM (1999) Constraints on Venus evolution from radiogenic argon. Icarus 139(1):32–39. https://doi.org/10.1006/icar.1999.6082
Kegerreis J, Eke V, Massey R, et al (2020) Atmospheric erosion by giant impacts onto terrestrial planets. Astrophys J 897(2):161
Keika K, Nosé M, Brandt PC, et al (2006) Contribution of charge exchange loss to the storm time ring current decay: IMAGE/HENA observations. J Geophys Res Space Phys 111(A11):A11S12. https://doi.org/10.1029/2006JA011789
Kempton EMR, Knutson HA (2024) Transiting exoplanet atmospheres in the era of JWST. Rev Mineral Geochem 90(1):411–464. https://doi.org/10.2138/rmg.2024.90.12
Kim J, Nagy AF, Fox JL, et al (1998) Solar cycle variability of hot oxygen atoms at Mars. J Geophys Res 103(A12):29339–29342. https://doi.org/10.1029/98JA02727
King MD, Platnick S, Menzel WP, et al (2013) Spatial and temporal distribution of clouds observed by modis onboard the terra and aqua satellites. IEEE Trans Geosci Remote Sens 51(7):3826–3852. https://doi.org/10.1109/TGRS.2012.2227333
Kirk J, Dos Santos LA, López-Morales M, et al (2022) Keck/NIRSPEC studies of He I in the atmospheres of two inflated hot gas giants orbiting K dwarfs: WASP-52b and WASP-177b. Astron J 164(1):24. https://doi.org/10.3847/1538-3881/ac722f
Kite ES, Barnett MN (2020) Exoplanet secondary atmosphere loss and revival. Proc Natl Acad Sci USA 117:18264–18271. https://doi.org/10.1073/pnas.2006177117
Kite ES, Fegley B Jr, Schaefer L, et al (2016) Atmosphere-interior exchange on hot, rocky exoplanets. Astrophys J 828(2):80
Knutson HA, Charbonneau D, Allen LE, et al (2007) A map of the day-night contrast of the extrasolar planet HD 189733b. Nature 447(7141):183–186. https://doi.org/10.1038/nature05782
Kobayashi K, Airapetian VS, Udo T, et al (2026) Proton irradiation of primitive atmospheres of young exoplanets and early Earth: N_2O greenhouse warming and prebiotic synthesis. Astrophys J Lett 1002:L12. https://doi.org/10.3847/2041-8213/ae5491
Komabayasi M (1967) Discrete equilibrium temperatures of a hypothetical planet with the atmosphere and the hydrosphere of one component-two phase system under constant solar radiation. J Meteorol Soc Jpn Ser II 45(1):137–139. https://doi.org/10.2151/jmsj1965.45.1_137

Kopparapu RK, Ramirez R, Kasting JF, et al (2013) Habitable zones around main-sequence stars: new estimates. Astrophys J 765(2):131. https://doi.org/10.1088/0004-637X/765/2/131
Kreidberg L, Bean JL, Désert JM, et al (2014) Clouds in the atmosphere of the super-Earth exoplanet GJ1214b. Nature 505(7481):69–72. https://doi.org/10.1038/nature12888
Kreidberg L, Koll DDB, Morley C, et al (2019) Absence of a thick atmosphere on the terrestrial exoplanet LHS 3844b. Nature 573(7772):87–90. https://doi.org/10.1038/s41586-019-1497-4
Krissansen-Totton J, Fortney JJ, Nimmo F (2021a) Was Venus ever habitable? Constraints from a coupled interior–atmosphere–redox evolution model. Planet Sci J 2(5):216
Krissansen-Totton J, Galloway ML, Wogan N, et al (2021b) Waterworlds probably do not experience magmatic outgassing. Astrophys J 913(2):107. https://doi.org/10.3847/1538-4357/abf560
Krissansen-Totton J, Thompson M, Galloway ML, et al (2022) Understanding planetary context to enable life detection on exoplanets and test the Copernican principle. Nat Astron 6:189–198. https://doi.org/10.1038/s41550-021-01579-7. arXiv:2202.10333 [astro-ph.EP]
Krissansen-Totton J, Wogan N, Thompson M, et al (2024) The erosion of large primary atmospheres typically leaves behind substantial secondary atmospheres on temperate rocky planets. Nat Commun 15(1):8374. https://doi.org/10.1038/s41467-024-52642-6
Kubyshkina D, Fossati L, Erkaev NV, et al (2018) Grid of upper atmosphere models for 1-40 $M_\oplus$ planets: application to CoRoT-7 b and HD 219134 b,c. Astron Astrophys 619:A151. https://doi.org/10.1051/0004-6361/201833737. arXiv:1809.06645 [astro-ph.EP]
Kubyshkina D, Way MJ, Dandouras I, et al (2026) Upper atmosphere dynamics and drivers of volatiles loss from terrestrial-type (exo)planets. Space Sci Rev 222(3):28. https://doi.org/10.1007/s11214-026-01283-w. arXiv:2602.15507 [astro-ph.EP]
Kurokawa H, Kurosawa K, Usui T (2018) A lower limit of atmospheric pressure on early Mars inferred from nitrogen and argon isotopic compositions. Icarus 299:443–459. https://doi.org/10.1016/j.icarus.2017.08.020
Lacedelli G, Pallé E, Luque R, et al (2024) Characterisation of TOI-406 as a showcase of the THIRSTEE program: a two-planet system straddling the M-dwarf density gap. Astron Astrophys 692:A238. https://doi.org/10.1051/0004-6361/202452244
Lagage PO, Mandell A, Giménez A, et al (2026) The future of rocky worlds exploration. Space Sci Rev 222(4):40. https://doi.org/10.1007/s11214-026-01297-4
Lambrechts M, Johansen A, Morbidelli A (2014) Separating gas-giant and ice-giant planets by halting pebble accretion. Astron Astrophys 572:A35. https://doi.org/10.1051/0004-6361/201423814
Lammer H, Lichtenegger HIM, Biernat HK, et al (2006) Loss of hydrogen and oxygen from the upper atmosphere of Venus. Planet Space Sci 54(13–14):1445–1456. https://doi.org/10.1016/j.pss.2006.04.022
Lammer H, Zerkle AL, Gebauer S, et al (2018) Origin and evolution of the atmospheres of early Venus, Earth and Mars. Astron Astrophys Rev 26(1):2. https://doi.org/10.1007/s00159-018-0108-y
Lammer H, Scherf M, Kurokawa H, et al (2020) Loss and fractionation of noble gas isotopes and moderately volatile elements from planetary embryos and early Venus, Earth and Mars. Space Sci Rev 216(4):74. https://doi.org/10.1007/s11214-020-00701-x
Lammer H, Brasser R, Johansen A, et al (2021) Formation of Venus, Earth and Mars: constrained by isotopes. Space Sci Rev 217(1):7. https://doi.org/10.1007/s11214-020-00778-4. arXiv:2102.06173 [astro-ph.EP]
Lammer H, Scherf M, Sproß L (2024) Eta-Earth revisited I: a formula for estimating the maximum number of Earth-like habitats. Astrobiology 24(10):897–915. https://doi.org/10.1089/ast.2023.0075
Laneuville M, Kameya M, Cleaves HJII (2018) Earth without life: a systems model of a global abiotic nitrogen cycle. Astrobiology 18(7):897–914. https://doi.org/10.1089/ast.2017.1700
Lavvas P, Coustenis A, Vardavas I (2008) Coupling photochemistry with haze formation in Titan's atmosphere, part ii: results and validation with Cassini/Huygens data. Planet Space Sci 56(1):67–99. https://doi.org/10.1016/j.pss.2007.05.027
Leblanc F, Modolo R, Curry S, et al (2015) Mars heavy ion precipitating flux as measured by Mars atmosphere and volatile EvolutioN. Geophys Res Lett 42(21):9135–9141. https://doi.org/10.1002/2015GL066170
Leblanc F, Martinez A, Chaufray JY, et al (2018) On Mars's atmospheric sputtering after MAVEN's first Martian year of measurements. Geophys Res Lett 45(10):4685–4691. https://doi.org/10.1002/2018GL077199
Lebrun T, Massol H, ChassefièRe E, et al (2013) Thermal evolution of an early magma ocean in interaction with the atmosphere. J Geophys Res Planets 118:1155–1176. https://doi.org/10.1002/jgre.20068
Leconte J, Forget F, Charnay B, et al (2013) Increased insolation threshold for runaway greenhouse processes on Earth-like planets. Nature 504(7479):268–271. https://doi.org/10.1038/nature12827
Leconte J, Wu H, Menou K, et al (2015) Asynchronous rotation of Earth-mass planets in the habitable zone of lower-mass stars. Science 347(6222):632–635. https://doi.org/10.1126/science.1258686. arXiv:1502.01952 [astro-ph.EP]

Ledvina SA, Brecht SH, Brain DA, et al (2017) Ion escape rates from Mars: results from hybrid simulations compared to maven observations. J Geophys Res Space Phys 122(8):8391–8408. https://doi.org/10.1002/2016JA023521
Lee EJ, Chiang E (2015) To cool is to accrete: analytic scalings for nebular accretion of planetary atmospheres. Astrophys J 811(1):41. https://doi.org/10.1088/0004-637X/811/1/41. arXiv:1508.05096 [astro-ph.EP]
Lee EJ, Chiang E (2016) Breeding super-earths and birthing super-puffs in transitional disks. Astrophys J 817(2):90. https://doi.org/10.3847/0004-637X/817/2/90
Lee EJ, Connors NJ (2021) Primordial radius gap and potentially broad core mass distributions of super-earths and sub-neptunes. Astrophys J 908(1):32. https://doi.org/10.3847/1538-4357/abd6c7
Lee EJ, Chiang E, Ormel CW (2014) Make super-earths, not jupiters: accreting nebular gas onto solid cores at 0.1 AU and beyond. Astrophys J 797(2):95. https://doi.org/10.1088/0004-637X/797/2/95
Lee EJ, Karalis A, Thorngren DP (2022) Creating the radius gap without mass loss. Astrophys J 941(2):186. https://doi.org/10.3847/1538-4357/ac9c66
Léger A, Fontecave M, Labeyrie A, et al (2011) Is the presence of oxygen on an exoplanet a reliable biosignature? Astrobiology 11(4):335–341
Lehmer OR, Catling DC, Buick R, et al (2020a) Atmospheric CO2 levels from 2.7 billion years ago inferred from micrometeorite oxidation. Sci Adv 6(4):eaay4644. https://doi.org/10.1126/sciadv.aay4644
Lehmer OR, Catling DC, Krissansen-Totton J (2020b) Carbonate-silicate cycle predictions of Earth-like planetary climates and testing the habitable zone concept. Nat Commun 11(1):6153. https://doi.org/10.1038/s41467-020-19896-2
Li Y (2024) The origin and evolution of Earth's nitrogen. Natl Sci Rev 11(6):nwae201. https://doi.org/10.1093/nsr/nwae201
Li H, He C, Wang S, et al (2025) The impact of organic hazes and graphite on the observation of CO_2-rich sub-Neptune atmospheres. Astrophys J Lett 990(2):L66. https://doi.org/10.3847/2041-8213/adfa87
Lichtenegger HIM, Dyadechkin S, Scherf M, et al (2022) Non-thermal escape of the Martian CO_2 atmosphere over time: constrained by Ar isotopes. Icarus 382:115009. https://doi.org/10.1016/j.icarus.2022.115009
Liggins P, Jordan S, Rimmer PB, et al (2022) Growth and evolution of secondary volcanic atmospheres: I. identifying the geological character of hot rocky planets. J Geophys Res Planets 127(7):e2021JE007123
Lillis RJ, Deighan J, Fox JL, et al (2017a) Photochemical escape of oxygen from Mars: first results from MAVEN in situ data. J Geophys Res Space Phys 122(3):3815–3836. https://doi.org/10.1002/2016JA023525
Lillis RJ, Deighan J, Fox JL, et al (2017b) Photochemical escape of oxygen from Mars: first results from MAVEN in situ data. J Geophys Res Space Phys 122(3):3815–3836. https://doi.org/10.1002/2016JA023525
Lin MY, Ilie R, Glocer A (2020) The contribution of n+ ions to Earth's polar wind. Geophys Res Lett 47(18):e2020GL089321. https://doi.org/10.1029/2020GL089321
Lingam M (2020) Implications of abiotic oxygen buildup for Earth-like complex life. Astron J 159(4):144. https://doi.org/10.3847/1538-3881/ab737f
Linsky J (2025) Host stars and their effects on exoplanet atmospheres: an introductory overview. Astrophysics and Space Science Library, vol 473. Springer, Cham. https://doi.org/10.1007/978-3-031-75208-7
Linsky JL, Yang H, France K, et al (2010) Observations of mass loss from the transiting exoplanet HD 209458b. Astrophys J 717(2):1291–1299. https://doi.org/10.1088/0004-637X/717/2/1291
Lock SJ, Stewart ST (2024) Atmospheric loss in giant impacts depends on preimpact surface conditions. Planet Sci J 5(2):28
Lockley IS, Armstrong DJ, Fernández Fernández J, et al (2025) The TOI-1117 multiplanetary system: 3 sub-Neptunes, 1 in both the Neptunian Desert and Radius Valley. Mon Not R Astron Soc 541(2):919–938. https://doi.org/10.1093/mnras/staf939
Lodders K, Fegley B (2026) Sulfur in the giant planets, their moons, and extrasolar gas giant planets. In: Harlov DE, Pokrovski GS (eds) The role of sulfur in planetary processes. Springer, Cham, pp 1447–1516. https://doi.org/10.1007/978-3-032-07705-9_19
Lopez ED, Fortney JJ, Miller N (2012) How thermal evolution and mass-loss sculpt populations of super-earths and sub-neptunes: application to the Kepler-11 system and beyond. Astrophys J 761(1):59. https://doi.org/10.1088/0004-637X/761/1/59
Lorenz RD, Lunine JI, McKay CP (1997) Titan under a red giant sun: a new kind of "habitable" moon. Geophys Res Lett 24(22):2905–2908. https://doi.org/10.1029/97GL52843
Loyd ROP, France K, Youngblood A, et al (2016) The MUSCLES treasury survey. III. X-ray to infrared spectra of 11 M and K stars hosting planets. Astrophys J 824(2):102. https://doi.org/10.3847/0004-637X/824/2/102
Luger R, Barnes R (2015) Extreme water loss and abiotic O_2 buildup on planets throughout the habitable zones of m dwarfs. Astrobiology 15(2):119–143

Luhmann JG, Kozyra JU (1991) Dayside pickup oxygen ion precipitation at Venus and Mars: spatial distributions, energy deposition and consequences. J Geophys Res 96(A4):5457–5467. https://doi.org/10.1029/90JA01753
Luhmann JG, Ledvina SA, Russell CT (2004) Induced magnetospheres. Adv Space Res 33(11):1905–1912. https://doi.org/10.1016/j.asr.2003.03.031
Luisi PL (2016) The emergence of life: from chemical origins to synthetic biology, 2nd edn. Cambridge University Press, Cambridge
Lundin R, Barabash S, Holmström M, et al (2013) Solar cycle effects on the ion escape from Mars. Geophys Res Lett 40(23):6028–6032. https://doi.org/10.1002/2013GL058154
Luque R, Pallé E (2022) Density, not radius, separates rocky and water-rich small planets orbiting M dwarf stars. Science 377(6611):1211–1214. https://doi.org/10.1126/science.abl7164
Luspay-Kuti A, Mandt K (eds) (2025) Triton and Pluto. 2514-3433, IOP Publishing. https://doi.org/10.1088/2514-3433/ad5278
Lyons TW, Reinhard CT, Planavsky NJ (2014) The rise of oxygen in Earth's early ocean and atmosphere. Nature 506(7488):307–315. https://doi.org/10.1038/nature13068
Macdonald E, Paradise A, Menou K, et al (2022) Climate uncertainties caused by unknown land distribution on habitable M-earths. Mon Not R Astron Soc 513(2):2761–2769. https://doi.org/10.1093/mnras/stac1040 arXiv:2110.04310 [astro-ph.EP]
MacKenzie SM, Birch SP, Hörst S, et al (2021) Titan: Earth-like on the outside, ocean world on the inside. Planet Sci J 2(3):112
Madhusudhan N, Agúndez M, Moses JI, et al (2016) Exoplanetary atmospheres—chemistry, formation conditions, and habitability. Space Sci Rev 205(1–4):285–348. https://doi.org/10.1007/s11214-016-0254-3
Madhusudhan N, Holmberg M, Constantinou S, et al (2025) Exploring the sub-Neptune frontier with JWST. Proc Natl Acad Sci USA 122(39):e2416194122. https://doi.org/10.1073/pnas.2416194122
Mahapatra G, Helling C, Miguel Y (2017) Cloud formation in metal-rich atmospheres of hot super-earths like 55 Cnc e and CoRoT7b. Mon Not R Astron Soc 472(1):447–464. https://doi.org/10.1093/mnras/stx1666
Mak MT, Mayne NJ, Sergeev DE, et al (2023) 3D simulations of the archean Earth including photochemical haze profiles. J Geophys Res, Atmos 128(20):e2023JD039343. https://doi.org/10.1029/2023JD039343
Mak MT, Sergeev DE, Mayne N, et al (2024) 3D simulations of TRAPPIST-1e with varying CO_2, CH_4, and haze profiles. Mon Not R Astron Soc 529(4):3971–3987. https://doi.org/10.1093/mnras/stae741. arXiv:2403.06928 [astro-ph.EP]
Mallik A, Li Y, Wiedenbeck M (2018) Nitrogen evolution within the Earth's atmosphere-mantle system assessed by recycling in subduction zones. Earth Planet Sci Lett 482:556–566. https://doi.org/10.1016/j.epsl.2017.11.045
Malsky I, Rogers LA (2020) Coupled thermal and compositional evolution of photoevaporating planet envelopes. Astrophys J 896(1):48. https://doi.org/10.3847/1538-4357/ab873f
Marcq E (2018) A simple model for the CO2 photochemistry in the upper atmosphere of Venus. Icarus 307:308–315. https://doi.org/10.1016/j.icarus.2018.02.024
Marley MS, Ackerman AS, Cuzzi JN, et al (2013) Clouds and hazes in exoplanet atmospheres. In: Mackwell SJ, Simon-Miller AA, Harder JW, et al (eds) Comparative climatology of terrestrial planets, pp 367–392. https://doi.org/10.2458/azu_uapress_9780816530595-ch015
Marois C, Zuckerman B, Konopacky QM, et al (2010) Images of a fourth planet orbiting HR 8799. Nature 468(7327):1080–1083. https://doi.org/10.1038/nature09684. arXiv:1011.4918 [astro-ph.EP]
Marty B (2012) The origins and concentrations of water, carbon, nitrogen and noble gases on Earth. Earth Planet Sci Lett 313:56–66. https://doi.org/10.1016/j.epsl.2011.10.040
Marty B, Zimmermann L, Pujol M, et al (2013) Nitrogen isotopic composition and density of the archean atmosphere. Science 342(6154):101–104. https://doi.org/10.1126/science.1240971
Maruyama S, Santosh M (2008) Models on Snowball Earth and Cambrian explosion: A synopsis. Gondwana Res 14(1–2):22–32. https://doi.org/10.1016/j.gr.2008.01.004
Matsui T, Abe Y (1986) Impact-induced atmospheres and oceans on Earth and Venus. Nature 322(6079):526–528. https://doi.org/10.1038/322526a0
Maurice M, Dasgupta R, Hassanzadeh P (2024) Volatile atmospheres of lava worlds. Astron Astrophys 688:A47. https://doi.org/10.1051/0004-6361/202347749
Mayor M, Queloz D (1995) A Jupiter-mass companion to a solar-type star. Nature 378(6555):355–359. https://doi.org/10.1038/378355a0
McDonald GD, Kreidberg L, Lopez E (2019) The sub-Neptune desert and its dependence on stellar type: controlled by lifetime X-ray irradiation. Astrophys J 876(1):22. https://doi.org/10.3847/1538-4357/ab1095. arXiv:2105.00142 [astro-ph.EP]
Meadows VS (2017) Reflections on O_2 as a biosignature in exoplanetary atmospheres. Astrobiology 17(10):1022–1052

Meadows VS, Reinhard CT, Arney GN, et al (2018) Exoplanet biosignatures: understanding oxygen as a biosignature in the context of its environment. Astrobiology 18(6):630–662. https://doi.org/10.1089/ast.2017.1727

Meier Valdes EA, Demory BO, Diamond-Lowe H, et al (2025) Hot Rocks Survey II: the thermal emission of TOI-1468 b reveals a hot bare rock. Astron Astrophys 698:A68. https://doi.org/10.1051/0004-6361/202453449

Meier R, Anderson G, Cantrell C, et al (1997) Actinic radiation in the terrestrial atmosphere. J Atmos Sol-Terr Phys 59(17):2111–2157. https://doi.org/10.1016/S1364-6826(97)00047-3

Mikhail S, Sverjensky DA (2014) Nitrogen speciation in upper mantle fluids and the origin of Earth's nitrogen-rich atmosphere. Nat Geosci 7(11):816–819. https://doi.org/10.1038/ngeo2271

Miller SL, Urey HC (1959) Organic compound synthesis on the primitive Earth: several questions about the origin of life have been answered, but much remains to be studied. Science 130(3370):245–251

Miller KE, Glein CR, Waite JH (2019) Contributions from accreted organics to Titan's atmosphere: new insights from cometary and chondritic data. Astrophys J 871(1):59. https://doi.org/10.3847/1538-4357/aaf561

Misener W, Schulik M, Schlichting HE, et al (2025) Blowin' in the nonisothermal wind: core-powered mass loss with hydrodynamic radiative transfer. Astrophys J 980(1):152. https://doi.org/10.3847/1538-4357/ada777

Mizuno H, Nakazawa K, Hayashi C (1980) Dissolution of the primordial rare gases into the Molten Earth's material. Earth Planet Sci Lett 50(1):202–210. https://doi.org/10.1016/0012-821X(80)90131-4

Mol Lous M, Mordasini C, Helled R (2024) Accretion of primordial H-He atmospheres in mini-Neptunes: the importance of envelope enrichment. Astron Astrophys 685:A22. https://doi.org/10.1051/0004-6361/202349039

Moldenhauer TW, Kuiper R, Kley W, et al (2022) Recycling of the first atmospheres of embedded planets: dependence on core mass and optical depth. Astron Astrophys 661:A142. https://doi.org/10.1051/0004-6361/202141955

Morbidelli A, Lambrechts M, Jacobson S, et al (2015) The great dichotomy of the Solar System: small terrestrial embryos and massive giant planet cores. Icarus 258:418–429. https://doi.org/10.1016/j.icarus.2015.06.003

Mordasini C (2014) Grain opacity and the bulk composition of extrasolar planets. II. An analytical model for grain opacity in protoplanetary atmospheres. Astron Astrophys 572:A118. https://doi.org/10.1051/0004-6361/201423702

Mordasini C (2020) Planetary evolution with atmospheric photoevaporation. I. Analytical derivation and numerical study of the evaporation valley and transition from super-earths to sub-neptunes. Astron Astrophys 638:A52. https://doi.org/10.1051/0004-6361/201935541

Moreira M, Charnoz S (2016) The origin of the neon isotopes in chondrites and on Earth. Earth Planet Sci Lett 433:249–256. https://doi.org/10.1016/j.epsl.2015.11.002

Mukhopadhyay S (2012) Early differentiation and volatile accretion recorded in deep-mantle neon and xenon. Nature 486(7401):101–104

Nagy AF, Cravens TE, Yee JH, et al (1981) Hot oxygen atoms in the upper atmosphere of Venus. Geophys Res Lett 8(6):629–632. https://doi.org/10.1029/GL008i006p00629

Nakajima S, Hayashi YY, Abe Y (1992) A study on the "runaway greenhouse effect" with a one-dimensional radiative–convective equilibrium model. J Atmos Sci 49(23):2256–2266. https://doi.org/10.1175/1520-0469(1992)049<2256,ASOTGE>2.0.CO;2

Nakayama A, Ikoma M, Terada N (2022) Survival of terrestrial N_2-O_2 atmospheres in violent XUV environments through efficient atomic line radiative cooling. Astrophys J 937(2):72. https://doi.org/10.3847/1538-4357/ac86ca

Narita N, Enomoto T, Masaoka S, et al (2015) Titania may produce abiotic oxygen atmospheres on habitable exoplanets. Sci Rep 5(1):13977

Navarro-González R, Molina MJ, Molina LT (1998) Nitrogen fixation by volcanic lightning in the early Earth. Geophys Res Lett 25(16):3123–3126. https://doi.org/10.1029/98GL02423

Navarro-González R, McKay CP, Mvondo DN (2001) A possible nitrogen crisis for Archaean life due to reduced nitrogen fixation by lightning. Nature 412(6842):61–64. https://doi.org/10.1038/35083537

Nicholls H, Lichtenberg T, Bower DJ, et al (2024) Magma ocean evolution at arbitrary redox state. J Geophys Res Planets 129(12):2024JE008576. https://doi.org/10.1029/2024JE008576

Nicholls H, Lichtenberg T, Chatterjee RD, et al (2026) Volatile-rich evolution of molten super-Earth L 98-59 d. Nat Astron 10:809–817. https://doi.org/10.1038/s41550-026-02815-8

Nielsen J, Johansen A, Bali K, et al (2025) A primordial radius valley as a consequence of planet formation. Astron Astrophys 695:A184. https://doi.org/10.1051/0004-6361/202450326

Nikolaou A, Katyal N, Tosi N, et al (2019) What factors affect the duration and outgassing of the terrestrial magma ocean? Astrophys J 875(1):11

Nilsson H, Stenberg G, Futaana Y, et al (2012) Ion distributions in the vicinity of Mars: signatures of heating and acceleration processes. Earth Planets Space 64(2):135–148. https://doi.org/10.5047/eps.2011.04.011

Noack L, Lasbleis M (2020) Parameterisations of interior properties of rocky planets-an investigation of planets with Earth-like compositions but variable iron content. Astron Astrophys 638:A129

Noack L, Breuer D, Spohn T (2012) Coupling the atmosphere with interior dynamics: implications for the resurfacing of Venus. Icarus 217(2):484–498

Odert P, Lammer H, Erkaev NV, et al (2018) Escape and fractionation of volatiles and noble gases from Mars-sized planetary embryos and growing protoplanets. Icarus 307:327–346. https://doi.org/10.1016/j.icarus.2017.10.031

Olson PL, Sharp ZD (2019) Nebular atmosphere to magma ocean: a model for volatile capture during Earth accretion. Phys Earth Planet Inter 294:106294. https://doi.org/10.1016/j.pepi.2019.106294

Ormel CW (2014) An atmospheric structure equation for grain growth. Astrophys J Lett 789. https://api.semanticscholar.org/CorpusID:119261293

Ormel CW, Shi JM, Kuiper R (2015) Hydrodynamics of embedded planets' first atmospheres - II. A rapid recycling of atmospheric gas. Mon Not R Astron Soc 447(4):3512–3525. https://doi.org/10.1093/mnras/stu2704

O'Rourke JG, Korenaga J (2015) Thermal evolution of Venus with argon degassing. Icarus 260:128–140. https://doi.org/10.1016/j.icarus.2015.07.009

O'Rourke JG, Wilson CF, Borrelli ME, et al (2023) Venus, the planet: introduction to the evolution of Earth's sister planet. Space Sci Rev 219(1):10. https://doi.org/10.1007/s11214-023-00956-0

Ortenzi G, Noack L, Sohl F, et al (2020) Mantle redox state drives outgassing chemistry and atmospheric composition of rocky planets. Sci Rep 10(1):10907

Osborne HLM, Van Eylen V, Goffo E, et al (2024) TOI-544 b: a potential water-world inside the radius valley in a two-planet system. Mon Not R Astron Soc 527(4):11138–11157. https://doi.org/10.1093/mnras/stad3837

Owen JE, Campos Estrada B (2020) Testing exoplanet evaporation with multitransiting systems. Mon Not R Astron Soc 491(4):5287–5297. https://doi.org/10.1093/mnras/stz3435

Owen JE, Jackson AP (2012) Planetary evaporation by UV & X-ray radiation: basic hydrodynamics. Mon Not R Astron Soc 425(4):2931–2947. https://doi.org/10.1111/j.1365-2966.2012.21481.x

Owen JE, Mohanty S (2016) Habitability of terrestrial-mass planets in the HZ of M Dwarfs - I. H/He-dominated atmospheres. Mon Not R Astron Soc 459(4):4088–4108. https://doi.org/10.1093/mnras/stw959

Owen JE, Wu Y (2013) Kepler planets: a tale of evaporation. Astrophys J 775(2):105. https://doi.org/10.1088/0004-637X/775/2/105

Owen JE, Wu Y (2016) Atmospheres of low-mass planets: the "boil-off". Astrophys J 817(2):107. https://doi.org/10.3847/0004-637X/817/2/107

Owen JE, Wu Y (2017) The evaporation valley in the Kepler planets. Astrophys J 847(1):29. https://doi.org/10.3847/1538-4357/aa890a

Parc L, Bouchy F, Venturini J, et al (2024) From super-earths to sub-neptunes: observational constraints and connections to theoretical models. Astron Astrophys 688:A59. https://doi.org/10.1051/0004-6361/202449911. arXiv:2406.04311 [astro-ph.EP]

Parker EN (1965) Dynamical theory of the solar wind. Space Sci Rev 4(5–6):666–708. https://doi.org/10.1007/BF00216273

Pavlov AA, Brown LL, Kasting JF (2001) UV shielding of NH_3 and O_2 by organic hazes in the Archean atmosphere. J Geophys Res 106(E10):23267–23288. https://doi.org/10.1029/2000JE001448

Payne JL, Boyer AG, Brown JH, et al (2009) Two-phase increase in the maximum size of life over 3.5 billion years reflects biological innovation and environmental opportunity. Proc Natl Acad Sci USA 106(1):24–27

Perez-Becker D, Chiang E (2013) Catastrophic evaporation of rocky planets. Mon Not R Astron Soc 433(3):2294–2309. https://doi.org/10.1093/mnras/stt895

Péron S, Moreira M, Colin A, et al (2016) Neon isotopic composition of the mantle constrained by single vesicle analyses. Earth Planet Sci Lett 449:145–154. https://doi.org/10.1016/j.epsl.2016.05.052

Persson M, Futaana Y, Fedorov A, et al (2018) H^+/O^+ escape rate ratio in the Venus magnetotail and its dependence on the solar cycle. Geophys Res Lett 45(20):10,805–10,811. https://doi.org/10.1029/2018GL079454

Petigura EA, Rogers JG, Isaacson H, et al (2022) The California-Kepler survey. X. The radius gap as a function of stellar mass, metallicity, and age. Astron J 163(4):179. https://doi.org/10.3847/1538-3881/ac51e3. arXiv:2201.10020 [astro-ph.EP]

Piaulet C, Benneke B, Almenara JM, et al (2023) Evidence for the volatile-rich composition of a 1.5-Earth-radius planet. Nat Astron 7:206–222. https://doi.org/10.1038/s41550-022-01835-4

Pierrehumbert RT (2010a) A palette of climates for Gliese 581g. Astrophys J Lett 726(1):L8
Pierrehumbert RT (2010b) Principles of planetary climate, 1st edn. Cambridge University Press, Cambridge. https://doi.org/10.1017/CBO9780511780783
Piso AMA, Youdin AN (2014) On the minimum core mass for giant planet formation at wide separations. Astrophys J 786(1):21. https://doi.org/10.1088/0004-637X/786/1/21
Podosek FA (2003) Noble gases. Treat. Geochem. 1:711. https://doi.org/10.1016/B0-08-043751-6/01066-5
Pollack JB, Yung YL (1980) Origin and evolution of planetary atmospheres. Annu Rev Earth Planet Sci 8:425–487. https://doi.org/10.1146/annurev.ea.08.050180.002233
Pollack JB, Hubickyj O, Bodenheimer P, et al (1996) Formation of the giant planets by concurrent accretion of solids and gas. Icarus 124(1):62–85. https://doi.org/10.1006/icar.1996.0190
Pont F, Knutson H, Gilliland RL, et al (2008) Detection of atmospheric haze on an extrasolar planet: the 0.55-1.05 μm transmission spectrum of HD 189733b with the Hubble Space Telescope. Mon Not R Astron Soc 385(1):109–118. https://doi.org/10.1111/j.1365-2966.2008.12852.x
Porcelli D, Pepin RO (2000) Rare gas constraints on early Earth history. In: Canup RM, Righter K, et al (eds) Origin of the Earth and Moon. University of Arizona Press, Tucson, pp 435–458
Porcelli D, Woolum D, Cassen P (2001) Deep Earth rare gases: initial inventories, capture from the solar nebula, and losses during Moon formation. Earth Planet Sci Lett 193(1–2):237–251. https://doi.org/10.1016/S0012-821X(01)00493-9
Powell D, Feinstein AD, Lee EKH, et al (2024) Sulfur dioxide in the mid-infrared transmission spectrum of WASP-39b. Nature 626(8001):979–983. https://doi.org/10.1038/s41586-024-07040-9
Quanz SP, Ottiger M, Fontanet E, et al (2022) Large Interferometer For Exoplanets (LIFE) I. Improved exoplanet detection yield estimates for a large mid-infrared space-interferometer mission. Astron Astrophys 664:A21. https://doi.org/10.1051/0004-6361/202140366
Radoman-Shaw B, McCanta MC, Filiberto J, et al (2022) Experiments on the reactivity of basaltic minerals and glasses in Venus surface conditions using the Glenn Extreme Environment Rig. Meteorit Planet Sci 57(9):1617–1633. https://doi.org/10.1111/maps.13902
Ramirez RM, Kasting JF (2017) Could cirrus clouds have warmed early Mars? Icarus 281:248–261
Ramirez RM, Levi A (2018) The ice cap zone: a unique habitable zone for ocean worlds. Mon Not R Astron Soc 477(4):4627–4640. https://doi.org/10.1093/mnras/sty761
Ramstad R, Barabash S (2021) Do intrinsic magnetic fields protect planetary atmospheres from stellar winds? Lessons from ion measurements at Mars, Venus, and Earth. Space Sci Rev 217(2):36. https://doi.org/10.1007/s11214-021-00791-1
Ramstad R, Barabash S, Futaana Y, et al (2018) Ion escape from Mars through time: an extrapolation of atmospheric loss based on 10 years of Mars Express measurements. J Geophys Res Planets 123(11):3051–3060
Ranjan S, Schwieterman EW, Harman C, et al (2020) Photochemistry of anoxic abiotic habitable planet atmospheres: impact of new H_2O cross sections. Astrophys J 896(2):148. https://doi.org/10.3847/1538-4357/ab9363
Ranjan S, Schwieterman EW, Leung M, et al (2023) The importance of the upper atmosphere to CO/O_2 runaway on habitable planets orbiting low-mass stars. Astrophys J Lett 958(1):L15. https://doi.org/10.3847/2041-8213/ad037c
Rappaport S, Levine A, Chiang E, et al (2012) Possible disintegrating short-period super-Mercury orbiting KIC 12557548. Astrophys J 752(1):1. https://doi.org/10.1088/0004-637X/752/1/1
Rappaport S, Barclay T, DeVore J, et al (2014) KOI-2700b—A planet candidate with dusty effluents on a 22 hr orbit. Astrophys J 784(1):40. https://doi.org/10.1088/0004-637X/784/1/40
Rauer H, Aerts C, Cabrera J, et al (2025) The PLATO mission. Exp Astron 59(3):26. https://doi.org/10.1007/s10686-025-09985-9
Raymond SN, Morbidelli A (2022) planet formation: key mechanisms and global models. In: Biazzo K, Bozza V, Mancini L, et al (eds) Demographics of exoplanetary systems: lecture notes of the 3rd advanced school on exoplanetary science. Astrophysics and Space Science Library, vol 466. Springer, Cham, pp 3–82. https://doi.org/10.1007/978-3-030-88124-5_1
Renggli CJ, Palm AB, King PL, et al (2019) Implications of reactions between SO2 and basaltic glasses for the mineralogy of planetary crusts. J Geophys Res Planets 124(11):3205–3226. https://doi.org/10.1029/2019JE006045
Ribas I, Guinan EF, Güdel M, et al (2005) Evolution of the solar activity over time and effects on planetary atmospheres. I. High-energy irradiances (1-1700 Å). Astrophys J 622(1):680–694. https://doi.org/10.1086/427977
Righter K, Herd CDK, Boujibar A (2020) Redox processes in early Earth accretion and in terrestrial bodies. Elements 16(3):161–166. https://doi.org/10.2138/gselements.16.3.161
Rimmer P, Shorttle O, Rugheimer S (2019) Oxidised micrometeorites as evidence for low atmospheric pressure on the early Earth. Geochem Perspect Lett 9:38–42. https://doi.org/10.7185/geochemlet.1903

Rimmer PB, Matthews JJK, Jordan S, et al (2023) The nature and implications of sulfur chemistry in Venus' cloud droplets. Proc Natl Acad Sci USA 120(28):e2220726120. https://doi.org/10.1073/pnas.2220726120

Rogers LA (2015) Most 1.6 Earth-radius planets are not rocky. Astrophys J 801(1):41. https://doi.org/10.1088/0004-637X/801/1/41

Rogers JG, Gupta A, Owen JE, et al (2021) Photoevaporation versus core-powered mass-loss: model comparison with the 3D radius gap. Mon Not R Astron Soc 508(4):5886–5902. https://doi.org/10.1093/mnras/stab2897

Rogers JG, Owen JE, Schlichting HE (2024a) Under the light of a new star: evolution of planetary atmospheres through protoplanetary disc dispersal and boil-off. Mon Not R Astron Soc 529(3):2716–2733. https://doi.org/10.1093/mnras/stae563

Rogers JG, Schlichting HE, Young ED (2024b) Fleeting but not forgotten: the imprint of escaping hydrogen atmospheres on super-Earth interiors. Astrophys J 970(1):47. https://doi.org/10.3847/1538-4357/ad5287

Rondanelli R, Lindzen RS (2010) Can thin cirrus clouds in the tropics provide a solution to the faint young sun paradox. J Geophys Res, Atmos 115:D2

Sakai S, Seki K, Terada N, et al (2018) Effects of a weak intrinsic magnetic field on atmospheric escape from Mars. Geophys Res Lett 45(18):9336–9343. https://doi.org/10.1029/2018GL079972

Sakakura K, Seki K, Sakai S, et al (2022) Formation mechanisms of the molecular Ion polar plume and its contribution to ion escape from Mars. J Geophys Res Space Phys 127(6):e29750. https://doi.org/10.1029/2021JA029750

Sakuraba H, Kurokawa H, Genda H (2019) Impact degassing and atmospheric erosion on Venus, Earth, and Mars during the late accretion. Icarus 317:48–58. https://doi.org/10.1016/j.icarus.2018.05.035. arXiv:1805.07094 [astro-ph.EP]

Salvador A, Samuel H (2023) Convective outgassing efficiency in planetary magma oceans: insights from computational fluid dynamics. Icarus 390:115265. https://doi.org/10.1016/j.icarus.2022.115265. arXiv:2209.06199 [astro-ph.EP]

Salvador A, Avice G, Breuer D, et al (2023) Magma ocean, water, and the early atmosphere of Venus. Space Sci Rev 219(7):51. https://doi.org/10.1007/s11214-023-00995-7

Salz M, Schneider PC, Czesla S, et al (2016) Energy-limited escape revised. The transition from strong planetary winds to stable thermospheres. Astron Astrophys 585:L2. https://doi.org/10.1051/0004-6361/201527042

Sanchis-Ojeda R, Rappaport S, Pallè E, et al (2015) The K2-ESPRINT project I: discovery of the disintegrating rocky planet K2-22b with a cometary head and leading tail. Astrophys J 812(2):112. https://doi.org/10.1088/0004-637X/812/2/112

Schaefer L, Fegley B (2007) Outgassing of ordinary chondritic material and some of its implications for the chemistry of asteroids, planets, and satellites. Icarus 186(2):462–483. https://doi.org/10.1016/j.icarus.2006.09.002

Schaefer L, Fegley B (2010) Chemistry of atmospheres formed during accretion of the Earth and other terrestrial planets. Icarus 208(1):438–448. https://doi.org/10.1016/j.icarus.2010.01.026

Scherf M, Lammer H (2021) Did Mars possess a dense atmosphere during the first ~400 million years? Space Sci Rev 217(1):2. https://doi.org/10.1007/s11214-020-00779-3. arXiv:2102.05976 [astro-ph.EP]

Scherf M, Lammer H, Erkaev NV, et al (2020) Nitrogen atmospheres of the icy bodies in the Solar System. Space Sci Rev 216(8):123. https://doi.org/10.1007/s11214-020-00752-0. arXiv:2011.00973 [astro-ph.EP]

Scherf M, Lammer H, Spross L (2024) Eta-Earth revisited II: deriving a maximum number of Earth-like habitats in the galactic disk. Astrobiology 24(10):e916–e1061. https://doi.org/10.1089/ast.2023.0076

Scherf M, Vorburger A, Wurz P, et al (2025) Future measurement needs for the atmospheres of Pluto and Triton. In: Luspay-Kuti A, Mandt K (eds) Triton and Pluto; the long lost twins of active worlds. IOP Publishing, pp 10–11. https://doi.org/10.1088/2514-3433/ad5278ch10

Schillings A, Slapak R, Nilsson H, et al (2019) Earth atmospheric loss through the plasma mantle and its dependence on solar wind parameters. Earth Planets Space 71(1):70. https://doi.org/10.1186/s40623-019-1048-0

Schirrmeister BE, Gugger M, Donoghue PC (2015) Cyanobacteria and the great oxidation event: evidence from genes and fossils. Palaeontology 58(5):769–785

Schlawin E, Agol E, Walkowicz LM, et al (2010) Exoplanetary transits of limb-brightened lines: tentative Si IV absorption by HD 209458b. Astrophys J Lett 722(1):L75–L79. https://doi.org/10.1088/2041-8205/722/1/L75

Schlecker M, Apai D, Lichtenberg T, et al (2024) Bioverse: the habitable zone inner edge discontinuity as an imprint of runaway greenhouse climates on exoplanet demographics. Planet Sci J 5(1):3. https://doi.org/10.3847/PSJ/acf57f

Schlichting HE, Young ED (2022) Chemical equilibrium between cores, mantles, and atmospheres of super-earths and sub-neptunes and implications for their compositions, interiors, and evolution. Planet Sci J 3(5):127. https://doi.org/10.3847/PSJ/ac68e6

Schlichting HE, Sari R, Yalinewich A (2015) Atmospheric mass loss during planet formation: the importance of planetesimal impacts. Icarus 247:81–94

Schmidt F, Way MJ, Costard F, et al (2022) Circumpolar ocean stability on Mars 3 gy ago. Proc Natl Acad Sci USA 119(4):e2112930118

Schmidt F, Way MJ, Quiquet A, et al (2025) Ancient Mars climate with a polar ocean and ice sheet dynamics. J Geophys Res Planets 130:e2025JE008970. https://doi.org/10.1029/2025JE008970

Schoonen MA (2016) Sulfur cycle. In: White W (ed) Encyclopedia of geochemistry. Encyclopedia of Earth Sciences Series. Springer, Cham, pp 1–4. https://doi.org/10.1007/978-3-319-39193-9_73-1

Schwieterman EW, Leung M (2024) An overview of exoplanet biosignatures. Rev Mineral Geochem 90(1):465–514. https://doi.org/10.2138/rmg.2024.90.13

Schwieterman EW, Kiang NY, Parenteau MN, et al (2018) Exoplanet biosignatures: a review of remotely detectable signs of life. Astrobiology 18(6):663–708

Schwieterman EW, Reinhard CT, Olson SL, et al (2019) A limited habitable zone for complex life. Astrophys J 878(1):19. https://doi.org/10.3847/1538-4357/ab1d52

Seki K, Elphic RC, Hirahara M, et al (2001) On atmospheric loss of oxygen ions from Earth through magnetospheric processes. Science 291(5510):1939–1941. https://doi.org/10.1126/science.1058913

Seki K, Nagy A, Jackman CM, et al (2015) A review of general physical and chemical processes related to plasma sources and losses for Solar System magnetospheres. Space Sci Rev 192(1–4):27–89. https://doi.org/10.1007/s11214-015-0170-y

Sembay S, Cheney A, Hampson R, et al (2025) The Soft X-ray Imager (SXI) on the SMILE mission. Space Sci Rev 221(8):113. https://doi.org/10.1007/s11214-025-01241-y

Semenov D, Henning T, Helling C, et al (2003) Rosseland and Planck mean opacities for protoplanetary discs. Astron Astrophys 410:611–621. https://doi.org/10.1051/0004-6361:20031279

Sharp RD, Johnson RG, Shelley EG (1977) Observation of an ionospheric acceleration mechanism producing energetic (keV) ions primarily normal to the geomagnetic field direction. J Geophys Res 82(22):3324. https://doi.org/10.1029/JA082i022p03324

Sharp ZD, McCubbin FM, Shearer CK (2013) A hydrogen-based oxidation mechanism relevant to planetary formation. Earth Planet Sci Lett 380:88–97

Shelley EG, Johnson RG, Sharp RD (1972) Satellite observations of energetic heavy ions during a geomagnetic storm. J Geophys Res 77(31):6104. https://doi.org/10.1029/JA077i031p06104

Shematovich VI, Ionov DE, Lammer H (2014) Heating efficiency in hydrogen-dominated upper atmospheres. Astron Astrophys 571:A94. https://doi.org/10.1051/0004-6361/201423573

Shkolnik EL, Barman TS (2014) HAZMAT. I. The evolution of far-UV and near-UV emission from early m stars. Astron J 148(4):64. https://doi.org/10.1088/0004-6256/148/4/64

Showman AP, Guillot T (2002) Atmospheric circulation and tides of "51 Pegasus b-like" planets. Astron Astrophys 385:166–180. https://doi.org/10.1051/0004-6361:20020101

Sing DK, Fortney JJ, Nikolov N, et al (2016) A continuum from clear to cloudy hot-Jupiter exoplanets without primordial water depletion. Nature 529(7584):59–62. https://doi.org/10.1038/nature16068

Slapak R, Schillings A, Nilsson H, et al (2017) Atmospheric loss from the dayside open polar region and its dependence on geomagnetic activity: implications for atmospheric escape on evolutionary timescales. Ann Geophys 35(3):721–731. https://doi.org/10.5194/angeo-35-721-2017

Solomatov VS (2000) Fluid dynamics of a terrestrial magma ocean. In: Canup RM, Righter K, et al (eds) Origin of the Earth and Moon. University of Arizona Press, Tucson, pp 323–338

Som SM, Catling DC, Harnmeijer JP, et al (2012) Air density 2.7 billion years ago limited to less than twice modern levels by fossil raindrop imprints. Nature 484(7394):359–362

Som SM, Buick R, Hagadorn JW, et al (2016) Earth's air pressure 2.7 billion years ago constrained to less than half of modern levels. Nat Geosci 9(6):448–451. https://doi.org/10.1038/ngeo2713

Sossi PA, Tollan PM, Badro J, et al (2023) Solubility of water in peridotite liquids and the prevalence of steam atmospheres on rocky planets. Earth Planet Sci Lett 601:117894

Sparrman V, Bladh S, Way MJ (2024) Multiple habitable phases on outer exosolar worlds. Astrophys J 962(1):83

Spencer JR, Rathbun JA, Travis LD, et al (2000) Io's thermal emission from the Galileo photopolarimeter-radiometer. Science 288(5469):1198–1201

Sproß L, Scherf M, Shematovich VI, et al (2021) Life as the only reason for the existence of N_2-O_2-dominated atmospheres. Astron Rep 65(4):275–296. https://doi.org/10.1134/S1063772921040077

Steinmeyer ML, Woitke P, Johansen A (2023) Sublimation of refractory minerals in the gas envelopes of accreting rocky planets. Astron Astrophys 677:A181. https://doi.org/10.1051/0004-6361/202245636

Stökl A, Erkaev N, Dorfi E, et al (2014) Origin and loss of nebula-captured hydrogen envelopes from 'sub'-to 'super-earths' in the habitable zone of sun-like stars. Mon Not R Astron Soc 439(4):3225–3238
Stökl A, Dorfi E, Lammer H (2015) Hydrodynamic simulations of captured protoatmospheres around Earth-like planets. Astron Astrophys 576:A87. https://doi.org/10.1051/0004-6361/201423638. arXiv:1505.06859 [astro-ph.EP]
Stüeken EE, Buick R, Guy BM, et al (2015) Isotopic evidence for biological nitrogen fixation by molybdenum-nitrogenase from 3.2 Gyr. Nature 520(7549):666–669. https://doi.org/10.1038/nature14180
Stüeken EE, Kipp MA, Koehler MC, et al (2016) Modeling pN_2 through geological time: implications for planetary climates and atmospheric biosignatures. Astrobiology 16(12):949–963. https://doi.org/10.1089/ast.2016.1537
Stüeken EE, Som SM, Claire M, et al (2020) Mission to planet Earth: the first two billion years. Space Sci Rev 216(2):31. https://doi.org/10.1007/s11214-020-00652-3
Tabataba-Vakili F, Grenfell JL, Grießmeier JM, et al (2016) Atmospheric effects of stellar cosmic rays on Earth-like exoplanets orbiting M-dwarfs. Astron Astrophys 585:A96. https://doi.org/10.1051/0004-6361/201425602
Tang Y, Fortney JJ, Murray-Clay R (2024) Assessing core-powered mass loss in the context of early boil-off: minimal long-lived mass loss for the sub-Neptune population. Astrophys J 976(2):221. https://doi.org/10.3847/1538-4357/ad8567
Taylor FW, Grinspoon DH, (2009) Climate evolution of Venus. J Geophys Res Planets 114:E00–B40. https://doi.org/10.1029/2008JE003316
The LUVOIR Team (2019) The LUVOIR Mission Concept Study Final Report. arXiv e-prints. arXiv:1912.06219
Thomas N, Bagenal F, Hill T, et al (2004) The io neutral clouds and plasma torus. Jupiter the planet, satellites and magnetosphere. Phys. Environ. Sci. 1:561–591
Thomas TB, Hu R, Lo DY (2023) Constraints on the size and composition of the ancient Martian atmosphere from coupled CO_2–N_2–Ar isotopic evolution models. Planet Sci J 4(3):41
Thompson MA, Krissansen-Totton J, Wogan N, et al (2022) The case and context for atmospheric methane as an exoplanet biosignature. Proc Natl Acad Sci USA 119(14):e2117933119. https://doi.org/10.1073/pnas.2117933119
Tian M, Heng K (2024) Atmospheric chemistry of secondary and hybrid atmospheres of super earths and sub-neptunes. Astrophys J 963(2):157. https://doi.org/10.3847/1538-4357/ad217c
Tian F, Kasting JF, Solomon SC (2009) Thermal escape of carbon from the early Martian atmosphere. Geophys Res Lett 36(2):L02205. https://doi.org/10.1029/2008GL036513
Tian F, France K, Linsky JL, et al (2014a) High stellar fuv/nuv ratio and oxygen contents in the atmospheres of potentially habitable planets. Earth Planet Sci Lett 385:22–27
Tian F, France K, Linsky JL, et al (2014b) High stellar FUV/NUV ratio and oxygen contents in the atmospheres of potentially habitable planets. Earth Planet Sci Lett 385:22–27. https://doi.org/10.1016/j.epsl.2013.10.024
Trainer MG, Pavlov AA, Curtis DB, et al (2004) Haze aerosols in the atmosphere of early Earth: Manna from heaven. Astrobiology 4(4):409–419. https://doi.org/10.1089/ast.2004.4.409
Trainer MG, Jimenez JL, Yung YL, et al (2012) Nitrogen incorporation in CH_4-N_2 photochemical aerosol produced by far ultraviolet irradiation. Astrobiology 12(4):315–326. https://doi.org/10.1089/ast.2011.0754
Turbet M, Boulet C, Karman T (2020) Measurements and semi-empirical calculations of CO_2 + CH_4 and CO_2 + H_2 collision-induced absorption across a wide range of wavelengths and temperatures. Application for the prediction of early Mars surface temperature. Icarus 346:113762
Turbet M, Bolmont E, Chaverot G, et al (2021) Day–night cloud asymmetry prevents early oceans on Venus but not on Earth. Nature 598:276–280. https://doi.org/10.1038/s41586-021-03873-w
Tyburczy JA, Frisch B, Ahrens TJ (1986) Shock-induced volatile loss from a carbonaceous chondrite: implications for planetary accretion. Earth Planet Sci Lett 80(3–4):201–207. https://doi.org/10.1016/0012-821X(86)90104-4
Tyburczy JA, Xu X, Ahrens TJ, et al (2001) Shock-induced devolatilization and isotopic fractionation of h and c from Murchison meteorite: some implications for planetary accretion. Earth Planet Sci Lett 192(1):23–30. https://doi.org/10.1016/S0012-821X(01)00429-0
Urata RA, Toon OB (2013) Simulations of the Martian hydrologic cycle with a general circulation model: implications for the ancient Martian climate. Icarus 226(1):229–250
Valley JW, Peck WH, King EM, et al (2002) A cool early Earth. Geology 30(4):351–354
Van Eylen V, Agentoft C, Lundkvist MS, et al (2018) An asteroseismic view of the radius valley: stripped cores, not born rocky. Mon Not R Astron Soc 479(4):4786–4795. https://doi.org/10.1093/mnras/sty1783

Van Looveren G, Güdel M, Boro Saikia S, et al (2024) Airy worlds or barren rocks? On the survivability of secondary atmospheres around the TRAPPIST-1 planets. Astron Astrophys 683:A153. https://doi.org/10.1051/0004-6361/202348079. arXiv:2401.16490 [astro-ph.EP]
Van Looveren G, Boro Saikia S, Herbort O, et al (2025) Habitable Zone and Atmosphere Retention Distance (HaZARD): stellar-evolution-dependent loss models of secondary atmospheres. Astron Astrophys 694:A310. https://doi.org/10.1051/0004-6361/202452998. arXiv:2502.09702 [astro-ph.EP]
Vazan A, Ormel CW, Brouwers MG (2024) How planets grow by pebble accretion. V. Silicate rainout delays the contraction of sub-Neptunes. Astron Astrophys 687:A262. https://doi.org/10.1051/0004-6361/202349137
Venturini J, Alibert Y, Benz W, et al (2015) Critical core mass for enriched envelopes: the role of H_2O condensation. Astron Astrophys 576:A114. https://doi.org/10.1051/0004-6361/201424008
Venturini J, Alibert Y, Benz W (2016) Planet formation with envelope enrichment: new insights on planetary diversity. Astron Astrophys 596:A90. https://doi.org/10.1051/0004-6361/201628828
Venturini J, Guilera OM, Haldemann J, et al (2020) The nature of the radius valley. Hints from formation and evolution models. Astron Astrophys 643:L1. https://doi.org/10.1051/0004-6361/202039141
Venturini J, Ronco MP, Guilera OM, et al (2024) A fading radius valley towards M dwarfs, a persistent density valley across stellar types. Astron Astrophys 686:L9. https://doi.org/10.1051/0004-6361/202349088. arXiv:2404.01967 [astro-ph.EP]
Vidal-Madjar A, Lecavelier des Etangs A, Désert JM, et al (2003) An extended upper atmosphere around the extrasolar planet HD209458b. Nature 422(6928):143–146. https://doi.org/10.1038/nature01448
Vilović I, Schulze-Makuch D, Heller R (2023) Variations in climate habitability parameters and their effect on Earth's biosphere during the Phanerozoic eon. Sci Rep 13(1):12663
Vissapragada S, Knutson HA, Jovanovic N, et al (2020) Constraints on metastable helium in the atmospheres of WASP-69b and WASP-52b with ultranarrowband photometry. Astron J 159(6):278. https://doi.org/10.3847/1538-3881/ab8e34
Vladilo G, Murante G, Silva L, et al (2013) The habitable zone of Earth-like planets with different levels of atmospheric pressure. Astrophys J 767(1):65. https://doi.org/10.1088/0004-637X/767/1/65
Wakeford HR, Sing DK, Deming D, et al (2018) The complete transmission spectrum of WASP-39b with a precise water constraint. Astron J 155(1):29. https://doi.org/10.3847/1538-3881/aa9e4e
Walbecq A, Samuel H, Limare A (2025) The effect of out-of-equilibrium outgassing on the cooling of planetary magma oceans. Icarus 434:116513. https://doi.org/10.1016/j.icarus.2025.116513
Walker JCG, Hays PB, Kasting JF (1981) A negative feedback mechanism for the long-term stabilization of Earth's surface temperature. J Geophys Res, Oceans 86(C10):9776–9782. https://doi.org/10.1029/JC086iC10p09776
Wallis M (1978) Exospheric density and escape fluxes of atomic isotopes on Venus and Mars. Planet Space Sci 26(10):949–953. https://doi.org/10.1016/0032-0633(78)90077-6
Watson Astron J, Donahue TM, Walker JCG (1981) The dynamics of a rapidly escaping atmosphere: applications to the evolution of Earth and Venus. Icarus 48(2):150–166. https://doi.org/10.1016/0019-1035(81)90101-9
Way MJ, Del Genio AD (2020) Venusian habitable climate scenarios: modeling Venus through time and applications to slowly rotating Venus-like exoplanets. J Geophys Res Planets 125(5):e2019JE006276
Way MJ, Del Genio AD, Kiang NY, et al (2016) Was Venus the first habitable world of our Solar System? Geophys Res Lett 43:8376–8383. https://doi.org/10.1002/2016GL069790. [astro-ph.EP]
Way MJ, Del Genio AD Aleinov I, et al (2018) Climates of warm Earth-like planets. I. 3d model simulations. Astrophys J Suppl Ser 239(2):24
Way MJ, Ostberg C, Foley BJ, et al (2023) Synergies between Venus & exoplanetary observations: Venus and its extrasolar siblings. Space Sci Rev 219(1):13
Wei Y, Fraenz M, Dubinin E, et al (2012) Enhanced atmospheric oxygen outflow on Earth and Mars driven by a corotating interaction region. J Geophys Res Space Phys 117(A3):A03208. https://doi.org/10.1029/2011JA017340
Weichbold F, Lammer H, Scherf M, et al (2025) First detection of deuterium in Venus's extended exosphere. Preprint. https://doi.org/10.21203/rs.3.rs-7720153/v1
Westall F, Höning D, Avice G, et al (2023) The habitability of Venus. Space Sci Rev 219(2):17. https://doi.org/10.1007/s11214-023-00960-4
Wignall PB (2011) Lethal volcanism. Nature 477(7364):285–286
Wilde SA, Valley JW, Peck WH, et al (2001) Evidence from detrital zircons for the existence of continental crust and oceans on the Earth 4.4 gyr ago. Nature 409(6817):175–178
Williams CD, Mukhopadhyay S (2019) Capture of nebular gases during Earth's accretion is preserved in deep-mantle neon. Nature 565(7737):78–81. https://doi.org/10.1038/s41586-018-0771-1
Woitke P, Herbort O, Helling C, et al (2021) Coexistence of CH_4, CO_2, and H_2O in exoplanet atmospheres. Astron Astrophys 646:A43

Wolff SG, Wang J, Stapelfeldt K, et al (2024) The roman coronagraph community participation program: observation planning. In: Coyle LE, Matsuura S, Perrin MD (eds) Space telescopes and instrumentation 2024: optical, infrared, and millimeter wave, pp 1309255. https://doi.org/10.1117/12.3020205. arXiv:2411.17868
Wong I (2021) Exoplanet phase curves from TESS: Results from the Primary Mission and future prospects. In: American Astronomical Society Meeting Abstracts #237, pp 302.02
Wood BJ, Walter MJ, Wade J (2006) Accretion of the Earth and segregation of its core. Nature 441(7095):825–833
Woods T, Rottman G, Harder J, et al (2000) Overview of the EOS SORCE mission. Proc SPIE 4135:192. https://doi.org/10.1117/12.494229
Wordsworth RD (2016) The climate of early Mars. Annu Rev Earth Planet Sci 44(1):381–408
Wordsworth R, Pierrehumbert R (2014) Abiotic oxygen-dominated atmospheres on terrestrial habitable zone planets. Astrophys J Lett 785(2):L20
Wordsworth R, Kalugina Y, Lokshtanov S, et al (2017) Transient reducing greenhouse warming on early Mars. Geophys Res Lett 44(2):665–671. https://doi.org/10.1002/2016GL071766
Wordsworth RD, Schaefer LK, Fischer RA (2018) Redox evolution via gravitational differentiation on low-mass planets: implications for abiotic oxygen, water loss, and habitability. Astron J 155(5):195. https://doi.org/10.3847/1538-3881/aab608
Yang J, Boué G, Fabrycky DC, et al (2014a) Strong dependence of the inner edge of the habitable zone on planetary rotation rate. Astrophys J 787:L2. https://doi.org/10.1088/2041-8205/787/1/L2
Yang J, Liu Y, Hu Y, et al (2014b) Water trapping on tidally locked terrestrial planets requires special conditions. Astrophys J Lett 796(2):L22
Yau AW, Abe T, Peterson WK (2007) The polar wind: recent observations. J Atmos Sol-Terr Phys 69(16):1936–1983. https://doi.org/10.1016/j.jastp.2007.08.010
Yokochi R, Marty B (2004) A determination of the neon isotopic composition of the deep mantle. Earth Planet Sci Lett 225(1–2):77–88. https://doi.org/10.1016/j.epsl.2004.06.010
Yoshida T, Terada N, Ikoma M, et al (2022) Less effective hydrodynamic escape of H_2-H_2O atmospheres on terrestrial planets orbiting pre-main-sequence M dwarfs. Astrophys J 934(2):137. https://doi.org/10.3847/1538-4357/ac7be7
Young ED, Shahar A, Schlichting HE (2023) Earth shaped by primordial H_2 atmospheres. Nature 616(7956):306–311. https://doi.org/10.1038/s41586-023-05823-0
Yung YL, Demore WB (eds) (1999). Photochemistry of planetary atmospheres. Oxford University Press
Zahnle KJ, Kasting JF (1986) Mass fractionation during transonic escape and implications for loss of water from Mars and Venus. Icarus 68(3):462–480. https://doi.org/10.1016/0019-1035(86)90051-5
Zahnle KJ, Gacesa M, Catling DC (2019) Strange messenger: a new history of hydrogen on Earth, as told by xenon. Geochim Cosmochim Acta 244:56–85
Zahnle KJ, Lupu R, Catling DC, et al (2020) Creation and evolution of impact-generated reduced atmospheres of early Earth. Planet Sci J 1(1):11. https://doi.org/10.3847/PSJ/ab7e2c
Zerkle AL, Poulton SW, Newton RJ, et al (2017) Onset of the aerobic nitrogen cycle during the great oxidation event. Nature 542(7642):465–467. https://doi.org/10.1038/nature20826
Zhang M, Knutson HA, Wang L, et al (2022) Detection of ongoing mass loss from HD 63433c, a young mini-Neptune. Astron J 163(2):68. https://doi.org/10.3847/1538-3881/ac3f3b
Zhang Z, Morley CV, Gully-Santiago M, et al (2023) Giant tidal tails of helium escaping the hot Jupiter HAT-P-32 b. Sci Adv 9(23):eadf8736. https://doi.org/10.1126/sciadv.adf8736
Zhang HL, Hirschmann MM, Lord OT, et al (2024) Ferric iron stabilization at deep magma ocean conditions. Sci Adv 10(42):eadp1752. https://doi.org/10.1126/sciadv.adp1752
Zieba S, Kreidberg L, Ducrot E, et al (2023) No thick carbon dioxide atmosphere on the rocky exoplanet TRAPPIST-1 c. Nature 620(7975):746–749. https://doi.org/10.1038/s41586-023-06232-z
Zilinskas M, van Buchem CPA, Miguel Y, et al (2022) Observability of evaporating lava worlds. Astron Astrophys 661:A126. https://doi.org/10.1051/0004-6361/202142984

Authors and Affiliations

Marie-Luise Steinmeyer[1] · Lena Noack[2] · Philipp Baumeister[2] · Keiko Hamano[3,4] · M.J. Way[5,6] · Doris Breuer[7] · Kanako Seki[8] · Caroline Brachmann[2,7] · Fabrice Gaillard[9] · Manuel Scherf[10] · Svetlana V. Berdyugina[11] · Brice-Olivier Demory[12]

✉ M.-L. Steinmeyer
msteinmeyer@phys.ethz.ch

[1] Institute for Particle Physics and Astrophysics, ETH Zurich, Wolfgang-Pauli-Strasse 27, 8093 Zurich, Switzerland

[2] Institute of Geological Sciences, Freie Universität Berlin, Malteserstr. 74-100, 12249 Berlin, Germany

[3] Division of Science, National Astronomical Observatory of Japan, 2-21-1 Osawa, Mitaka, 181-8588 Tokyo, Japan

[4] Earth-Life Science Institute, Institute of Science Tokyo, 2-12-1 Ookayama, Meguro-ku, 152-8550 Tokyo, Japan

[5] NASA Goddard Institute for Space Studies, 2880 Broadway, 10025 New York, USA

[6] Theoretical Astrophysics, Department of Physics and Astronomy, Uppsala University,Uppsala, Sweden

[7] DLR, Institute of Space Research, Rutherfordstrasse 2, 12489 Berlin, Germany

[8] Department of Earth and Planetary Science, University of Tokyo, Komaba 4-6-1, Meguro-ku, 153-8904, Tokyo, Japan

[9] Institut des Sciences de la Terre d'Orléans, Université d'Orléans-CNRS-BRGM, Orléans, France

[10] Space Research Institute, Austrian Academy of Sciences, Schmiedlstrasse 6, Graz, 8042, Austria

[11] Istituto ricerche solari Aldo e Cele Daccó (IRSOL), Faculty of Informatics, Universitá della Svizzera italiana, Via Patocchi 57, Locarno, 6605, Switzerland

[12] Center for Space and Habitability, University of Bern, Gesellschaftsstrasse 6, Bern, 3012, Switzerland